TRIBOLOGICAL CHARECTERIZATION OF A NOVEL UHMWPE HYBRID NANOCOMPOSITE COATING FOR BIOMEDICAL APPLICATIONS

BY

ZAHID AHMED UWAIS

A Thesis Presented to the
DEANSHIP OF GRADUATE STUDIES

KING FAHD UNIVERSITY OF PETROLEUM & MINERALS

DHAHRAN, SAUDI ARABIA

In Partial Fulfillment of the
Requirements for the Degree of

MASTER OF SCIENCE

In

MECHANICAL ENGINEERING

DECEMBER 2017

KING FAHD UNIVERSITY OF PETROLEUM & MINERALS

DHAHRAN- 31261, SAUDI ARABIA

DEANSHIP OF GRADUATE STUDIES

This thesis, written by Zahid Ahmed Uwais under the direction of his thesis advisor and approved by his thesis committee, has been presented and accepted by the Dean of Graduate Studies, in partial fulfillment of the requirements for the degree of **MASTER OF SCIENCE IN MECHANICAL ENGINEERING.**

Dr. Nasser Al-Aqeeli
(Advisor)

Dr. Zuhair M. A. Gasem
Department Chairman

Dr. Abdul Samad, Mohammed
(Co-Advisor)

Dr. Salam A. Zummo
Dean of Graduate Studies

Dr. Laoui, Tahar
(Member)

Dr. Mohamed Abdrabou Hussein
(Member)

2/4/18
Date

Dr. Madhan Kumar
(Member)

Dedicated to my family

ACKNOWLEDGMENTS

It is a genuine pleasure to express my deep sense of thanks and gratitude to my advisor, the Dean of Scientific Research (DSR) **Professor Nasser Al-Aqeeli**. This work would have hardly been completed without his continuous optimism, enthusiasm, encouragement, and support. I am much obliged to my co-advisor **Dr. Abdul Samad** for his unrelenting support and guidance. His timely scholarly advice and scientific approach have helped me accomplish this task.

I owe a deep sense of gratitude to my committee member **Professor Taher Laoui** for his inspiration, timely suggestions with kindness, enthusiasm, dynamism and keen interest in me at every stage of my research. I would also like to thank the remaining committee members **Dr. Mohamed Abdrabou** and **Dr. Madhan Kumar** for their input and guidance in this research work.

I acknowledge the support provided by King Abdulaziz City for Science and Technology (KACST) through the Science & Technology Unit at King Fahd University of Petroleum & Minerals (KFUPM) for funding this work through **project # 15-ADV4632-04** as part of the National Science, Technology and Innovation Plan.

I am extremely thankful to my research group members Dr. AkeemYusuf Adesina, Dr. Ismaila Aliyu and especially Mr. Umar Azam for keeping me on track. Finally, it is a privilege to thank my parents and my wife, for their constant encouragement and relentless prayers thought my research period.

TABLE OF CONENTENTS

LIST OF TABLES

LIST OF FIGURES

LIST OF ABBREVIATIONS

UHMWPE	**:**	Ultrahigh Molecular Weight Polyethylene
MWCNT	**:**	Multi-walled Carbon Nanotube
CNT	**:**	Carbon Nanotubes
HA	**:**	Hydroxyapatite
TJR	**:**	Total Joint Replacement
Wt%	**:**	weight percentage
GO	**:**	Graphene Oxide
DLC	**:**	Diamond Like Carbon
COF	**:**	Coefficient of Friction
WR	**:**	Wear Rate
SEM	**:**	Scanning Electron Microscopy
PT	**:**	Pure Titanium
Ti64	**:**	Ti6Al4V
SWR	**:**	Specific Wear Rate
SBF	**:**	Simulated Body Fluid
SCE	**:**	Saturated Calomel Electrode
OCP	**:**	Open Circuit Potential
EIS	**:**	Electrochemical impedance spectroscopy

ABSTRACT

Full Name : Zahid Ahmed Uwais

Thesis Title : Tribological Characterization of a Novel UHMWPE Hybrid Nanocomposite Coating for Biomedical Applications

Major Field : Materials and Manufacturing

Date of Degree : December 2017

Titanium and its alloys are extensively used in the medical field for biomedical applications for dental and orthopedic implants. However, due to its poor wear resistance, several studies have been conducted to improve the surface properties of titanium and its alloys through several methods of surface modification.

A new approach of using a polymer hybrid nanocomposite coating to modify the surface of commercially available titanium (pure titanium and Ti6Al4V) and a newly developed titanium alloy (Ti20Nb13Zr) is explored in this study. The coating is achieved by implementing a novel electrostatic spray coating process. Ultra-high molecular weight polyethylene (UHMWPE) has been selected as the parent matrix for the coating due to its excellent biocompatibility and tribological properties. However, due to its low-load bearing capacity carbon nanotubes (CNT's) are used as reinforcement. CNT's in the nanocomposite coating bridge the polymer chains by anchoring them, ensuring excellent mechanical properties. CNT content was optimized based on its tribological performance using three different wt% of CNT (0.5, 1.5 and 3).

Hydroxyapatite (HA) was introduced into the optimized nanocomposite coating to enhance the biocompatibility of the coating. HA increases the biocompatibility due to its ability to bond directly to the natural bone, thus, accelerating bioactivity and osteocoductivity. This is possible due to its similar mineral constituents to natural bone and teeth. Therefore, the hybrid nanocomposite coating was optimized for varied wt% of HA (0.5, 1.5, 3 and 5).

The dispersion of CNT's and HA was evaluated by Raman spectroscopy and SEM images. Higher shifting of the G-band was observed for 1.5wt% CNT compared to 0.5 and 3wt% CNT indicating good dispersion, SEM images showed an even distribution for 1.5wt% CNT and 3wt% HA in the polymer matrix. An increase in 37% of hardness was observed upon addition of CNT from 0wt% to 3wt% into the UHMWPE matrix.

Best tribological and scratch results were achieved for UHMWPE reinforced with 1.5wt% CNT and 3wt% HA, the coating was able to sustain 250,000 cycles without failure, for a load of 12N at a sliding velocity of 0.1m/s, whereas pristine UHMWPE failed at 3600 cycles, for the same parameters. UHMWPE reinforced with 1.5wt% CNT and 3wt% HA coating did not fail for a linear progressive scratch for an end load of 30N. The developed hybrid nanocomposite coating showed excellent tribological performance in terms of low friction, low wear rate and protecting the counterface material as compared to all the bare substrates.

ملخص الرسالة

الاسم الكامل: زاهيد احمد عويس

عنوان الرسالة: الخصائص التريبولوجية للطلاء بمواد UHMWPE الهجينة النانوية للتطبيقات الطبية الحيوية

التخصص: المواد والتصيع

تاريخ الدرجة العلمية: ديسمبر 2017

يستخدم التيتانيوم وسبائكه على نطاق واسع في المجال الطبي للتطبيقات الطبية الحيوية فى زراعة الأسنان و العظام و تطبيقات اخرى .و نظرا لان مقاومة التيتانيوم للبرى منخفضة ، قد أجريت العديد من الدراسات لتحسين خصائص سطح التيتانيوم وسبائك التيتانيوم عن طريق استخدام طرق عديدة لتعديل السطح.

تم في هذه الدراسة استكشاف طريقة جديدة لاستخدام طلاء هجين من النانو البوليمر لتعديل سطح التيتانيوم المتاح تجاريا (التيتانيوم النقي و Ti6Al4V) و سبيكة تيتانيوم مطورة حديثا (Ti20Nb13Zr). يتم اجراء الطلاء باستخدام عملية الطلاء بالرذاذ. و تم اختيار البولي ايثيلين عالي الوزن الجزيئي (UHMWPE) كمصفوفة للطلاء بسبب توافقها الاستثنائي مع الخصائص التريبولوجية. ومع ذلك، نظرا لانخفاض قدرتها على تحمل الاحمال فان أنابيب الكربون النانوية (CNT's)تم استخدامها كمدعم. وتعمل أنابيب الكربون النانوية في طلاء النانو على رسو سلاسل البوليمر ، التي لها خصائص ميكانيكية ممتازة. تم اختيار الوزن الامثل لمحتوى أنابيب الكربون النانوية بناء على الخصائص التريبولوجية باستخدام ثلاثة نسب وزن مختلفة (0.5، 1.5 و 3).

تم إدخال هيدروكسيباتيت في الطلاء المركب النانومترى الأمثل لتعزيز التوافق الطبى للطلاء نظرا لقدرتها على ربط مباشرة إلى العظام الطبيعية، وبالتالي، تسريع النشاط الحيوي والعظمية. هذا ممكن بسبب مكوناته المعدنية المماثلة إلى العظام الطبيعية والأسنان. ولذلك، تم تحسين طلاء نانوكومبوسيت الهجين لنسب مختلفة من وزن الهيدروكسيباتيت (0.5، 1.5، 3 و 5).

تم تقييم تشتت أنابيب الكربون النانوية و هيدروكسيباتيت من قبل مطياف رامان الطيفي و صور الميكروسكوب الالكترونى . وقد لوحظ ارتفاع التحول من االنطاق G ل 1.5 wt٪ من أنابيب الكربون النانوية مقارنة مع 0.5 و 3wt٪ أنابيب الكربون النانوية تشير إلى التشتت جيدة، وأظهرت الصور الميكرسكوب الالكترونى توزيع حتى ل 1.5wt٪ أنابيب الكربون النانوية و 3wt٪ هيدروكسيباتيت في مصفوفة البوليمر. لوحظت زيادة في 37٪ من صلابة عند إضافة أنابيب الكربون النانوية من 0wt٪ إلى 3wt٪ في مصفوفة UHMWPE.

وقد تحققت أفضل النتائج التريبولوجية والخدش ل UHMWPE المعززة مع 1.5wt٪ أنابيب الكربون النانوية و 3wt٪ هيدروكسيباتيت ، وكان الطلاء قادرة على الحفاظ على 250،000 دورة دون الفشل، لحمل 12نيوتن بسرعة انزلاق 0.1 متر/ ثانية، في حين فشل UHMWPE في 3600 دورة، لنفس الشروط . UHMWPE عززت مع 1.5wt٪ أنابيب الكربون النانوية و 3wt٪ طلاء هيدروكسيباتيت لم تفشل خدش التقدمي الخطي لحمل نهاية من 30 نيوتن. وأظهر طلاء النانو الهجين المركب المطور أداء تريبولوجيا ممتازا من حيث الاحتكاك المنخفض، ومعدل التآكل المنخفض، وحماية المواد المواجهة بالمقارنة مع جميع الركائز الاساسية.

CHAPTER 1

INTRODUCTION

1.1 Background

Aging of the world population cannot be prevented as the life expectancy is exponentially rising due to significant improvement in the general living and health conditions. Joint diseases and osteoporotic (porous bone) fractures are common chronic diseases elders are battling. The most common locations of porous bone fractures include the hip, spine, and forearm. Large bone fractures and defects are repaired using commercially available bone implants developed by biomaterials [1].

Biomaterials refer to materials that are biocompatible, and biocompatibility is a descriptive term which specifies the ability of a material to perform with an appropriate host response, in a specific application [2]. Some of the key factors that determine materials, suitability for biomedical application include mechanical properties, corrosion resistance, bio-adhesion, bio-functionality, excellent tribological properties (high wear resistance and low friction), and biocompatibility [3].

The function and quality of patient can be improved by using artificial joints (implants). However, currently due to aseptic loosing caused by periprosthetic osteolysis (defined as the progressive destruction of periprosthetic bony tissue) [4], the lifespan of artificial joins is reduced to 10-15 years. Studies show that the root cause of osteolysis is linked to fatigue fracture and the body's response to the wear debris of biomaterials [5, 6]. Therefore it is crucial to modify the surface of biomaterials, which will improve its wear resistance and mechanical properties resulting in an increase in lifespan of the implant.

Depending on the biomedical application the implant must be capable of withstanding the dynamic loads, simulated when the body is exposed to aggressive environments [7, 8]. Several experiments around the world are being conducted aiming to improve the reliability and durability of artificial joints and implants in order to confidently use the implant for a long period of time. Wear debris generation can be lowered by using a highly wear resistant surface during artificial joint replacement [5].

Surface properties of the biomaterial can be enhanced by using an appropriate highly wear resistant coating or surface treatment techniques. Modifying the surface of the biomaterial can impact several surface properties such as Hardness, elastic strain, wettability, friction, and wear. Coating materials are usually deposited by physical vapor deposition (PVD), chemical vapor deposition (CVD), electrodeposition, thermal treatment in molten salts, laser implantation and ion implantation [5].

The use of polymer coatings for engineering applications is significantly increasing due to their amazing properties such as exceptional corrosion and wear resistance, low cost, self-lubricating properties, and the ability to coat onto any complex shapes [9]. For some applications where the surface are in constant motion the wear properties of the polymer coating may play a very important role since the thickness of the coating compared to the metal substrate is very thin [10]. Ultra-High-Molecular- weight-polyethylene (UHMWPE) in the bulk state has proven to be a good wear-resistant polymer with a moderate coefficient of friction when tested against a steel counterface [11-13, 20]

Since 1962, when UHMWPE was introduced it has been used in several biomedical applications due to its High strength and biocompatibility. In addition, its high stiffness

and strength make it useful in structural materials and fiber production [10]. Its outstanding properties such as abrasive resistance, notched impact strength and low coefficient of friction make it feasible to be used in highly stressed part for instance in total joint replacement, UHMWPE is still commercially used in the manufacturing of cups and tibial inserts. UHMWPE is also used in bearing applications [9,10, 12].

Recent studies on the tribological properties of UHMWPE as a thin film on bare Silicon and surface modified silicon has shown that UHMWPE is an attractive candidate as thin film coating due to its high strength, extraordinary wear resistance and low coefficient of friction against metallic and ceramic components [11,13].

Despite its excellent tribological properties, the use of UHMWPE in numerous tribological applications have been limited due to its low load-bearing capacity and thermal instability, thus tackling this issue has been the focus of considerable scientific research. Reinforcing carbon nanotubes (CNT's) in to the polymer matrix, is one possible solution to overcome this issue.[13]

Carbon nanotubes (CNT's) are cylinders of graphite sheets either in the form of Multi-walled (MW) or single-walled (SW) assemblies [14]. Several studies have shown that the reinforcement of CNT's into polymer matrices in bulk form has significant improvement in the mechanical properties such as elastic modulus and strength, this is owing to the exceptional properties of CNT's such as high tensile strength, high stiffness, excellent electrical and thermal properties [13].

Hydroxyapatite ($Ca_{10}(PO_4)_6(OH)_2$, HA) is an attractive biomaterial due to its similar chemical semblance with bone and teeth. The biocompatibility and bioactivity of HA

flourish osteoblasts, therefore HA coatings have been used in several biomedical applications such as dental implants, skeletal implants bone repair scaffolds , body insert material etc.[15]. Lately, substantial research has been devoted to the development of HA coatings on titanium and other biomaterials, where the mechanical properties and ensured by the metal substrates while HA contributes in enhancing the biocompatibility [14].

If two different elements are mixed together they are known as composites, whilst if one of the two elements is a nanomaterial, it is denoted as nanocomposite. Moreover integrating more than one element to the matrix is referred to as hybrid. Individual elements are mixed together to improve the property of the composite hybrid from different perspective, such as mechanical properties, biocompatibility, corrosion behavior etc.

1.2 Biomaterials and Orthopedic Implants

Orthopedic implants are devices surgically placed into the body designed to restore function by replacing or reinforcing damaged structure such as knee, hip and shoulder replacements. These implants are exposed to great challenges during their use. Sliding wear, cyclic loads and the human body ambient are demanding factors for the materials employed.

Substituting bone constituents lost due to traumatic events has been the main objective in the development of orthopedic application, leading to the increase in production of artificial hard tissue replacement implants, thus an ideal option for orthopedic implant are for hard tissue replacement materials are metallic materials [14].

1.2.1 Types of biomaterials and their limitations

A good combination of mechanical strength, pore size and dimensions, and elastic modulus, biocompatibility and corrosion and wear resistance, are key factors to ensure a successful implant [16].

As already noted, only a certain number of biomaterials are currently used for making surgical implants Table 1 summarizes, the most common biomaterials, currently being used for orthopedic implants.

Table 1: Common biomaterials [3]

Metals	Gold, Tantalum, 316L Stainless Steel, Co-Cr Alloys, Ti and Titanium alloys
Ceramics	Alumina, Zirconia, Carbon, Titania, Bioglass, Hydroxyapatite
Polymers	Ultra-high molecular weight polyethylene (UHMWPE), Polyurethane(PE), Polyurethane (PU), polytetrafuoroethylene (PTFE), Polyacetal (PA), Polymethylmethacrylate (PMMA), Polyethylene Terepthalate (PET), Silicone Rubber (SR), Polyetheretherketone (PEEK), Poly(lactic acid) (PLA), Polysulfone (PS)
Composite	Silica/SR, CF/UHMWPE, CF/PTFE, HA/PE, CF/epoxy, CF/PEEK, CF/C, Al2O3/PTFE)

Table 2 shows a list of materials used for Orthopedic Implants, with respect to their major and minor application. Osteosynthesis is a process to alleviate bone fixation of a bone fracture, using implants and arthroplasty is a surgical procedure to mimic the function of a joint.

Table 2: Biomaterials used for orthopedic implant [16]

Biomaterial	Major/Minor Application	Limitations
Stainless Steel	Osteosynthesis/ Joint arthroplasty	High friction coefficient, wear debri generation, aseptic loosening
Cobalt alloys	Joint arthroplasty /Osteosythesis	Wear debri generation, can cause hypersensitivity & inflammatory reaction, higher modulus of elasticity
Pure Titanium	Osteosynthesis	Poor tribological properties, low abresive resistance, low mechanical stability
Ti alloys	Joint arthroplasty & osteosynthesis	

The use of orthopedic implants, such as total hip or knee replacement has positively influenced the quality of patient's life by reducing pain and returning the function. Hence, for the last decade masses of research are being conducted for the development of advance biomaterial, to perfect the integration with the human body.

However there are concerns of the materials biocompatibility, negative tissue reaction, corrosion and wear rate, which can result in loosening of the implant due to uneven stress distribution [14].

Implant loosening can also occur due to unacceptable host reaction which may result, because of poor wear resistant since wear debris can occur at articulating joint surfaces by itself or following its degradation through corrosion. Thus wear resistance plays an important role in joint replacement implants [17].

The biomaterials listed in table 2, have been briefly discussed below, along with their limitations.

1.2.2 Stainless steel

Stainless steel was one of the initially used materials for biomedical applications [17], mainly in hip and joint replacement, it was used as the original stem in femoral head material, however its high coefficient of friction and wear debris generation against polyethylene acetabular, makes stainless steel unappealing compared to recently fabricated biomaterials [12,14] . The stainless steel most widely used in biomedical application is austenitic stainless steel AISI 316L [11,14], , L represents a low carbon content, nonetheless stress corrosion, pitting and crevice have been reported for AISI 316L implants, besides studies have shown that the Nickle content in the stainless steel causes allergic reactions, thus, new research is being led to fabricate Nickle free stainless steel [13,15] .

Furthermore, the wear resistance of austenitic stainless steel is very low and it was discarded due to high friction, in metal on metal contact in joints such as hip, in TJR's. The poor tribological properties and wear debris particle that was produced led to rapid implant loosening. This is the reason why the Cobalt-Chromium-molybdenum alloy was introduced in hip prostheses [20].

1.2.3 Pure cobalt and cobalt alloys

From a material science point of view, one of the most challenging implants are total hip replacement, usually in a hip replacement the femoral head is made of metallic alloys such as stainless steel, titanium alloys, and cobalt alloys, or ceramics such as Aluminum oxide and zirconium oxide and the acetabular cup is generally made of UHMWPE [18]. Moreover, implant loosening is one of the major factors that affect total hip replacement.

Wear and adverse tissue response are factors that contribute to implant losing which results in early stage failure of the implant.

Cobalt alloys, such as Co-Cr-Mo alloy are usually used as the femoral head due to its high strength, ductility and wear resistance. Studies show that cobalt alloys have a higher wear resistance compare to titanium alloys and stainless steel, the high wear resistance is achieved by the dispersion of carbides or via deformation induced transformation from the (γ) metastable phase to the (ε) martensitic phase [21].

Patients with metal on metal prostheses have blood with high level of Co and Cr concentration due to wear debris of the Co alloy. This can lead to hypersensitivity and inflammatory reaction. Furthermore the Co and Cr ions in the body can result in chromosome breakage and DNA damage, cell apoptosis and subsequent necrosis [16,17].

Despite the development in design, material composition and roughness, to optimize prosthesis an alternative solution is to coat the surface of the implant with a protective functional film, to improve properties such as wear, corrosion and biological reactions that lead to implant degradation [18].

1.2.4 Pure titanium and titanium alloys

Due to its high specific strength and good fatigue resistance Titanium and titanium alloys are best choices for biomedical applications. The formation of thin passive layers by means of electrochemical oxidation of titanium due to low electrical conductivity of titanium is a key characteristic for titanium to be considered biocompatible, since the oxide layer provides a high resistance to corrosion [24].

Titanium and its alloys are used in various biomedical implants which replace damaged hard tissue since the 70's. Few examples of Titanium used in biomedical applications include, pacemakers, artificial hearts, bone plates, cornea back plates, artificial hip/knee joints, screws for fracture fixation, cardiac valve prostheses, dental and orthopedic implants [24].

It is also feasible to combine a more wear and fatigue resistant alloy such as Cobalt alloys or a ceramic with Titanium alloy as a stem to reduce wear for hip joint replacement. However relative movement and fretting can occur due to inter component junctions [17]. Hardness and wear resistance play a vital role for "metal on metal" or "metal on polyethylene" hip joints for long term services.

The low modulus, excellent biocompatibility and corrosion resistance of titanium alloys makes it a better choice for orthopedic materials compared to stainless steel and cobalt alloys. Thus numerous devices are being made from titanium alloys for biomedical applications. Nevertheless, few of the limiting parameters of titanium alloys, is there poor tribological properties, low abrasive resistance and lack of mechanical stability of the oxide layer [25].

These negative factors of titanium alloys may affect the long-term success of TJR, and could be co-relate to aseptic loosening and osteolysis and may not meet all the clinical requirements. Therefore several surface modification technologies pertaining to titanium and titanium alloys are being investigated, such as, mechanical treatment, thermal spraying, chemical and electrochemical treatment, and ion implantation techniques to improve the wear resistance and hardness of the surface [19,20] .

Different methodologies have been explored to modify the surface of titanium to tackle the negative factors of titanium and its alloys. Based upon extensive literature review no study of polymer hybrid nanocomposite coating (UHMPWE reinforced with CNT and HA) on titanium and its alloys for the improvement of tribology properties has been reported hence the focus of the present study is to evaluate the feasibility of using a hybrid nanocomposite coating on titanium substrate to enhance its tribological properties. UHMWPE has been selected as the parent polymer matrix for the coating due to its exceptional biocompatibility and tribological properties, thus phase 1 of this study will be the tribological optimization of pristine UHMWPE using different loading conditions. In the second phase, CNT's are introduced into the UHMWPE matrix to enhance the load bearing capacity of UHMPWE. This nanocomposite coating will then be optimized by tribological analysis for different compositions of CNT's. The final phase of this study is to incorporate different wt% of HA and investigate its tribological performance, HA is added to improve the biocompatibility of the hybrid nanocomposite coating. The dispersion of the constituents is evaluated by Raman spectroscope and SEM images, and the coatings are further characterized by hardness and scratch tests.

1.3 Objective

The Objective of the present research is to develop a novel hybrid nanocomposite coating, Ultra high molecular weight polyethylene (UHMWPE) reinforced with multi walled carbon nanotubes (MCNT) and hydroxyapatite (HA) and modify the surface of commercially available titanium (pure titanium and Ti6Al4V) and a newly developed titanium alloy (Ti20Nb13Zr) to improve its tribological properties for use in biomedical application. Surface modification is achieved by using electrostatic spray coating technology to obtain a smooth surface overcoat on the surface of titanium and its alloys.

The performance of the coating will be evaluated by tribological characterization along with hardness, scratch test, Raman spectroscopy and scanning electron microscopy (SEM). Finally, the corrosion properties of the coating will be evaluated by electrochemical analysis.

1.4 Research Methodology

In order to achieve these objectives more efficiently, the overall project was divided into different phases and tasks. During the optimization process, only pure titanium was used as the substrate. Once the coating has been optimized it will be characterized on the titanium alloys (Ti6Al4V and Ti20Nb13Zr).

1.4.1 Phase 1 – Optimization and characterization of pristine UHMWPE

This phase is focused on optimizing the UHMWPE coating on pure titanium by manipulating various coating parameters and heat treatment.

Task 1: Optimization of coating procedure for pristine UHMWPE

Task 2: Selection of an appropriate pre-treatment for the substrate to enhance the adherence of the coating

Task 3: Tribological characterization of pristine UHMWPE

Task 4: Physical and chemical characterization of pristine UHMWPE

1.4.2 Phase 2 – Optimization and characterization of the UHMWPE nanocomposite coating reinforced with different loadings of CNT's

In this phase Carbon Nanotubes (CNT) are reinforced into the UHMWPE matrix, by sonication and mechanical mixing.

Task 1: Optimize the parameters of sonication and mechanical mixing for the reinforcement of CNT's into the polymer UHMWPE matrix

Task 2: Optimizing the wt% of CNT for better load bearing capacity

Task 3: Tribological characterization of UHMWPE reinforced with CNT's

Task 4: Material characterization of optimized UHMWPE reinforced with CNT nanocomposite coating using: Raman spectroscopy and SEM images.

1.4.3 Phase 3 – Optimization and characterization of the UHMWPE hybrid nanocomposite coating reinforced with CNT's and different loadings of HA

The final phase includes the integration of Hydroxyapatite into the optimized UHMWPE reinforced with CNT.

Task 1: The ideal parameters need to be assessed upon the addition of hydroxyapatite into the "UHMWPE reinforced with CNT" matrix, which will be achieved by sonication and mechanical mixing.

Task 2: Tribological characterization of UHMWPE hybrid nanocomposite coating reinforced with CNT's and HA

Task 3: Material characterization of optimized UHMWPE hybrid nanocomposite coating reinforced with CNT and HA using: raman spectroscopy, SEM and corrosion test.

CHAPTER 2

LITERATURE REVIEW

2.1 Surface modification

It is evident that Surface properties and biocompatibility play major roles in the response of biomaterial, Thus to enhance the performance of biomaterial in a biological system, there is a crucial need for their surface to be modified [27].

Without changing the bulk material, the surface properties of the material can be altered by surface modification. Usually, the atoms, compounds, or molecules on the surface are changed to some extent chemically, physical, or by coating a different material on the surface [28].

Surface modification can improve the substrates; Energy, adhesion, biocompatibility, corrosion resistance, and degradation and most importantly its tribological properties [27].

The three main branches of surface modification include biological, mechanical and physicochemical methods. Figure 1, shows several examples of physicochemical method of surface modification. This study focuses on overcoat and surface gradient techniques.

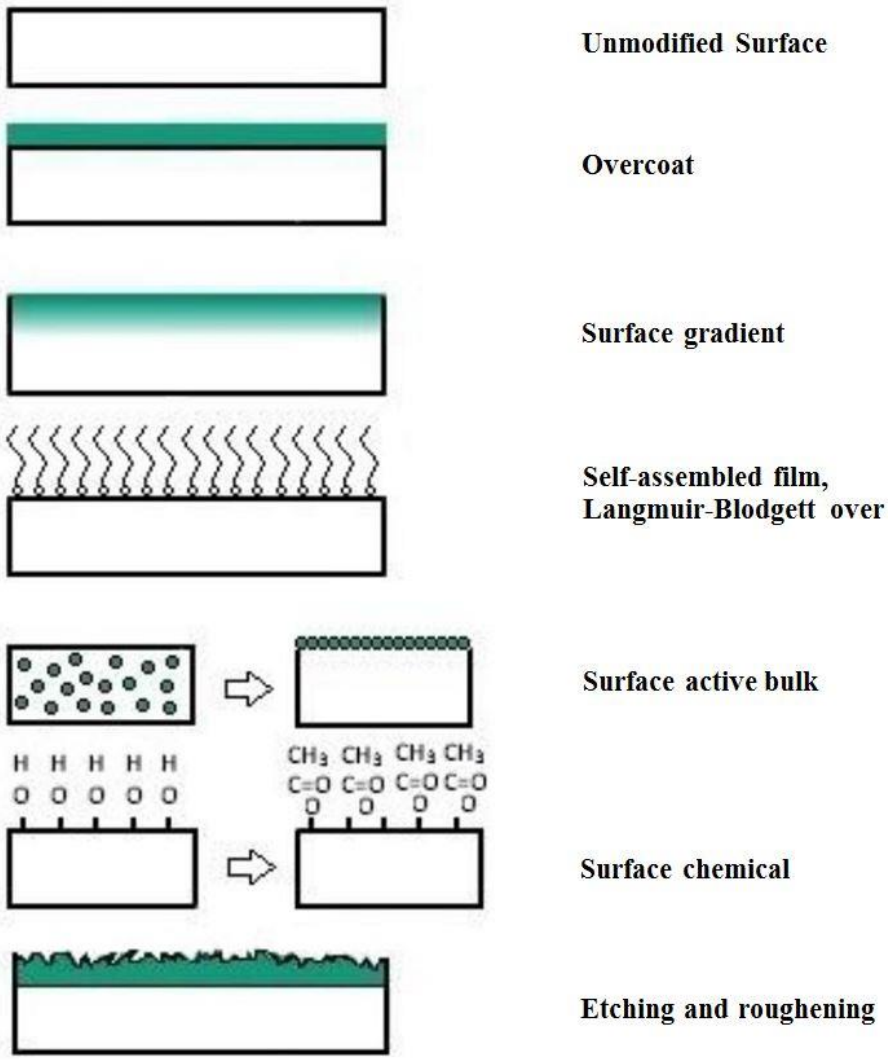

Figure 1: Schematic illustrations of methods to modify surfaces [29]

Figure 2, shows a simple flow diagram intended to show various biocompatible coatings (over coat) and surface treatments (surface gradient) performed on biomaterials. Solid arrows in the diagram indicate, the surface modification conducted on a biomaterial and tribological study performed. Whereas the dashed arrows represents only surface modification on biomaterial, since this review focuses on the tribological outcome only

the materials and techniques used for surface modification (solid arrows) are briefly explored [29].

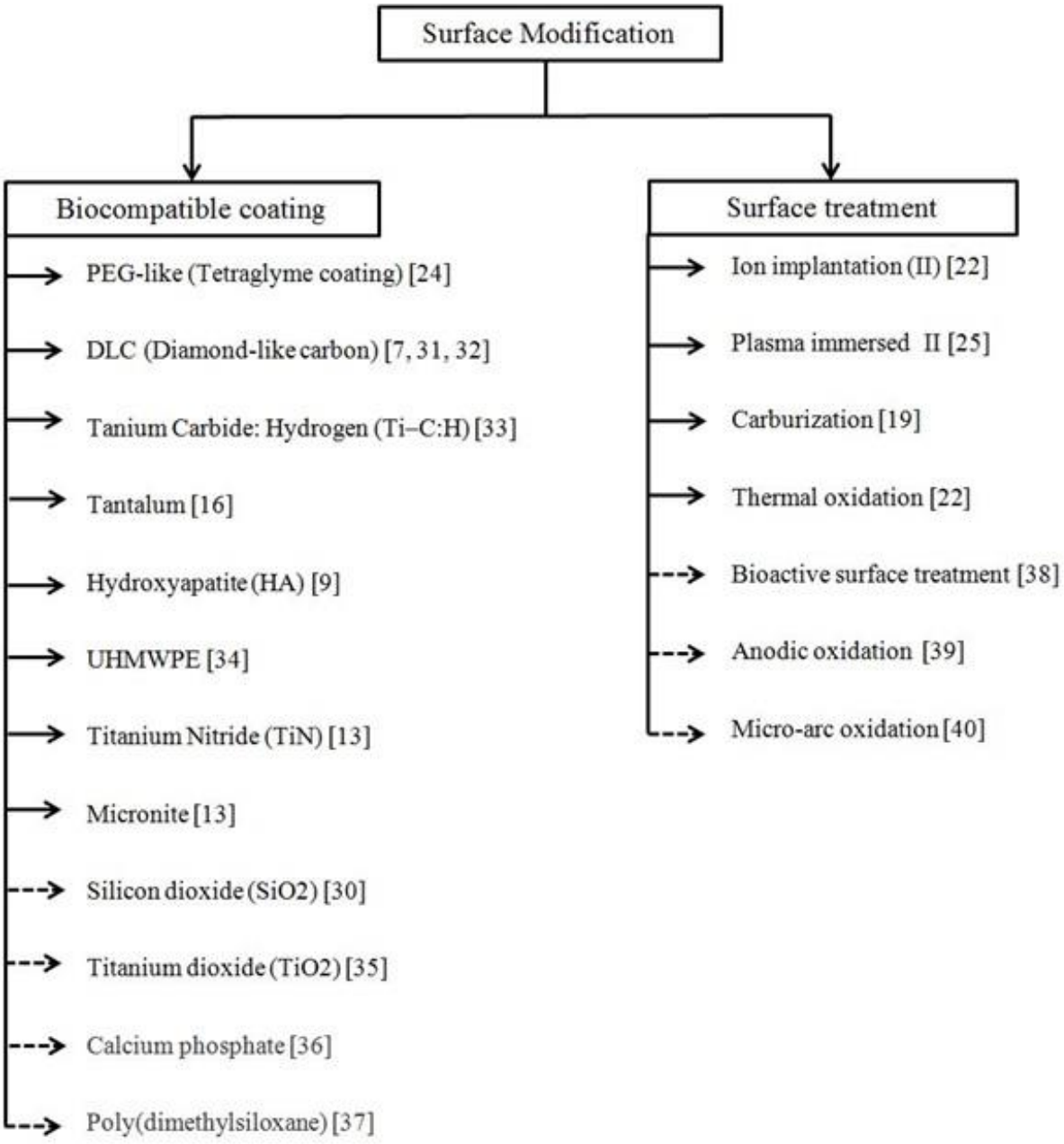

Figure 2: Flow diagram of Surface modification

2.2 Biocompatible coating materials

2.2.1 PEG-like (Tetraglyme coating)

The tetraglyme coating material, which is similar to polyethylene glycol (PEG), is a lubricous flexible linear polymer, constructed of CH_2CH_2O repeated units, It is hydrophilic and resistant to protein absorption and its biocompatibility has found many use in biomedical application. The PEG-like Tetraglyme coating is used as a conjugation to drugs in order to decrease antigenicity and the degradation of enzymes. It is also used to alleviate phagocytosis of liposomes. The chemical characterization of the coating has shown an antithrombogenic surface [30].

2.2.2 DLC and Tetrahedral amorphous carbon

Diamond like carbon (DLC) coatings has currently been a great interest in research, owing to its outstanding properties as a thin film coating. It is known to have properties similar to diamond, such as hardness, chemical inertness and elastic modulus. It also has high electrical resistivity, low friction, wear rate, transparency and good bio and hemocompatibilities[7,17] . Nowadays, commercially available implants coated with DLC are heart valves and artificial joints. DLC coatings are very resistant to abrasive and adhesive wear making it suitable for many application, for instance, In 2001, the femur portion in an artificial joint was coated with DLC coating and sold by a company [19]. Recent advances in the industrial sector using ion implantation technique for surface modification using DLC film have shown drastic improvement in corrosion and tribological properties [31]. Experiments and computer (molecular dynamic) modeling

has shown, during sliding wear the outer layer of DLC transforms to graphite, resulting in very low coefficient of friction [32].

DLC can exist in several different forms, DLC coatings can be made amorphous and flexible. tetrahedral amorphous carbon or ta-C is one of the strongest, hardest and slickest of such mixture. Thin firm of Tetrahedral amorphous carbon (ta-C) shows several interesting properties for practical application [18].

2.2.3 Ti–C:H

Similar to commercially used biomaterials such as Titanium alloys and steel, the a-C:H coating also show lower adhesion making them useful for biomedical applications [33]. They possess excellent corrosion and wear resistance properties and exhibit low friction characteristics under appropriate conditions [34].

When CH_4 is used as a reactive gas, an (a-C:H) layer will be formed due to the increase in carbon content owing to the excess of reactive $C:H_x$ species created in the discharge. Using different carbon content to fabricate metal-C:H films is now widely being used [35].

However the interlayer generally used for a-C:H coatings are Tungsten carbide or chromium, these materials are not biocompatible, thus making their use in questionable [33].

2.2.4 Tantalum

Tantalum metal has gained the attention of researches in recent years due to their excellent biocompatibility, corrosion resistance, MRI compatibility, high radiopacity and

histocompatibility, as well as bioactive and biologically bonds to bone [36]. Which arose their interest firstly in the bulk form, such as plates and suture wires, and then porous structure, finally tantalum or tantalum oxide films [5,45] .

Currently scaffolds for bone replacement and acetabular caps are made of 99% pure tantalum. It has shown outstanding scaffolds for bone ingrowth and mechanical attachment in vitro [2,50]. Porous Ta components offer a low modulus of elasticity, high surface frictional characteristics and excellent osseointegration properties [38].

Ta coatings exhibit excellent cellular adhesion. This is attributed to the wettability characteristic of its structure. Ta surface has lower contact angles and higher surface energy and is therefore able to improve cell–material interaction [5]. Furthermore Tantalum films could be used for cardiac and vascular devices thanks to its hemocompatible properties [37].

2.2.5 CNT-reinforced HA

Hydroxyapatite ($Ca_{10}(PO_4)_6(OH)_2$, HA) is a naturally occurring mineral form of calcium apatite that has the ability to bond directly to the natural bone, due to the similar mineral constituents of natural bone and teeth. Therefore it is widely used in variety of biomedical applications in dentistry and orthopedics [39]. HA are commonly used to coat titanium implants, to reduces the release of metallic ions by acting as a barrier, additionally it enhance the bone bioactivity [40]. Nevertheless, HA coatings have poor load bearing capacity attributed to its brittle nature and poor strength [41], which prevents its use in certain applications. The fracture toughness and load bearing capacity can be

increased by adding a secondary element to HA such as carbon nano tubes (CNT's), alumina (Al2O3), Yttria-stabilized zirconia (YSZ) or Titanium alloys [42].

Carbon nanotubes (CNT's), are cylinders of graphite sheets which exists in the form of single-walled (SW) or multi-walled (MW), they possess brilliant mechanical properties and exceptional chemical stability. Thus introducing CNT's into a material will enhance the materials mechanical properties [43]. The addition of CNT's onto HA, enhances the tribological properties by connecting the splats in a bridged manner. Substantial research is being conducted to use HA as a coating for biomaterials for implants [14]. Therefore, hydroxyapatite composite coatings reinforced with CNTs have exceptional properties including high strength and good bioactivity [41].

2.2.6 UHMWPE

Due to their ease in fabrication, impact loading performance and low price, polymer coatings have caught the interests of researchers. Ultra-high molecular weight polyethylene (UHMWPE) is a linear homopolymer with a simple composition of only hydrogen and carbon that is produced by the polymerization of ethylene (C2H4) gas. The molecular weight number is greater than 2 million plus a sungle molecular chain can consist of as many as 200, 000 ethylene repeated units [44].

UHMWPE is a unique polymer that has the highest abrasion resistance and highest notched impact strength compared to any commercial plastic. Moreover UHMWPE exhibit excellent tribological properties. Studies have shown, that, a thin film of UHMWPE has significantly increased the wear resistance and decreased the coefficient of friction when coated on Silicon, steel and aluminum substrates [32,34, 52-54] .

2.2.7 Titanium Nitride and Micronite

Titanium nitride is a gold color coating commonly coated by physical vapor deposition (PVD) or chemical vapor deposition (CVD) [48].

(TiN) coatings improve corrosion, thermal and tribological properties of the coated substrate. Its good mechanical, anticorrosive and biocompatible properties make it feasible to be used in biomedical application [49]. TiN coating are also used in the field of dental implants, TiN-coated dental implants show higher physico-mechanical properties [50]

Micronite is a specially treated TiN coating with a considerably lower coefficient of friction and wear. It is prepared by depositing a high molecular material onto a specially treated PVD coated Titanium nitride [19].

2.2.8 Coating techniques

There is several coating methods that can be used to modify the surface of the substrate by overcoat, few of the conventional methods are listed below:

- Dip coating
- Spin coating
- Electrostatic spray coating
- Wire spray
- High velocity oxyfuel and plasma spray
- Pulsed laser deposition
- Electrostatic fluidized bed.

Electrostatic spray coating technique will be elaborated since that is the method we will be implementing in this study due to its numerous advantages.

The Electrospraying method is a process by means of which liquid or solid particles are transformed into a fine mist. This transformation occurs due to the application of a high voltage electric field to the capillary nozzle. The generated electric charge on the droplet contends with the surface tension of the droplet, which results in a breakdown, to micro or nano droplets. [51] .A controlled and defined surface topography can be achieved by electrospraying deposition method [52]. Figure 3 shows a schematic of the apparatus for electrospraying.

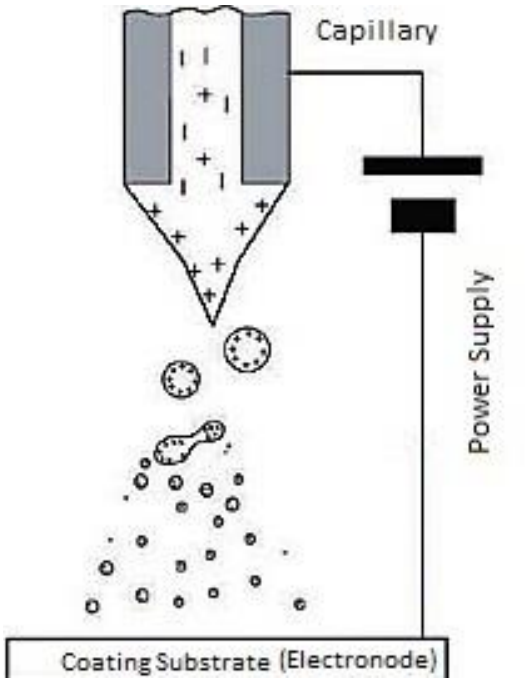

Figure 3: Electro static spray coating

Several solutions of bio-macromolecules and synthetic polymers can be deposited in the form of nano-sized particles or nano-fiber using the Electrospraying technique. Adhesion to the coating substrate occurs with the aid of electrostatic force.

When the sample stored in the capillary is supplied with a very high voltage relative to the counter electrode. Due to the effect of electric field concentration, a strong electric field is generated at the end of the capillary.

A conical shape with the electrically charged ions gathered on its surface begins to form as the liquid begins to exit the capillary a phenomenon known as Tylor cone. Consequently, when the electrostatic force exceeds the surface tension the liquid begins to erupt from the tip of the capillary to form a fine jet. As a result of the highly charged jet, the liquid instantly turns into fine droplets , with the aid of electrostatic force spray is generated with each droplet split from the next (This phenomenon is knows as Coulomb Explosion) [51].

Tiny droplets are formed by means of electrospray. Thus the solvent immediately evaporates and tries within in a few seconds, which results in formation of fine nano particles. These charged nano particles are attracted to the substrate (electronode) by electro static force. They can be deposited in numerous patterns [51].

Some of the advantages of electro static spray coating method are listed below:

- Low investment costs
- High availability
- High temperature operation not required
- Particles instantly dry during the process, further drying stems not required.

- The distribution and pattern of the particles can be easily controlled, by electrostatic force.
- Conducted in room temperature and pressure.

Provided these advantages of electrostatic spray coating technique and cross referring the latest literature reviewed in the beginning of this chapter, we realize there is a gap in the field of biocompatible coatings using the electrostatic spray coating technique, furthermore there has not been any study conducted on UHMWPE reinforced with CNT and HA as an overcoat on biomaterial to enhance tribological properties. Therefore this study aims to fill that gap in the literature and study of biocompatible coatings.

2.3 Surface treatment techniques

2.3.1 Ion implantation

Amongst several methods of surface treatment, ion implantation offers distinctive advantages, making this technique suitable for medical applications [53].

Ion implantation is a kinetic doping process in which acceleration ions are focused to the surface of the target material. Ions impinge the surface, penetrating the surface layer due to high initial energy usually in the range of 20 – 200 KeV [54], it is a low temperature process (almost room temperature) preventing change to the initial properties of the bulk material. Additionally, any kind of dopant can be introduced into any solid material. Ion implantation can also be used as a method of energy transfer into surface layer of materials [53].

Main disadvantages of the technique are high cost and low penetration depth. However, for the purpose of biomedical application these downsides are no critical since implants are usually expensive [53].

2.3.2 Plasma immersed ion implantation

Recent developed Plasma immersed ion implantation (PII) has been showing progressive potential for its adaptable process of plasma modification, ion implantation and non-line-of sight process which makes it suitable for biomedical applications [55]. In PII, the material is immersed in a plasma and ions are introduced to the entire surface at the same time, providing a faster and more cost-effective treatment accordingly [56]. Furthermore Thermal deformation of the material is minimized since it is a low temperature treatment process [57].

2.3.3 Carburization

Carburization can offer great combination of mechanical properties, thus it is one of the most extensively used surface hardening technique for metals such as steel. During the carburizing process, generally low carbon-steel of approximately 0.10 to 0.25% Carbon is heated at high temperature, in the presence of a carbon rich medium, the heating process usually occurs at a temperature range of 900 to 1100 ^{o}C Carbon atoms tend to diffuse in the surface of iron (FCC structure) at a temperature of 910^{o}C [58]. A carbon-enriched layer is produced on the surface, the depth of the layer can be manipulated by controlling the holding time. Finally the iron surface will have a carburized layer, this layer can be hardened by quenching directly from the carburizing temperature or by reheating and quenching [59].

Depending on the nature and choice of the work different carburizing medium can be used such as, Solid liquid or gaseous. The purpose of the carburizing medium is to discharge carbon atoms at the surface of the substrate at the carburizing temperature so that they will be absorbed interstitially into the metal surface [59].

2.3.4 Thermal Oxidation (TO)

Surface characteristics of metals such as Titanium and its alloys can be improved by using thermal oxidation treatment. Development of a crystalline oxide film is promoted by oxidation usually at a temperature over 200 ^{o}C. A thick oxide layer is formed due to high temperature, which is accompanied with oxygen beneath it [60].

Scaling or surface hardening can be prevented while effectively hardening Ti alloys by thermal oxidation process. In fact the benefits by thermal oxidation process can be ascribed to both the formation of a thin oxide layer and an oxygen diffusion zone [61].

2.4 Literature results

The main objective of coatings and surface treatments in biomedical applications such as Hip or knee replacement is to ensure bio-tolerance and to enhance the biomaterials ability to withstand high cyclic loading, with or without body fluids. Furthermore the wear rate and friction coefficient can be alleviated by an appropriate coating or surface treatment technique [5].

A detailed literature review on various coating material and surface treatment techniques carried out on various biomaterial and there results on their tribological outcome, mainly with respect to friction and wear has been reviewed.

2.4.1 Tribology characteristics for coating materials

Kane, R.S., et al [24] coated, clean Ultra-high molecular weight polyethylene (UHMWPE) with tetraglyme with the aid of a plasma science parallel plate reactor. The UHMWPE surface was activated using a high power argon treatment to endorse covalent bonding of the coating. Furthermore the tetraglyme coating was plasma polarized onto the surface, different range of coating thickness was achieved by manipulating the time.

Reciprocating Wear test for the coating was led using a pin-on-disk tribotester. UHMWPE pins were tested against CoCr disks simulating the hip or knee, therefore a contact pressure of 3 and 21 MPa was used, along with a sliding distance of 2500 and 500m, respectively. After the wear tests the coating survival were determined by rinsing the UHMWPE pins in deionized water and inspecting by ATR-FTIR. The wear resulted are shows in table 3.

Table 3: Wear results [24]

Coating thickness (nm)	Pressure (Mpa)	Sliding Distance (m)	Condition	No. of Pins	Result
>140	21	500	knee	5	All pins coating Entirely wore off
>200	3	2500	Hip	4	1 pin coating wore off entirely

Manhabosco, T. M., & Muller, I, L., [7] coated pure titanium with two types of DLC coating. DLC from acetonitrile and N,N-dimethyl Formamide (DMF). Ball on plate, reciprocating configuration was used for the wear test. There wear track were examined using a surface profilometer. On each wear track six profile measurements were taken and knowing the track length the wear volume was estimated. It was concluded that, DLC obtained from acetonitrile had similar wear volume when compared to the wear volume

of pure titanium. Whereas in the case of DLC obtained from DMF the wear volume was decreased by a factor of 20 indicating super wear resistance. Furthermore, it was seen that the coefficient of friction was almost similar for both coating, about 0.1.

Loir, A. S., et al., [18] deposited tetrahedral-amorphous carbon films (ta-C) onto stainless steel (AISI 316L) and evaluated the tribological results, using UHMWPE as the counterface. Wear rate and friction tests were conducted in room temperature with a contact pressure of 500MPa and 50,000 cycles using a pin-on flat disk configuration. The parameters used for testing was severe compared to a natural hip joint contact; however the duration for testing was low. The wear coefficient for the DLC films were in the range of 10^{-8} – 10^{-9} mm^3 $(Nm)^{-1}$ and Friction results indicated, the film deposited on stainless steel displayed an average coefficient of friction in the range of 0.1-0.2. However, when the test was conducted using ringer solution as a lubricant the coefficient of friction dropped to a range of 0.04-0.05. Suggesting the feasibility of using tetrahedral-amorphous carbon films (ta-C) as a coating material for stainless steel.

Vitu, T., et al., [33] coated 10 samples of Titanium alloy, with Ti-C:H coating varying the titanium and carbon content. Identical conditions were used for all tribological measurements using a pin-on-disk configuration. The coatings wear rates were performed by evaluating the wear track profile and optical microscopy was used to measure the spherical wear cap of the balls.

It took 300 cycles to reach the maximum coefficient of friction during the running in period and 1500 cycles to reach the steady state value. It was noticed that increasing the C:H value the local friction's maximum value was drastically decreasing. The highest

C_2H_2 flow displayed the best frictional and wear properties. Therefore, the sample that showed the least coefficient had a C_2H_2 flow of 40 sccm and a chemical composition of 33 at % Ti and 67 at % C. Figure 4 shows the graph of the ball wear rate Vs. C2H2 Flow rate.

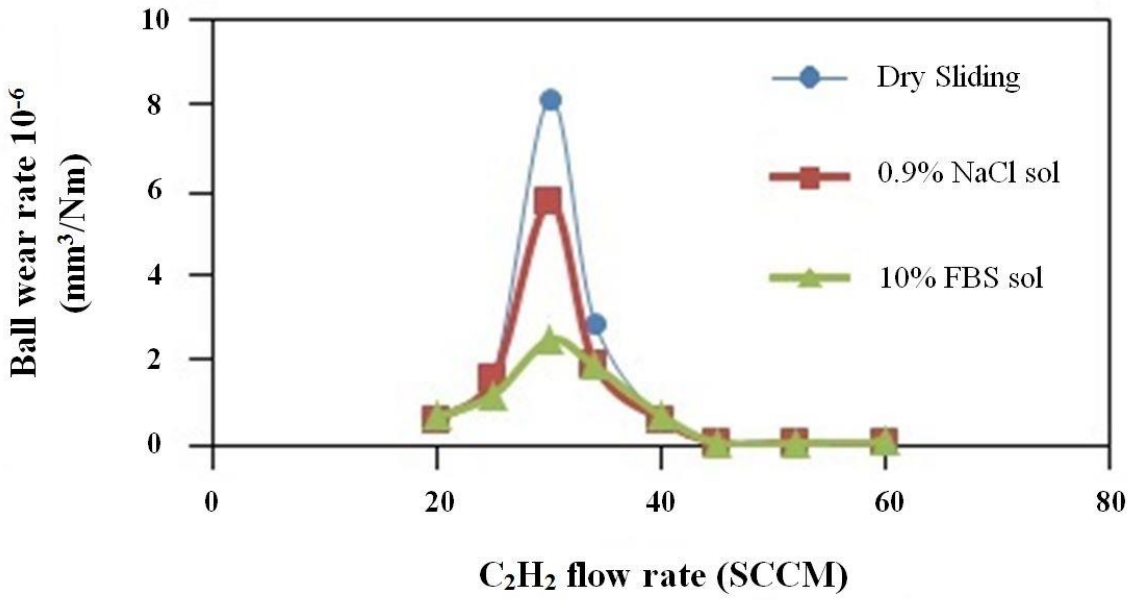

Figure 4: Wear rate of steel ball against varied Ti-C:H coatings [33]

Balagna, C., Faga, M. G., & Spriano, S., [22] coated, high carbon cobalt–chromium–molybdenum alloy with tantalum based coating. Wear and friction coefficient studies were evaluated with three different coupling corresponding to a typical arthroprosthesis. The testing configurations used were Metal on polymer (MoP), Metal on metal (MoM), Ceramic on Metal (CoM). Friction and wear results were assessed by a pin/ball on a rotating disk, with a fixed velocity of 10 cm/s. Table 4 shows the coupling and materials used for different configurations along with several testing parameters and wear outcomes.

Table 4: Coupling and materials used [22]

Test	Couple	Material		Load (N)	Laps	Sliding distance (m)	Track depth (µm)	Track volume (mm^3)	Wear rate (mm^3/Nm)
Pin on disk	MoP	Polythelene pin	Untreated disc Disk 970 Disk 990	7	10,000	251	-	-	-
	MoM	Pin Pin 970	Untreated disk Disc 970	10	1 million	43,960	2.5 ± 0.5 5 ± 1	0.1 ± 0.03 0.2 ± 0.1	$(2 \pm 1) \times 10^{-7}$ $(4 \pm 2) \times 10^{-7}$
Ball on disk	CoM	Alumina ball	Untreated disc Disc 970 Disc 990	7	25.000	1099	3.0 ± 0.3 0.7 ± 0.005 0.7 ± 0.001	$(2 \pm 0.5) \times 10^{-2}$ $(3 \pm 0.3) \times 10^{-3}$ $(4 \pm 0.3) \times 10^{-3}$	$(3 \pm 1) \times 10^{-6}$ $(4 \pm 0.4) \times 10^{-7}$ $(5 \pm 0.3) \times 10^{-7}$
			Untreated Disc Disc 970 Pre-treated Disc 970	10	1 million	18.840	89 ± 3 33 ± 1 78 ± 2	2 ± 0.05 $(2 \pm 1) \times 10^{-7}$ 1 ± 0.04	$(9 \pm 0.3) \times 10^{-6}$ $(2 \pm 0.1) \times 10^{-6}$ $(7 \pm 0.2) \times 10^{-6}$

For the MoP contact, the material used for the pin was a reticulate polythenene whereas for the disk, three different disks were evaluated. (1) Untreated, (2) treated at 970 ^{o}C and (3) treated at 990^{o}C. the friction coefficient after averaging the results were 0.11 ± 0.008 for the untreated disk, 0.08 ± 0.003 for the treated disk at 970 ^{o}C and 0.09 ± 0.003 for the treated disk at 990^{o}C. it was concluded that surface treating the metal counterpart could be useful.

For the MoM contact, for the untreated surface the friction coefficient was about 0.35± 0.02 and for the surface treated at 970 ^{o}C the friction coefficient was 0.25 ± 0.011. and finally for the CoM couple, the untreated surface showed a coefficient of friction of 0.19 ± 0.011 and the 970^{o}C treated couple showed a coefficient of friction of about 0.14 ± 0.006 and 0.16 ± 0.015 for treated metal. It was concluded that the coating material was very effective in reducing the coefficient of friction.

Balani, k., et al., [9] coated Ti6Al4V with Hydroxyapatite (HA) reinforced with CNT. A wear rate of 90.23 gm^{-2} per 10, 000 revolutions was observed for the bare substrate, the wear rate dropped to 60.15 gm^{-2} and 38.92 gm^{-2} for the same number of revolutions for the HA coating and the HA-CNT coating respectively. After 100 min of wear test the total weight loss was estimated, the bare substrate had a weight loss of 0.0051 g, HA coating 0.0034g and HA-CNT coating 0.0022g. The CNT reinforced in HA act as bridges connecting splats, which is attributed to the excellent wear resistance of the HA-CNT coating.

Panjwani, B., Satyanarayana, N., Sinha, S. K., [45] coated Ti6Al4V sample with UHMWPE and an additional lubricant layer of PFPE and evaluated the tribological

properties using a silicon nitride (Si3N4) ball as a counterface, on a ball on disk tribometer. Bare Ti6Al4V Vs Ti6Al4V coated with UHMWPE was compared. The test parameters used for the COF study was, a normal load of 4N and a spindle speed of 400 rpm, the bare Ti6Al4V showed a very high coefficient of friction of approximately between 0.5-0.6, this is attributed to adhesive wear due to elevated surface energy and formation of unstable titanium oxide film. After the UHMWPE coating, the coefficient of friction dropped to about 0.05.

Using the same normal load and a speed of 1000 rpm the wear life and COF were evaluated with and without the PFPE layer, it was noticed that absent the PFPE layer the COF of the Ti6Al4V with UHMWPE started to increase from 0.1 after about 20,000 cycles and had a wear life of 28,000 ± 8000 cycles whereas in case of the PFPE as a top lubricant layer the coefficient of friction started to increase from 0.1 after 50, 000 cycles and the wear life was improved to 60,000 ± 14,000 cycles., figure 5, shows the wear life at 1000 RPM.

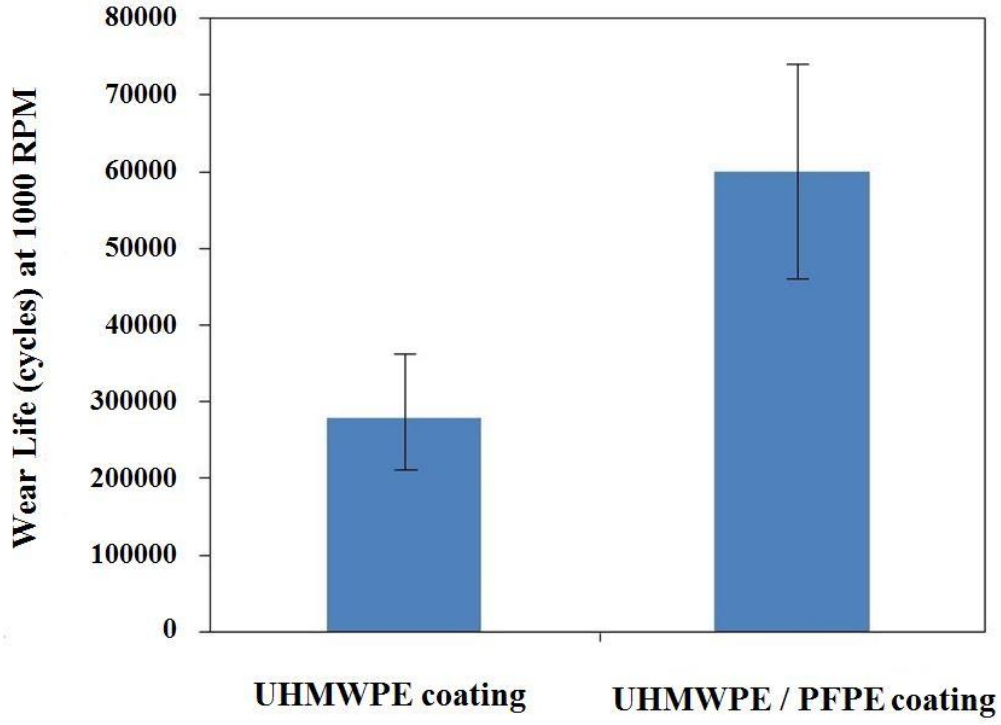

Figure 5: Wear life cycles at 1000 RPM [45]

Hoseini, M., et al., [13] coated Stainless steel (316L) with Titanium Nitride and Micronite, and evaluated the tribological properties by sliding it against UHMWPE pins using a pin-on disk configuration. A linear regression model was used to assess the specific wear, data was taken from the steady state period during sliding from 10Km to 18Km. The coefficient of friction (COF, μ) was calculated by dividing the applied force of 63 N by the mean friction force. The specific wear and the COF were defined by their mean values and standard deviation. Student's t-test (significant level $p = 0.05$) was used to evaluate the statistical differences.

The PVD coating technique altered the surface topography of the substrate increasing its surface roughness after the coating. Since the surface coating procedure altered the surface roughness two stages were used in performing the experiment. In Stage 1, the

tribological experiments were performed on surfaces having the same surface roughness on the substrate before the coating. In Stage 2, tribological experiments were performed on surfaces having similar roughnesses after the coating. Table 5 shows the change in surface roughness, Figure 6a shows the change in specific wear and figure 6b shows the change in coefficient of friction before and after the coating. The results indicated that the enhanced tribological behavior of the Micronite/UHMWPE sliding pair might be used as a material combination in artificial joints

Table 5: Change in surface roughness, per & post coating [13]

	Before coating			After coating		
	Ra (µm)	COF (µ)	Spec. wear (µm)	Ra (µm)	COF (µ)	Spec. wear (µm)
316L	0.025	0.088	1.39	0.104	0.158	21.15
Ti N	0.052	0.139	3.11	0.169	0.115	5.44
Micronite	0.228	0.140	4.12	0.176	0.104	4.14

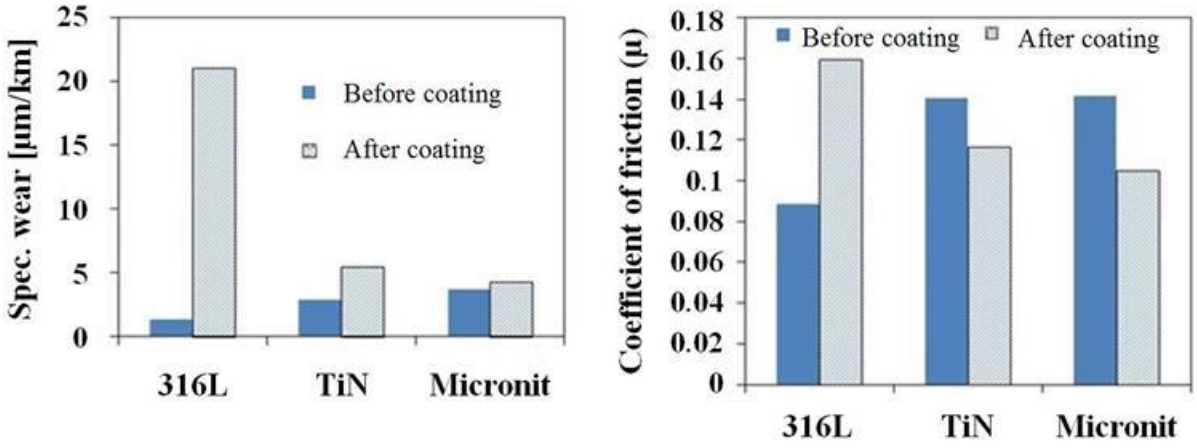

Figure 6a: Specific wear, pre & post coating and Figure 6b: Coefficient of Friction, pre & post coating [13]

2.4.2 Tribology characteristics for surface treated materials

Xiong, D., Gao, Z., & Jin., Z.., [62] studied the friction and wear behavior of UHMWPE sliding against ion implanted Titanium alloy. The friction and wear properties were assessed by using a pin-on-disk machine using distilled water as a lubricant. Table 6 and Figure 7 present's the wear factors of UHMWPE sliding against ion implanted and unplanted Ti6Al4v counterface. From the chart it is clear that un-implanted Ti64 has a very high wear rate almost 40 times greater than the ion-implanted surface

Table 6: Wear rate of ion implanted and un-implanted Titanium alloy [62]

#	Substrate	Wear rate 10^{-6} (mm^3/Nm)
-	Un-implanted	23
#1	$1X10^{18}$ O^+/ cm^2, 100^{oC}	0.52
#2	$5X10^{18}$ O^+/ cm^2, 100^{oC}	0.58
#3	$1X10^{18}$ O^+/ cm^2, 300^{oC}	0.56
#4	$5X10^{18}$ O^+/ cm^2, 300^{oC}	0.48

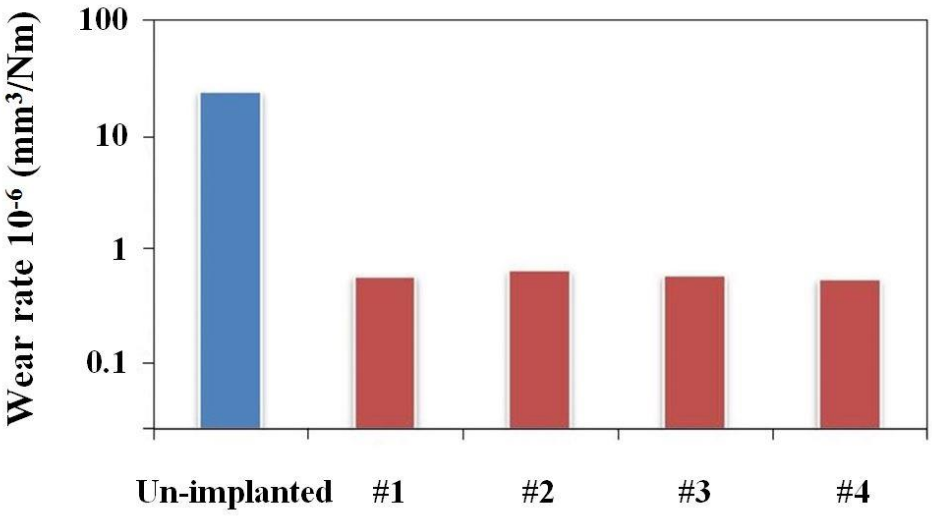

Figure 7: Wear rate of Ion Implanted and un-implanted Titanium alloy bar chart [62]

Figure 8 shows the friction coefficient of the UHMWPE and Ti6Al4V couple. From the graph it is seen that when the test was initiated the friction coefficient was very high for all the cases, and then rapidly drops and stabilizes with sliding distance. The mean value of the four ion-implanted surfaces has been plotted along with the un-implanted surface.

All the ion implanted Ti6Al4V cases the coefficient of friction drops from 0.2 to 0.04, this is attributed to the formation of Titanium-oxide and Titanium nitride (TiO-TiN) layer on Ti6Al4V alloy. Furthermore, the friction coefficient alleviated almost 5 times under water lubrication.

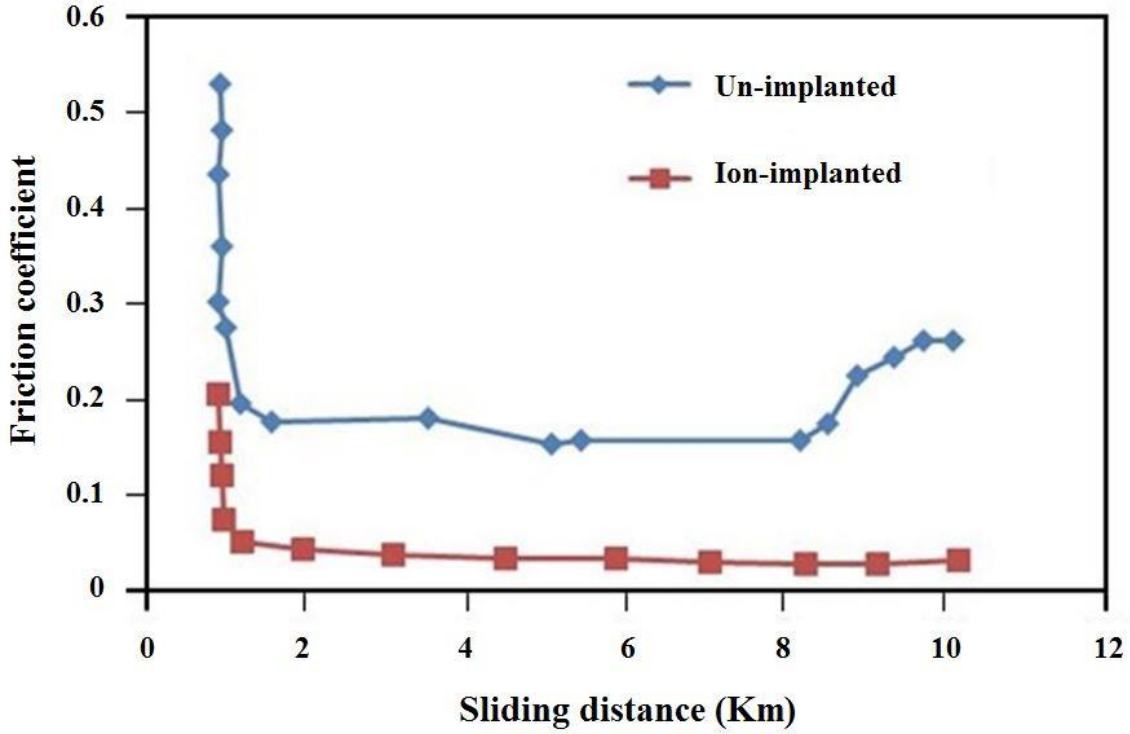

Figure 8: Friction coefficient of UHMWPE and Ti6Al4V couple [62]

Wen, S., & Han-shan, D.,[63] studied the tribological properties of nitrogen ion implanted UHMWPE sliding against thermal oxidized (TO) Ti6Al4V using a pin-on disk tribometer. Ti6Al4V was used as a disk and was set to a constant sliding speed of 0.25 m/s, the normal contact pressure was 5 Mpa, the coefficient of friction results obtained for untreated UHMWPE and untreated Ti6Al4V was about 0.150 whereas in case of the Nitrogen ion implanted UHMWPE and Thermal oxidized Ti6Al4V the coefficient of friction dropped from 0.150 to 0.025. Figure 9 shows the wear factor for three cases 1) Ion implanted UHMWPE/TO treated, 2) untreated UHMWPF/ TO treated Ti6A14V, 3) Ti6AI4V untreated UHMWPE/untreated Ti6AI4V.

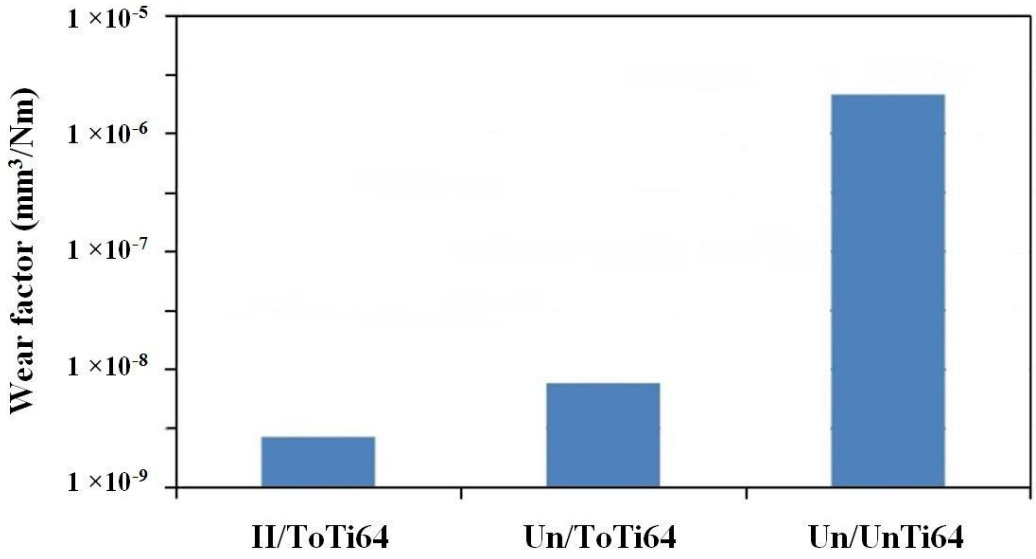

Figure 9: Wear factor for three cases [63]

Tai, Z., et al., [64] modified UHMWPE surface, by reinforcing different wt% of graphene oxide and evaluated there tribological performance. There was increase in COF as the percentage of GO was increased. However, there was a great reduction in the wear rate of UHMWPE (see figure 10), owing to the fact that graphene oxide acts as nano filler.

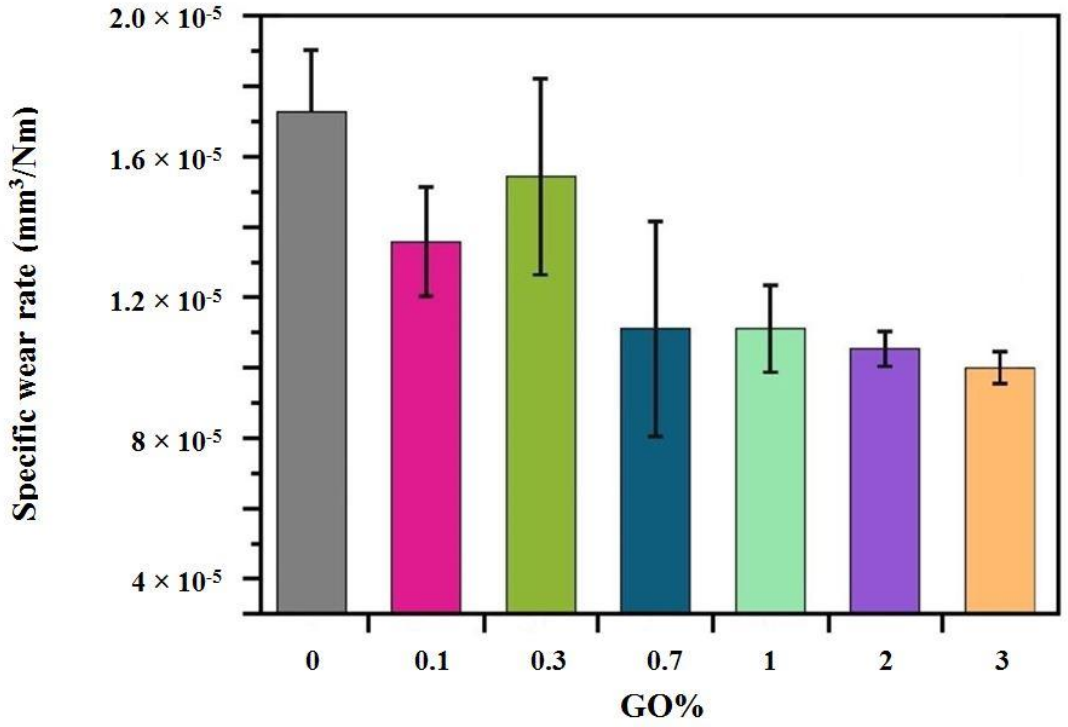

Figure 10: Wear rate Vs Go% [64]

Luo. Y., et al., [19] modified the surface properties of titanium alloy by nitrogen ion implantation and carburization, and assessed the tribological behavior of the substrate. A ball-on flat test was performed in bovium serum lubrication under dry friction condition on a universal multi-functional tester. After the wear test, in order to investigate the mechanism of the worn surface, SEM was used with an energy disperse spectrum and the wear debris distribution were analyzed by a laser granularity analyzer. Figure 11 shows the volumetric wear rate of the nitrogen implanted and carburized Ti64, it is evident that the wear rate significantly drops from 6.28x10-4 to 2.87x10-4 and 1.80x10-4 mm3/Nm for the nitrogen ion implanted sample and the carburization sample respectively indicating a highly wear resistant surface.

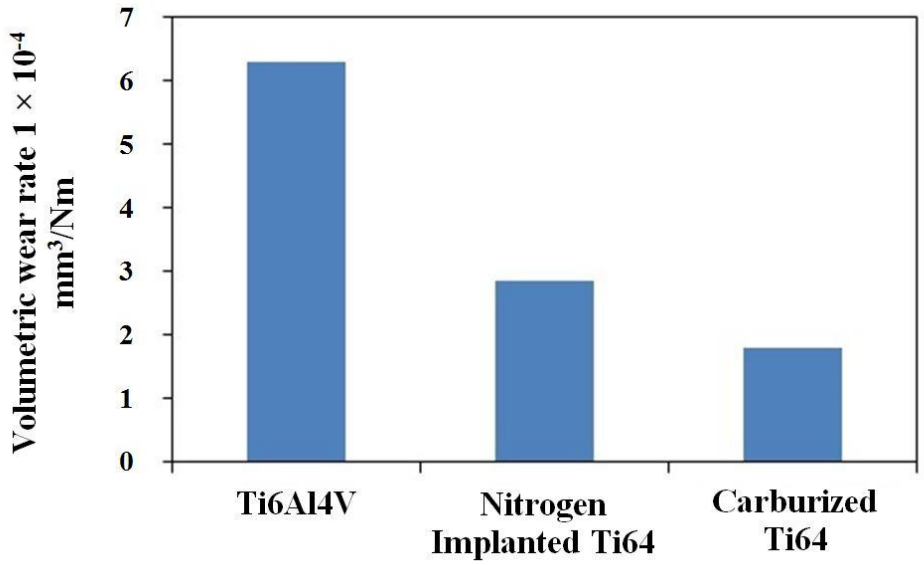

Figure 11: Volumetric wear rate surface treated Ti64 [19]

Diaz, C., et.al., [54]- evaluated the tribological outcome of surface modified titanium and cobalt alloy by ion implantation and plasma immersed ion implantation. Friction and wear were evaluated, on a pin/ball on disk machine, with the samples immersed in Hank's solution to mimic the human body fluid. The study concluded that, there was no major effect in friction coefficient when the sample was tested in hanks solution; the coefficient of friction for the treated Titanium and cobalt alloys was similar to their reference value. The wear coefficient for the two ion implanted material with varying temperature is tabulated in table 7.

Table 7: Wear coefficient of Ion implanted material [54]

Materials	Implanted ion	Temperature (^oC)	Wear coefficient ($x10^{-15}$)
Ti_6Al_4V	Reference	-	229.7
	N2	80	244.1
	O2	700	9.7
	O2	580	137.6
	O2	400	268.6
Co28Cr6Mo	O2	480	4.9
	O2	400	4.3

Spriano, s., et al., [65] modified the surface of pure cobalt and cobalt micro-melt alloy producing significant tantalum enrichment by thermal treatment in molten salt. And evaluated there tribological behavior. Friction coefficient was determined by using a pin on disk and a ball on disk configuration. The same material was used in case of the pin and disk tests. However, in case of the ball on disk configuration Alumina (Al_2O_3) balls were used for all tests. The sliding rate of the disk was set to a constant speed of 10 cm/s and a load in the range of 0.7 – 4.8 MPa was applied. Dilute bovine serum was used as a lubricant, and the tests were conducted at 37^oC (similar to the body temperature). The results obtained from the tests are tabulated in table 8

It was concluded that modifying the layers displayed low coefficient of friction on itself as well as on the alumina ball and a significant scratch and wear resistance.

Table 8: Abrasive wear rate and Coefficient of Friction [65]

Material	Load (N)	Track depth (µm)	Track volume (μm^3)	Abrasive wear rate (mm^3/Nm) $x10^{-4}$	COF
Alloy-60-1000	5	0.99	0.49	1.249	0.19
Alloy-60-1000	7	0.94	0.41	0.755	0.18
Co-60-800	5	1.74	0.84	2.129	0.18
Co-60-800	7	4.15	3.57	6.489	0.19
Co-120-800	5	1.9	0.94	2..385	0.19
Co-120-800	7	4.6	4.58	8.336	0.19
Untreated alloy	5	2.8	1.58	4.034	0.23
Untreated alloy	7	5.99	3.14	5.723	0.22

Kose ki et al.,[31] used carbon ion implantation (CII) and diamond-like carbon (DLC) film by Plasma source ion implantation to modify the surface of Wrought Co–Cr– Mo alloy, and studied the friction and wear behavior of the surface treated alloy. A pin on plate configuration was used for the study. The pin had a diameter of 6mm with a length of 20 mm.5000 running cycles were used for the test. The tests were conducted using two different lubricating conditions. For the first case pure water was used as a lubricant and for the second case bovine serum was used. All three samples displayed a lower coefficient of friction in the serum lubricant compare to pure water. Figure 12 shows the wear rate of the plates; from the bar chart it is clear that carbon ion implanted plate has the lowest wear rate.

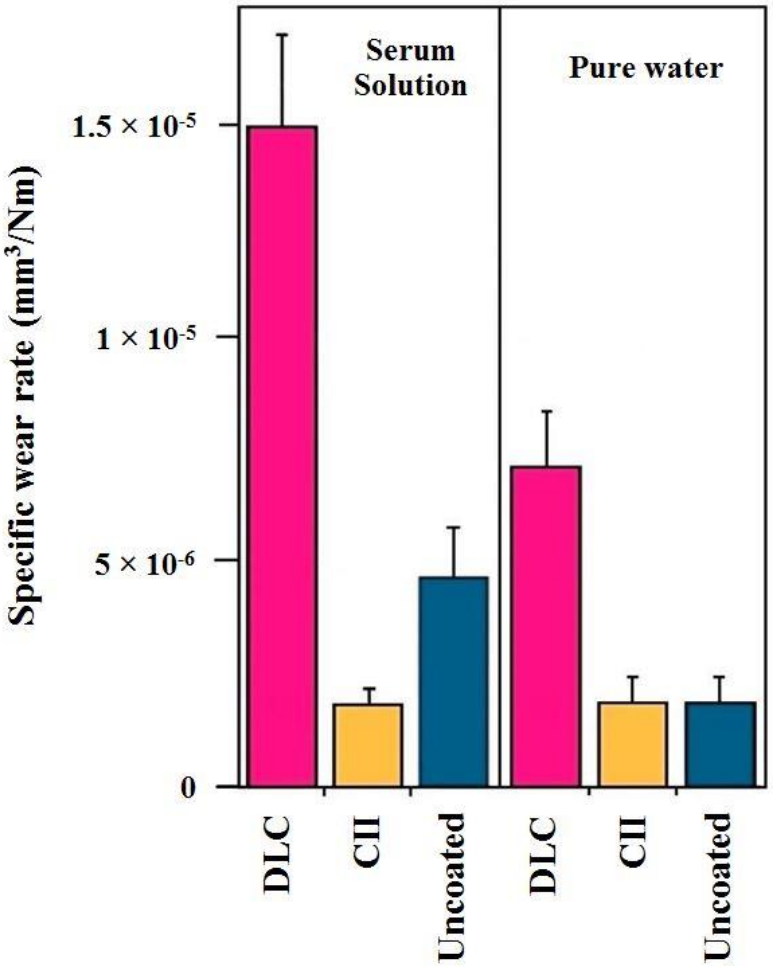

Figure 12: Wear rate of the plates [31]

2.4.3 Wear outcome (for coating materials)

Ref	Coating Substrate	Coating	Coating technique	Test parameters	wear test results
[30]	UHMWPE	Tetraglyme polyethylene glycol) (PEG)-Like coating	Parallel plate reactor Frequency:13.56 MHz, Power:550 W RF Generator Temp: 508^{o}C High-power argon treatment: (400 W, 250 sccm, 3 min) Tetraglyme was plasma polymerized onto the surface. 50 W, 30 sccm argon, with 6 mL/h tetraglyme flow through a 130^{o}C heated tube, for 20–40 min to generate a range of coating thicknesses.	Custom -built pin-on-disk tribometer UHMWPE pins: Diameter: 2 mm RMS roughness 0.030 µm CoCr disk, Ra 0.027, Speed: 36 mm/sec, room temperature, Lubricant: bovine calf serum Contact pressure: (3 or 21 MPa) Sliding distance: (2500 or 500 m)	For 21 MPa and 5pins > 140 nm thick coating coating wore off completely in all pins For 3 MPa and 4pins > 200nm thick coating Coating was present in 3pins Coating wore off completely in 1 pin
[7]	Pure titanium (Grade 1)	DLC from acetonitrile DLC from DMF	Electrodeposition Potential 0 to 1200 V Time 4 h Temp 25 C.	Ball-on-plate 5 mm diameter alumina ball Applied force of 2N Velocity 2mm/s Linear wear track of 2 mm.	Wear volume for DLC from acetonitrile = wear volume for pure titanium, about 3 x 10E-9 Wear volume for DLC from DMF 20 x less COF: 0.1
[18]	Stainless steel AISI 316L	Tetrahedral amorphous carbon (ta-C)	femtosecond Pulsed Laser deposition	Pin-on-flat configuration UHMWPE counterface Room temperature Contact pressure of 500 MPa50,000 cycles.	Stainless Steel WR: 10E-8 - 10E-9 mm^{3} (N m)$^{-1}$ Avg COF: 0.1-0.2 COF with lubricant: 0.04-0.05
[33]	Titanium alloys	Ti–C:H Varying content of C:H Interlayer for DLC coating	PECVD Deposition Reactive gas acetylene (C2H2) Magnetron sputtering C:H content varied by controlling C2H2 flowrate Ar (In atmosphere) flow rate of 75 sccm Coating thickness: 2.5 to 3.5 µm	Pin-on-disc CSM Tribometer 5000 cycles, Normal load 5 N Linear speed 0.05 ms−1 Room temperature 440C steel spherical counterpart diameter of 8 mm Relative air humidity 40±5%, 0.9% NaCl water solution, 10% fetal bovine serum, dissolved in Ringer's saline solution.	Best wear properties were achieved for the highest C2H2 flows

[22]	high carbon cobalt–chromium–molybdenum alloy	tantalum coating	Thermal treatment in molten salts by diffusion mechanism Multilayered tantalum carbides (TaC and Ta2C) Single layer of carbide (TaC) Temp 970 or 990^{oC}	Pin/ball on rotating disc Metal on Polymer (MoP) Metal on metal (MoM) Ceramic on Metal (CoM)	Coating on CoM had best wear resistance [(5 ± 0.3) x 10^{-7}] Mean value of COF was re duced for all couplings
[14]	Ti6Al4V	CNT-reinforced HA	Plasma spraying (Praxair SG-100 gun)	Pin-on-disc wear tester (Simulated Body Fluid) Pin: Length 50 mm diameter 3mm, zirconia (ZrO2) Disk: coated specimens. 100rpm, 8.8 N, 10,000 revolutions, 100min	HA (wear rate ~ 60.15 gm^{-2}) HA-CNT (wear rate ~ 38.92 gm^{-2}) Bare substrate (wear rate ~ 90.23 gm^{-2})
[45]	Ti6Al4V-ELI Grade 5	UHMWPE and PFPE as top lubricant layer	Dip coating Dipping and withdrawal speeds: 1.9 mm/s Intermediate soaking time: 35s Air exposure time: 1 min. Afterward, samples were heated at 100 ◦C (for 20 h) in clean air furnace. Cooled slowly to room temperature.	ball-on-disk mode Counterface : Si3N4 ball 4 mm diameter ,Roughness of 5 nm Track radius = 2mm Normal Load = 4N Spindle Speed= 1000 rpm 96,000 cycles	UHMWPE on Ti6Al4V , Wear life: 28,000 ± 8000 cycles COF: started to increase from 20,000 cycles UHMWPW/PFPE on Ti6Al4V, Wear life: 60,000 ± 14,000 cycles. COF: started to increase from 50,000 cycles
[19]	Stainless Steel 316L (SS)	Titanium Nitride and Micronite	Coatings were made by Micromy (Taby,Stockholm) Using a magnetic sputtering PVD Temperature: 300 ◦C Coating thickness: about 3 µm	Pin on disk Disc: SS, SS/TiN, SS/Micronite Pin: UHMWPE Sliding velocity: 60 rpm, 100 mm/s Running period: 48 h, 17.3 km Contact pressure (load/area): 9MPa Contact area 7mm^2 Temperature: 37±1 ◦C Lubricant: Bovine calf serum	Specific wear of 316L was 4-5 x higher compared to TiN and Micronite respectively

2.4.4 Wear outcome (for surface treated)

Ref	Substrate	Surface Modification technique	Wear test parameters	wear test results
[62]	Ti6AL4V	Two-step plasma immersion ion implantation technique Titanium oxide and titanium nitride film formed on the subsurface of Ti6Al4V alloy	Pin on disk tribometer Pin: UHMWPE Length: 20 mm, Diameter: 5mm Ra = 0.08 µm. Disk: Ti6AL4V Dimensions Ø45×4 mm2	WR of un-implanted Ti64 $23x10^{-6}$ $mm^3(N.m)^{-1}$ Avg WR of ion-implanted Ti64 $0.535x10^{-6}$ $mm^3(N.m)^{-1}$ Avg COF of ion – implanted 0.04
[66]	Ti6AI4V	Ion implantation of UHMWPE and Thermal Oxidation (TO) treatment of titanium alloy UHMWPE specimens were ion implanted In nitrogen atmosphere at 10^{-3} Pa 80 kV to a dose of 1 x 10^{-15} ions cm^{-2}	pin-on-disc tribometer Pin: UHMWPE Ra = 0.02 µm Disk: Ti6Al4V Diameter: 100mm, Thickness: 10mm Sliding speed: 0.25 m/s Contact pressure: 5 MPa	untreated UHMWPE/untreated Ti6AI4V WR: $5.5x10^{-6}$ - $1x10^{-6}$ $mm^3(N.m)^{-1}$ COF:0.150 Ion implanted UHMWPE/TO treated Ti6AI4V WR: $5.5x10^{-9}$ - $1x10^{-9}$ $mm^3(N.m)^{-1}$ COF: 0.025
[64]	UHMWPE	Optimized toluene-assisted mixing followed by hot-pressing Graphene Oxide	Ball-on- disc tribometer Ball: Zirconia Diameter: 4mm, Hardness: 7.0 Roughness: Ra = 0.03 µm RH 70%, Room temperature Load: 5 N, Avg sliding speed 9 cm/s Time 5,600 s	0% of GO: WR: $17x10^{-6}$ - $18x10^{-6}$ $mm^3(N.m)^{-1}$ COF (at 5000s): 0.100 3% of GO; WR: 10 $x10^{-6}$ $mm^3(N.m)^{-1}$ COF (at 5000s): 0.105
[25]	Titanium alloys	Nitrogen ion implantation and carburization nitrogen ion implantation: multi-function ion implanting system, Pressure: 10^{-5} Pa Energy: 40 keV, Nitrogen dose: 2.1×10^{17} ions/cm2. Carburization: Vacuum gas carburizing furnace three titanium specimens	Ball-on-flat Ball: ZrO2 Diameter: 5mm Load of 1.96 N, c Contact stress : 500MPa Time: 3 h Distance: 356 m Bovine serum lubrication dry friction condition	After nitrogen ion implantation, 6.28×10^{-4} to 2.87×10^{-4} mm^3/Nm After carburization, 6.28×10^{-4} to 1.80×10^{-4} mm3/m 71.3% decrease of wear rate

[54]	Ti6Al4V and Co28Cr6Mo	Ion implantation and plasma immersed ion implantation Ion implantation of nitrogen (I^2) Nitrogen dose: 4 x 10^{17} ions/cm2 Energy: 90 keV PI^3 oxygen implantations Pressure <10^{-4} Pa Working pressure: 0.2 Pa Plasma generation: 40.68 MHz. One Sample: Voltage: 30 kV, Incident fluence of 6 x 10^{18} oxygen atoms/ cm2 Temperature of 700 ^{o}C, Time: 3 h For the rest of the samples: Voltage: 15 kV, Temperatures: 580, 480 and 405 ^{o}C , Time: 2 h	pin/ball-on-disk tribometer Counter body: 3 mm-diameter Al2O3 bearing ball Applied load: 100g; Humidity: 45% Cycles: 30,000 cycles Linear speed: 0.1 m/s	Wear coefficient for Ti alloy samples, reduced by 95% at 700 ^{o}C and about 50% at 580 ^{o}C
[65]	Pure cobalt and a cobalt micro-melt alloy	Tantalum enrichment by Thermal treatment in molten salts After mirror polishing samples were place in a graphite crucibles filled with a solid salt mixture: NaCl 47 wt.%, K2TaF7 52 wt.% and Ta 1 wt.%. Argon flux, Linear heating: 800 - 1000 ^{o}C Isothermal heating: 1–2 h Isothermal treatment (60–90–120 min)	Ball-on-disk tribometer Alumina ball Diameter: 6mm Load: 5 or 7N Sliding rate: 10 cm/s Distance: 785 m (25,000 rev). Contact pressure: 1.3 GPa (5N) , 1.7 GPa (7N) Lubricant: bovine serum.	Alloy-60-1000 (7N) WR: 0.755x10^{-4} $mm^3(N.m)^{-1}$ COF: 0.18 Co-120-800 (7N) WR: 8.336 x10^{-4} $mm^3(N.m)^{-1}$ COF: 0.19
[31]	Wrought Co–Cr– Mo alloy	Carbon ion implantation (CII) and diamond-like carbon (DLC) film by Plasma source ion implantation Time: 2 h Pulse repetition rate: 100 Hz Pulse width: 50 μs with a −20 kV target bias Two samples were prepared, for three specimen types: uncoated, CII, and DLC.	Pin on plate test Pin:Diameter: 6mm Length: 20 mm Plate:Tests samples Load: 5.5 N. Reciprocating velocity: 15mm/s Stroke length: of 30mm. Cycles: 5000 Lubricant: 30 wt.% fetal bovine serum and pure water Temperature: 23±1 °C	WR in pure water: Uncoated: 1.9 x10^{-6} $mm^3(N.m)^{-1}$ CII: 1.9 x10^{-6} $mm^3(N.m)^{-1}$ DLC: 7.3 x10^{-6} $mm^3(N.m)^{-1}$ WR in serum solution: Uncoated: 4.8 x10^{-6} $mm^3(N.m)^{-1}$ CII: 1.9 x10^{-6} $mm^3(N.m)^{-1}$ DLC:1.5 x10^{-5} $mm^3(N.m)^{-1}$

2.5 Literature review summary

Orthopedic implants, that replace the function of a joint in the human body, fail due to several factors. One of the chief factors linked to implant failure at these locations are attributed to friction and wear. The tribological behavior of various biocompatible coatings and surface treatments on biomaterial were comprehensively reviewed. The friction and wear characteristics of the coatings and surface treated biomaterials were briefly discussed and summarized systematically. The following conclusion can be drawn from these studies:

2.5.1 Titanium and its alloys:

- DLC obtained from DMF showed best wear resistance compared to that obtained from acetonitrile. However, both coatings showed a similar reduction in friction coefficient to about 0.1.
- The highest C_2H_2 flows during PECVD showed better tribological characteristics during deposition of functional Ti–C:H layers.
- CNT-reinforced hydroxyapatite coating on Ti–6Al–4V substrate showed higher wear resistance compared to HA coating on SBF. And the addition of CNT contributed in alleviating wear debris.
- UHMWPE coating on Ti–6Al–4V substrate had a reduction in COF to about 0.05 compared to a COF of 0.5-0.6 for uncoated substrate and the addition of a PFPE as a top lubricant significantly improved the wear life.
- A graded titanium oxide–titanium nitride film ion-implanted on Ti6Al4V alloy increased the microhardness and improved the wear rate by 40 times and reduced the COF to 0.04 from 0.2.

- Nitrogen ion implanted UHMWPE and Thermal oxidized Ti6Al4V had a reduction of COF from 0.150 to 0.025 and had an improved wear resistance.
- Nitrogen ion implantation and carburization improved the wear resistance of Ti alloy however Carburization had a reduction in wear rate up to twice as compared to nitrogen ion implantation.
- Implantation and plasma immersed ion implantation for Ti6Al4V showed no major effect in friction coefficient. However, there was a reduction in wear coefficient which was temperature dependent.

2.5.2 Stainless steel AISI 316L:

- DLC can be used as a protective coating for articular joints it has shown low wear and friction coefficients in an artificial physiological liquid.
- Micronite showed higher wear resistance compared to TiN and 316L substrates respectively. Micronite/UHMWPE sliding pair showed enhanced tribological behavior and may be used in pair as artificial joints.

2.5.3 Co–Cr–Mo alloy:

- Tantalum carbide coatings showed a reduction in coefficient of friction and the multilayer tantalum carbide coatings on a high carbon cast Co–Cr–Mo alloy exhibit higher wear resistance.
- The surface chemical composition of an implant cobalt alloy was modified, producing relevant tantalum enrichment. The modified surface presented low friction coefficients.

- Ion implantation and plasma immersed ion implantation $Co_{28}Cr_6Mo$ showed no major impact on friction coefficient.
- Carbon ion implantation (CII) on Co–Cr alloy showed improvement in wear resistance and reduction in friction coefficient, offering potential advantages as a hard coating for articulating joints.

Based upon the extensive literature review presented above, it has been observed that only few studies have been reported on the surface modification of titanium and its alloys with polymer/polymer nanocomposite coatings for biomedical applications. Hence identifying the need for further research in this direction, we propose to develop a novel hybrid polymer nanocomposite coating for titanium and its alloys, using UHMWPE as the polymer matrix for its excellent tribological properties, reinforced with CNTs for improved load bearing capacity and HA for better biocompatibility.

CHAPTER 3

MATERIALS AND METHOD

This chapter presents properties of material and experimental procedure during the synthesis and characterization of Hybrid nanocomposite coating. The following flow chart shown in figure 13 summarizes all the process undertaken during surface modification of titanium and its alloys.

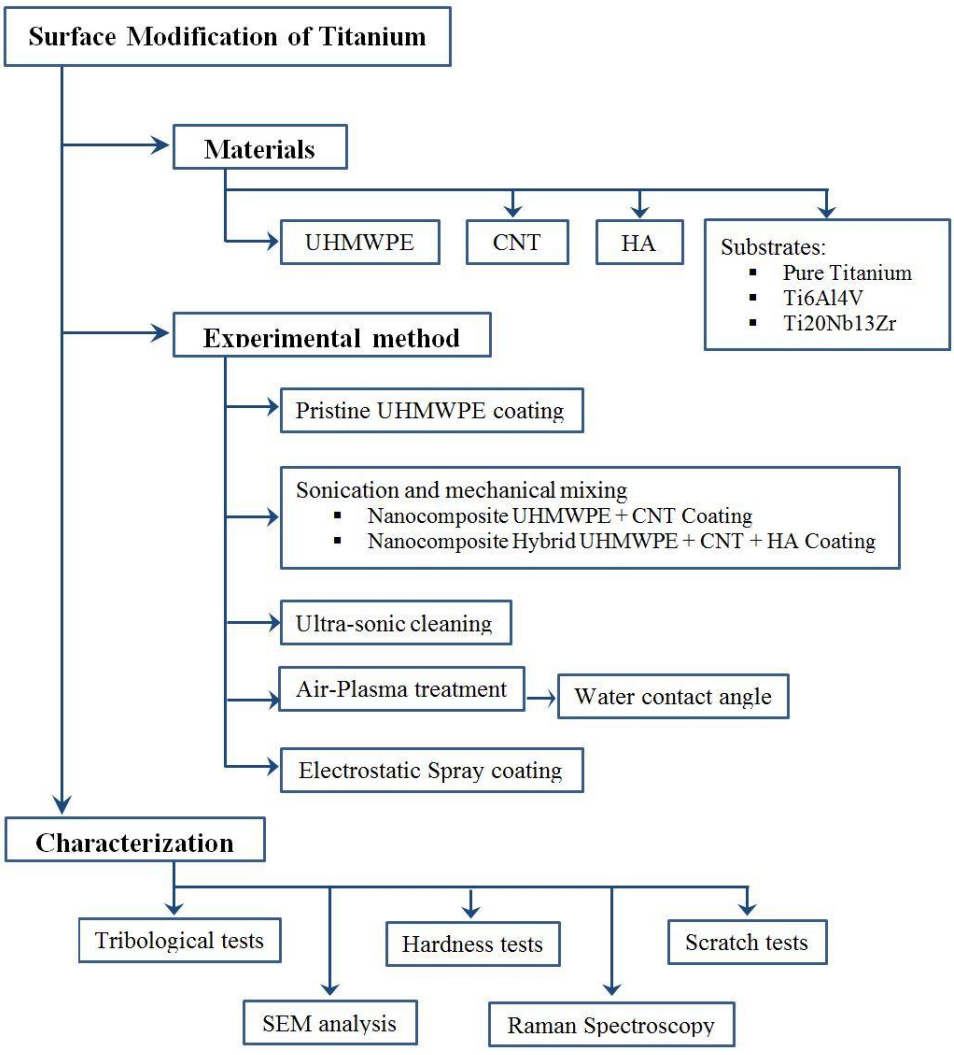

Figure 13: Flowchart summarizing the experimental methodology

3.1 Ultra high molecular weight polyethylene (UHMWPE)

UHMWPE used in this study was purchased from Good fellow corporation, USA. The average particle size ranged between 80 – 120 µm, with a melting point of 140^{o}C and a flash point of 341^{o}C. The characteristic appearance of the powder was white color which was in the form of solid granules. Figure 14 shows the SEM image of the pristine UHMWPE.

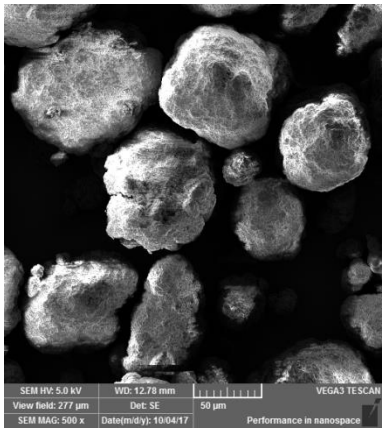

Figure 14: SEM image of Pristine UHMWPE

3.2 Multi-walled carbon nanotube (MWCNT)

MWCNT was used as reinforcement in the UHMWPE matrix to enhance tribological properties of the coating, the MWCNT used in this study was purchased from "Nanostructured & Amorphous materials Inc.: Houston, Texas, USA. The diameter of the MWCNT ranged from 40-60nm with a length of 1-2 µm and a specific surface area of 60-70 m^2/g. Figure 15 shows the SEM image of MWCNT's.

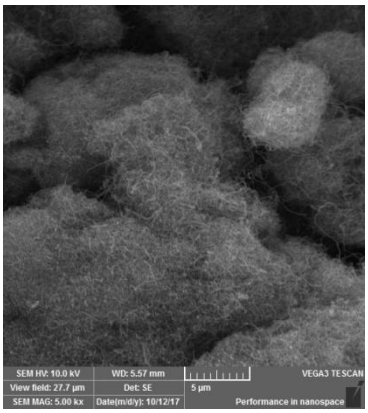

Figure 15: SEM image of MWCNT

3.3 Hydroxyapatite (HA)

HA, as described in chapter 2 was used as filler in this study, for better biocompatibility and enhanced mechanical properties. HA was prepared in house using the method by Paz, Adrian et al [67]. 0.555g of $CaCl_2$ (Calcium chloride), 0.150g of NaH_2PO_4 (Sodium dihydrogen phosphate) and 0.073g of $NaHCO_3$ (Sodium bicarbonate) were dissolved in 500 mL of distilled water. The solution was stirred for 24 hours at 37^oC and 80 rpm. At the end of the procedure the precipitate was washed with deionized water and dried at 110^oC for 2 hours in an oven. The quantity of HA yielded was very little, in sufficient for this study, therefore the constituents used for the preparation of HA were multiplied by x50 which resulted in a higher yielding of HA. Figure 16 shows the SEM images of HA, The characteristic appearance of the powder was white in color and had a plate like structure with a thickness ranging from 0.3-0.5 µm.

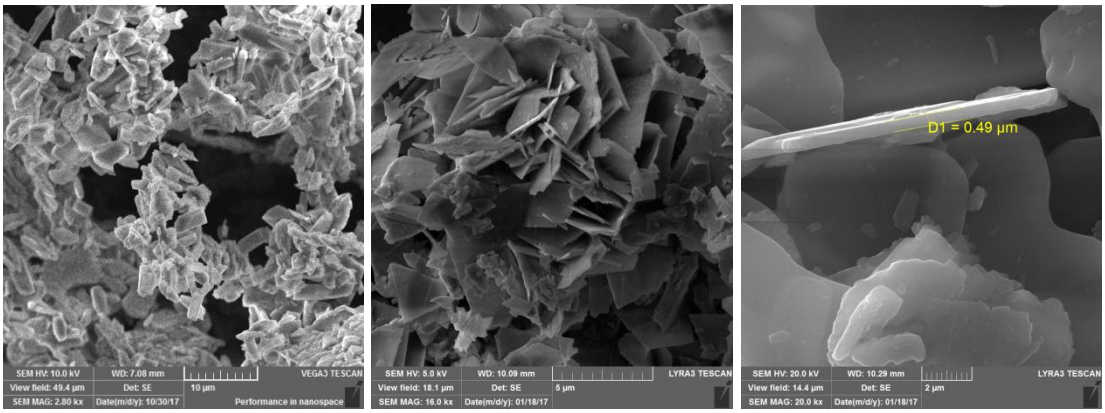

Figure 16: SEM image of HA

3.4 Sample preparation

Commercially available titanium sheets of dimension 1m x 0.5m x 0.003m were purchased from Xi'an Saite Metal Materials Development Co.Ltd Ti Grade 2 – ASTM F67 (pure titanium) and Titanium Grade 5 – ASTM F136 (Ti6Al4V). The third substrate used in this study was a newly developed and patented nanostructured titanium alloy (Ti20Nb13Zr) [68,69]. It possesses improved hardness, resistance to plastic deformation, and corrosion resistance in SBF compared to commercial Ti and Ti6Al4V alloys [70], and bioactivity [71].

From the 1m x 0.5 m and 3mm thick sheet of pure titanium, 0.5 m long strip of width 25mm was cut using the gelatin machine, figure 17, shows the gelatin machine used to cut the titanium strip. The same machine was used to cut the strip into small 25mm x 25mm square samples.

Figure 17: Gelatin machine which was used to cut a strip of titanium from a sheet

All the substrates used in this study were grinded using 320 & 180 Grit size papers to remove impurities on the surface and to maintain an even surface roughness throughout all tests.

3.5 Experimental Methodology

3.5.1 Sonication and mechanical mixing

The powders were mixed by sonication and mechanical mixing method. For 10g of UHMWPE reinforced with X% of CNT, the following steps were followed:

1. Using the weigh balance X g of CNT was weighed on a piece of paper and emptied into a 100 ML clean empty beaker
2. The beaker was filled with ethanol up to the 50 ML mark
3. The sonicator probe (see figure 18) was placed inside the beaker and was initiated for 10 min, (Total sonication time takes 15 min due to 5 seconds interval after every 20 seconds)

4. After the sonication process is completed the beaker is placed in a magnetic stirrer and stirred at 1000 RPM, after 2min of stirring (10-X) g of UHMWPE powder was added gradually, and the stirring process was let to continue for 60min.

Figure 18: Probe sonicator

5. Once the stirring process is complete, the beaker was placed on a hot plate with the temperature set to 80^{o}C for the complete evaporation of ethanol.
6. After 24 hours the beaker was ethanol free and UHMWPE reinforced with CNT powder was collected and stored for subsequent characterization and tests.

For 10g of UHMWPE reinforced with Xwt% CNT and Y% HA the method used by Kwok.C.T et al. [40] was employed.

1. Y% of HA was added to a 50ml of ethanol and magnetically stirred for 10min
2. After the stirring process HA was sonicated for 30min
3. X% of CNT was added into the beaker containing HA and sonicated for another 30 min. The remaining steps are similar to section 3.5.1 steps 4-6.

3.5.2 Ultra sonic cleaner

"Craftsman" powder spray coating gun was used to coat the samples. Prior to spray coating the samples are placed in a beaker, soaked in acetone and cleaned by using an ultra-sonic bath for 15min. the ultra-sonic bath used is shows in figure 19. After Ultra-sonic cleaning samples are dried using air blowers.

Figure 19: Ultra-sonic cleaner

3.5.3 Plasma treatment

Air- Plasma treatment was selected as a pre-treatment process for all the substrates before coating for better adhesion of the coating. Studies have shown the effect of adhesion for a thin film of coating on a metallic substrate pre-treated by Air-plasma [72-74]. It is one of the most effective surface adhesion enhancement techniques.

The electrons in the molecules and atoms get separated from the nuclei when air is subjected to very high energy due to electric sparks. Air-plasma is termed subsequent to the stream of ionized air containing independently moving electrons and nuclei. Various gasses such as oxygen, nitrogen, argon etc., can be used with the plasma to functionalize

specific functional groups on the surface to improve the quality of the coating on the surface. Contaminated surfaces are cleaned by plasma treatment resulting in an enhanced wettability and adhesion of coating due to the increase in surface energy.

Due to dust in the atmosphere surfaces that come in contact with the atmosphere contains organic or inorganic contaminates such as CO_2 and hydrocarbons, thus resulting in poor adhesion of the coating. When these surfaces are exposed to air plasma discharge are subjected to very high energy bombarding electrons, breaking the molecular bonds on the surface. When the carbon reacts with the free oxygen radicals in the plasma CO_2 is formed and removed this is known as the carbon cleaning effect. In addition oxidation effect [73] is referred to the formation of functional groups in the surface due to the oxidization of the oxygen radicals in the plasma, this helps in improving the wettability and the adhesion property of the surface, the principle of air plasma treatment is shown in figure 20

The titanium substrates were Air-plasma treated using Harick plasma cleaner. The samples were placed in the plasma chamber and the pump was turned on for 5 min to create a vacuum. After 5min the plasma treatment was commenced setting the RF value to high. Figure 21 shows the Harick plasma cleaning equipment used.

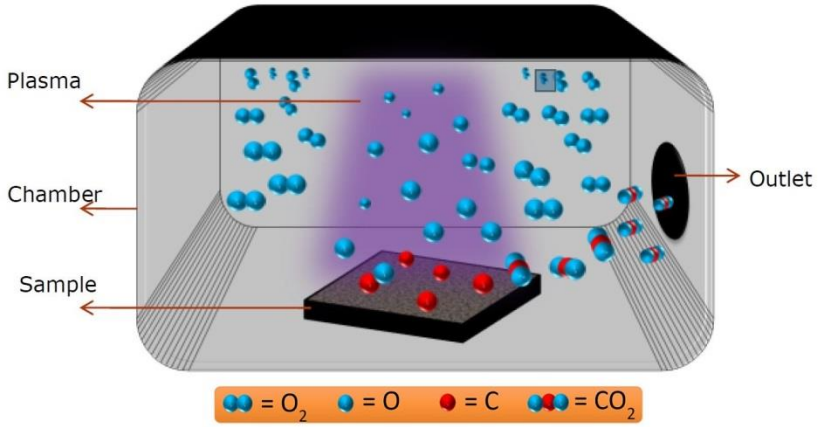

Figure 20: Air plasma treatment - working principle

Figure 21: Harick plasma cleaning equipment

3.6 Water contact angle

Wettability of a surface can be determined by a method known as contact goniometry, Surface energy can also be determined by this technique. The interface at which water meets a solid surface is called the water contact angle. Intermolecular interaction occurs when, liquid comes in contact with a solid, wetting depends on the energy (or surface tension) of the interface and the contact angle describes the degree of wetting [75].

If the solid surface attracts the liquid, and the liquid is strongly attached, the contact angle will be nearing zero, and the liquid will completely spread out. These surfaces are known as hydrophilic surfaces. If the water contact angle is greater than 90 ^{o}, the solid surface is said to be Hydrophobic. A super hydrophobic surface is achieved at a water contact angle above 150 ^{o}. figure 22 shows there schematic of different wettability levels of surfaces. Along with the Young's equation which relates the water contact angle with the interaction energy between the surface and the liquid. [75].

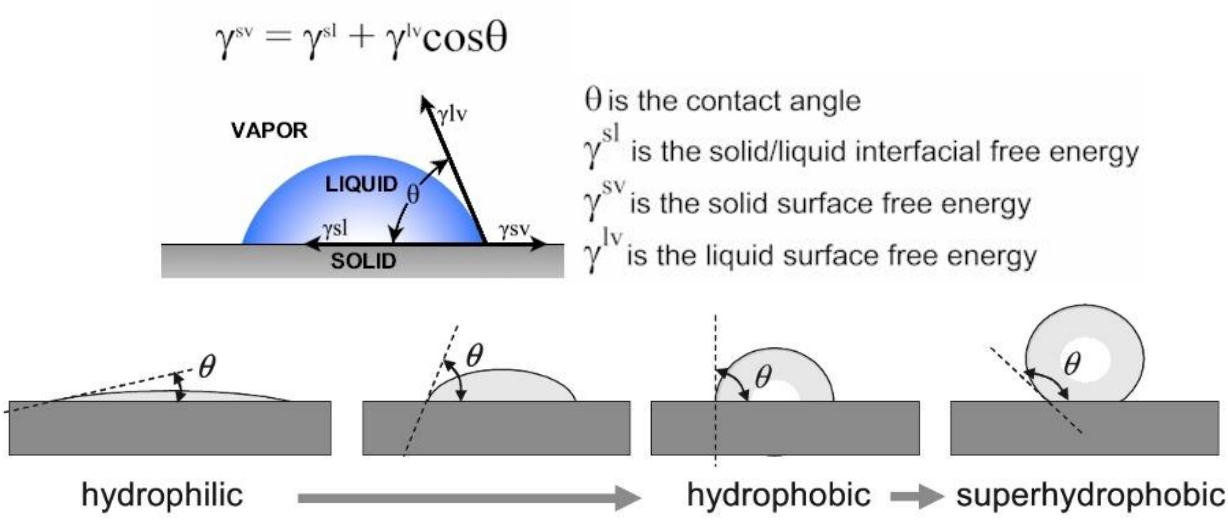

Figure 22: Different wettability levels on the surface

Water contact angle measurements were conducted for 3 samples before and after plasma treatment. The titanium samples were placed on a stage that could move in X or Y axis direction. An injection needle containing distilled water (that could move in the Z axis) was used to drop a 30 µL water droplet on to the surface of the sample. The equipment used and set up is shown in figure 23.

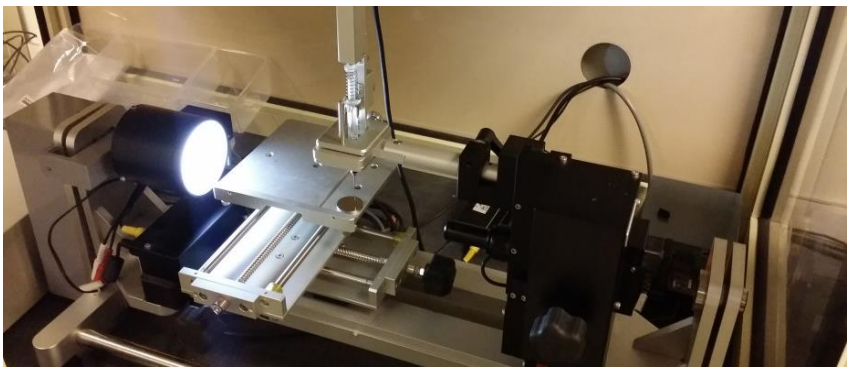

Figure 23: Water contact angle measurement, equipment

To evaluate the surface properties of the untreated and plasma-treated titanium substrate ATR-FTIR Spectroscopy was performed on a Nicolet 6700 by Thermo-Scientific before and after plasma treatment.

3.7 Spray coating

Immediately after plasma treatment the samples are placed on a hot plat for 5min, with the temperature set to 180^{o}C. the samples are electrostatic spray coated using the Craftsman spray gun, powder coat system with an input of 24VDC, 1 amp and output: 15KVDC, 15 micro amp. Initially the ground wire is clamped to an aluminum foil to ground the samples. The removable cup powder holder is filled with the required powder and attached to the spray gun. When the trigger is pushed the powder is charged as it

passes through the tip electrode at the emitter and a smooth layer is deposited on to the substrate. Figure 24 shows the complete spray coating system.

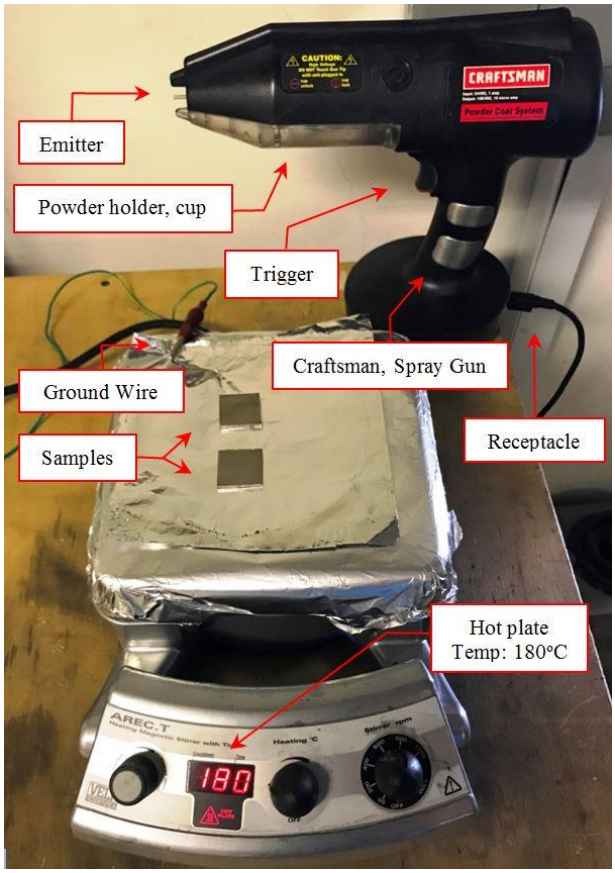

Figure 24: Spray coating gun and Hotplate

The powder is only held on to the metal surface by static electricity, the samples are left on the hot plate for 25-30 min for the powder to completely melt and form an even coating.

Figure 25 (Left) shows a pure titanium sample coated with pristine UHMWPE, and figure 25 (right) shows a coating of UHMWPE reinforced with 1.5%CNT on the same substrate. Visually the coatings seem even, smooth and well adhered to the substrate,

however the ability to with stand a certain load and there coefficient of friction can only be determined by tribological studies.

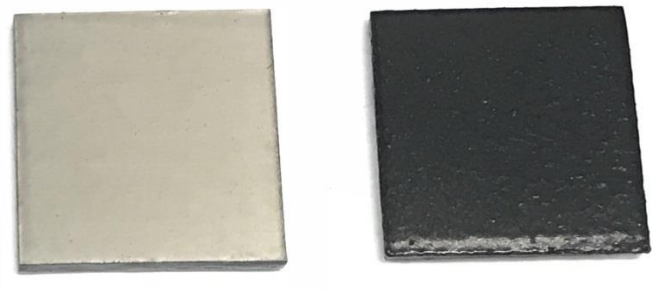

Figure 25: Pristine UHMWPE (left) and UHMWPE reinforced with 1.5wt% CNT (right) coated on Pure Titanium

3.7.1 Coating thickness

The thickness of the coating was evaluated using the Field Emission Scanning Electron microscope (FE-SEM). Two samples of each composition were used. Two sides were grinded for each sample and three readings were recorded. The average value were evaluated. Average values of the coating along with the FESEM Image of one reading for three coating composition are shown in figure 26.

	UHMWPE			
	Sample 1		Sample 2	
	Side 1	*Side 2*	*Side 1*	*Side 2*
	137.56	143.2	142.7	140.36
	142.2	136.7	145.2	146.58
	140.62	141.38	139.58	143.8
Avg:	140.13	140.43	142.49	143.58
Overall Avg: 141.66				

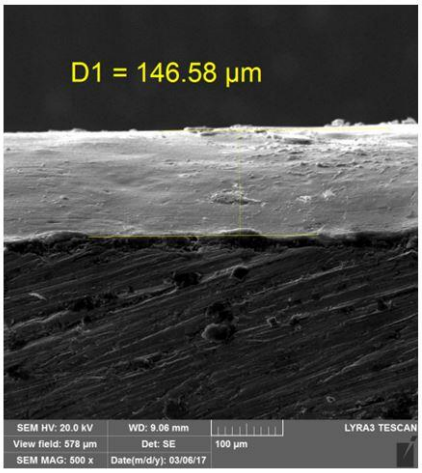

	UHMWPE + 1.5% CNT			
	Sample 1		Sample 2	
	Side 1	*Side 2*	*Side 1*	*Side 2*
	187.96	172.99	178.3	187.36
	181.7	187.96	174.66	185.2
	184.64	182.97	171.33	190.6
Avg:	184.77	181.31	174.76	187.72
Overall Avg:181.24				

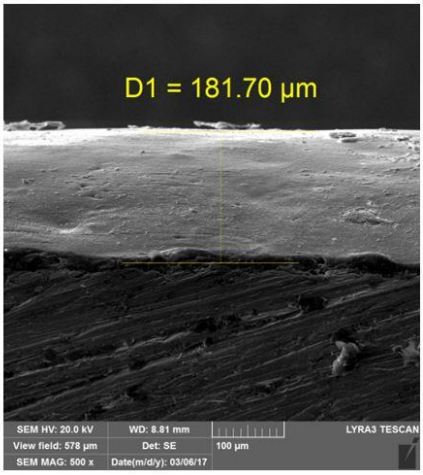

	UHMWPE + 1.5% CNT + 3%HA			
	Sample 1		Sample 2	
	Side 1	*Side 2*	*Side 1*	*Side 2*
	187.96	182.97	177.98	177.98
	186.3	194.62	191.29	185.36
	171.33	194.62	189.63	186.3
Avg:	181.86	190.74	186.30	183.21
Overall Avg:185.53				

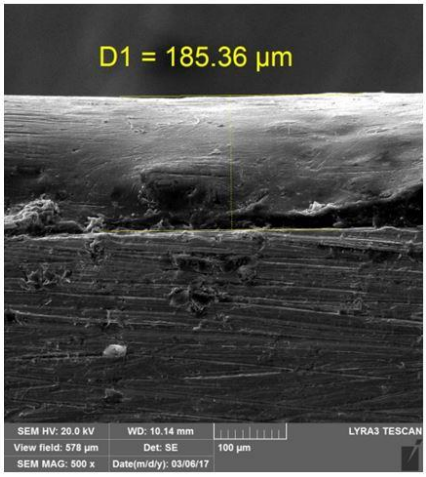

Figure 26: Average coating thickness and FESEM images of coating thickness

3.8 Tribology test

Bruker UMT-3 Tribometer, with a ball on disk configuration was used to conduct all the tribological tests in this study. A stainless steel ball with diameter of 6.3mm and hardness of RC 38 was used as a counterface. Initially a load of 7N for 5000 cycles at 478 rpm and 0.1 m/s was used to optimize the coatings; the coatings were further optimized for a load of 9N for 50,000 cycles. The rpm and velocity were kept constant throughout the test. The optimized coating was tested at 100,000 cycles and 250,000 cycles for a 12N load.

Table 9 shows the test parameters used in this study. The following equations were used to calculate the test parameters. Figure 27 shows the UMT-3 Tribometer system used in this study.

- $v = 2\pi rN$
- $S = vt$
- $t = \frac{Cycles}{N}$
- $v = \omega r$

v : Sliding velocity (m/s)
r : Track radius (m)
N : Revolution per minute (rpm)
S : Distance (m)
t : Time (s)
ω : Angular velocity

Table 9: Tribology testing parameters

R (m)	V (m/s)	Distance (m)	N (rpm)	Cycles	Time (min)
0.002	0.1	63.0	478	5000	10.5
0.002	0.1	627.6	478	50000	104.6
0.002	0.1	1255.2	478	100000	209.2
0.002	0.1	3138.0	478	250000	523.0

.

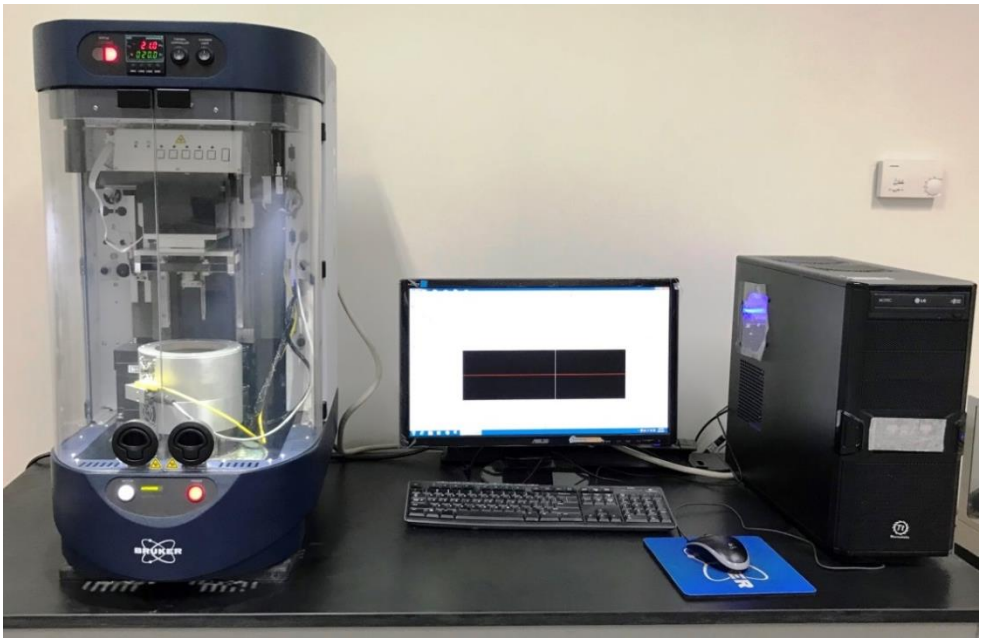

Figure 27: Tribometer connected to the PC system

Criteria to evaluate coating failure are listed below:

1. Sudden spike and too many fluctuation in the COF graph
2. Optical microscopic assessment for wear and tear on counter face ball
3. Wear track analysis by SEM
4. EDX analysis of wear track

Hertzian contact stress was evaluated for a normal load of 12N using the following equation:

$$P_{max} = \frac{3F}{2\pi a^2}, \quad a = \sqrt[3]{\frac{3rF}{2E_*}}$$

$$\frac{1}{E_*} = \frac{1}{2}\left(\frac{1-v_1^2}{E_1} + \frac{1-v_2^2}{E_2}\right)$$

a : Contact radius
r : Ball radius
F: Normal Load
E : Elastic Modulus
v : Poisson's Ratio

The calculated maximum Hertzian contact stress P_{max} = 68 Mpa

Many investigators have calculated the maximum contact pressure at the knee and hip joints In vitro and in vivo. The tibiofemoral joint (knee joint) evaluated by finite element analysis resulted in an average maximum pressure of 2.21 MPa. [76, 77]

For Hip joint, In vitro peak contact stresses measured using piezoelectric pressure sensors, pressure-sensitive film and transducers range between ~5 and ~10MPa. An instrumented prosthesis measured peak pressures of up to ~10MPa in vivo during activities of daily living. In addition pressure-sensitive film measured peak contact stress

at 13.8 ± 2.8 MPa and FE models with average cartilage predicted peak contact stress at 16.4 ± 7.8 MPa. [78, 79]

3.9 Hardness measurement

Vickers Hardness tests were conducted on the coated sample using the Micro-Combi Tester (See figure 28), with a contact force of 0.01N and an approach speed of 16.6 µm /min. The maximum applied load was 0.1N with a loading and unloading rate of 0.20 N/min. Measurement were carried out on 3samples of each type with the average value of 20 reading at different locations.

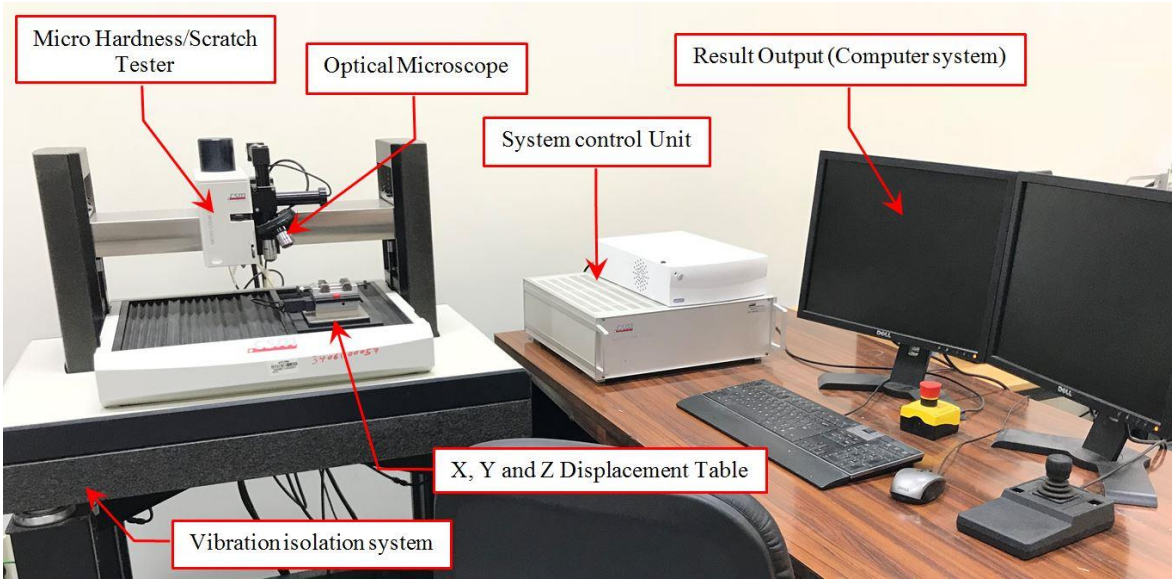

Figure 28: Micro-Combi Tester for hardness and scratch test

3.10 Scratch test

Linear, progressive scratch test was performed for the optimized coatings using the Micro-Combi tester as previously shown in figure 27. A rigidly mounted diamond having a Rockwell C geometry with a radius of 100 µm was used as the indenter to perform these tests. An initial load of 0.03N and an end load of 30N with a Loading rate of 15 N/m and a scratch length of 10mm were defined as test parameters.

3.11 Optical profilometer

Surface measurement determines the surface topography, usually essential to confirm the surfaces suitability for a given function. Conceptually surface measurement includes; Surface finish, Surface roughness, surface texture and structural characterization.

There are various techniques used to measure the surface topography of a sample [80], some of the techniques include:

- Mechanical Stylus Method
- Optical Method
- Scanning Probe Microscopy Methods
- Electrical Method
- Electron Microscopy Methods

The technique used to measure the surface topography in this study is the optical method. A 3D optical profilometer as shown in figure 29 is used. The 3D profilometer is connected to the computer, surface analysis is displayed in the monitor by a program.

Wear depth and wear volume, Specific wear rate was calculated using the Optical profilometer.

Specific wear rates are calculated by initially finding the area under the curve for a 2-D plot which is provided by the computer and multiplying it with the track circumference i.e. 2πr, where r stands for the track radius, to calculate the wear volume. The wear volume is then divided by the applied normal load and distance traveled by the ball as shown in the equation below:

$$Specific\ Wear\ rate = \frac{Wear\ volume}{Applied\ Normal\ load\ \times Distance} = \frac{mm^3}{Nm}$$

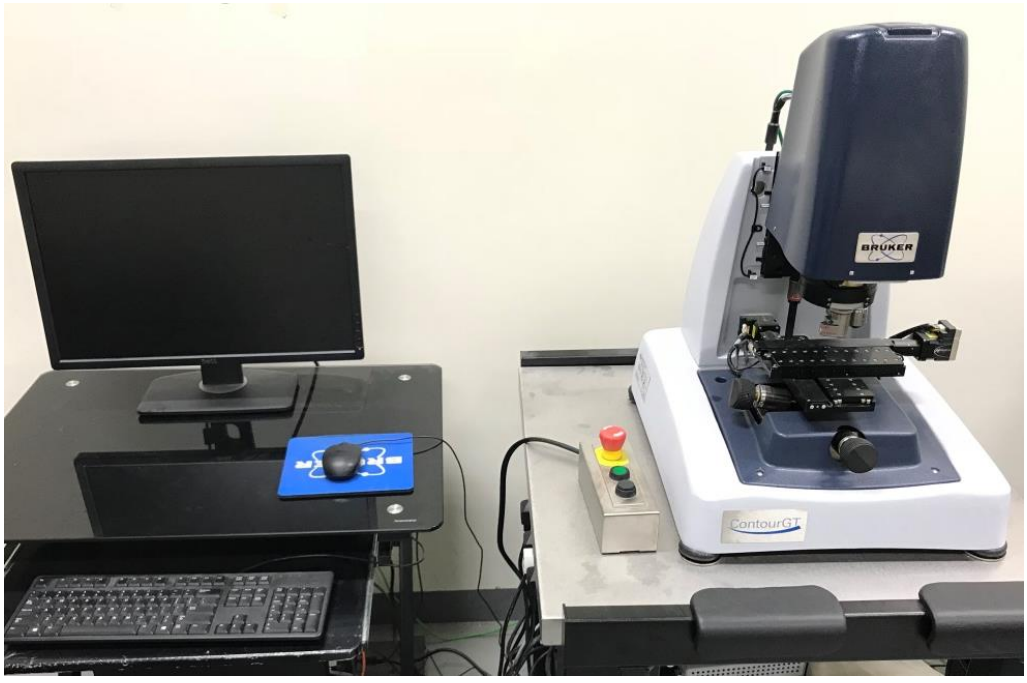

Figure 29: 3D Optical profilometer

3.12 Metallurgical microscope

The Metallurgical microscope by MEIJI TECHNO CO., LET was used to examine the ball images after the tribology tests. The ball images were captured using an EPI 10x/0.25 lens with work distance (WD) = 7.7 and F=200, the microscope model used was MT7100 with a vertical illuminator. Figure 30 illustrates the metallurgical microscope used in our study.

Figure 30: Metallurgical microscope

3.13 Raman spectroscopy

Raman spectroscopy is a powerful technique that can give information on the interaction of CNT's with the polymer chains and the structure of individual CNT's.

Test samples are exposed to electromagnetic radiation of single wave length. There is an inelastic and elastic scattering, depending on the samples interaction with

electromagnetic radiation. Raman Scattering is termed when the electromagnetic radiation is scattered inelastically, implying that light being scattered from the sample is of different frequency compared to the source of radiation. The Raman spectrum is represented by the intensity of absorbed radiation plotted against the wave number.

The variance of the incident beam and the intensity of scattering carries information regarding the stretching of molecules and bonds and vibration. Therefore by observing the raman shift in the band, the interfacial interaction can be characterized. The shifting of bands from one wave number to another can be a result of stretching, vibrational and conformational modes of the bonds in interaction. [73,74,75,76]

Raman spectroscopy was performed for UHMWPE reinforced with CNT coatings to investigate the interaction of CNT's with the UHMWPE matrix. Figure 31 shows the Raman spectroscopy system used in this study.

Figure 31: Raman spectroscopy system

3.14 SEM imaging

Tescan VEGA3 Scanning electron microscope was used to analyze the dispersion of CNT's and HA in the UHMWPE Matrix. VEGA3 is a fully PC-controlled scanning electron microscope that uses a tungsten heated filament and consists of a powerful four lens wide field optics design that offers variety of working and displaying modes. VEGA3 Control software was used to process the SEM images using the PC. Figure 32, shows the SEM system used. Prior to SEM imaging the samples were sputter coated with gold using the "Fine Coat Ion Sputter JFC-1100".

Figure 32: Scanning Electron Microscope (SEM)

3.15 Electrochemical corrosion analyses

Electrochemical corrosion analyses were carried out using a typical three-electrode cell with the Gamry Instrument potentiostat/galvanostat/ZRA (Reference 3000). A saturated calomel electrode (SCE) was used as a reference electrode and a graphite rod as a counter

electrode see figure 33. The simulated human body fluid (SBF) solution was used as electrolyte for electrochemical characterization. The preparation of SBF and the procedure for conducting the experiments was adopted using previous reports [70,71]. The exposed area of each sample was 1.76 cm^2. Open circuit potential (OCP) monitoring was done for about 30 minutes. Electrochemical impedance spectroscopy (EIS) measurements were done in a frequency range from 100 kHz to 10 mHz with a sinusoidal AC voltage of 10 mV amplitude. The results of the EIS data are represented as a Bode plot.

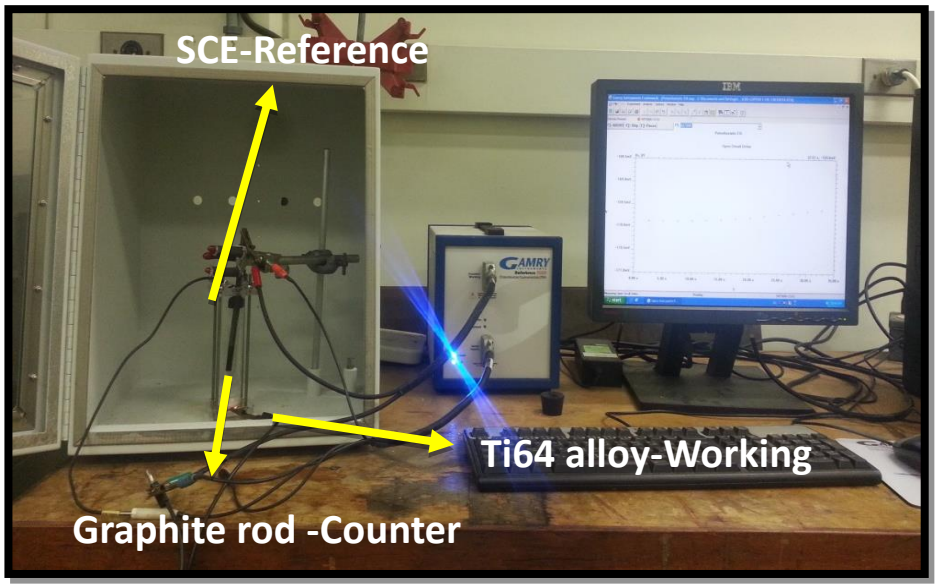

Figure 33: Electrochemical corrosion analyses setup

CHAPTER 4

RESULTS AND DISCUSSION

4.1 Phase 1 – Optimization and characterization of pristine UHMWPE coating

4.1.1 Effect of plasma treatment on the water contact angle

Water contact angle measurment was conducted on Pure titanium substrate before and after plasma treatment. A 30µL water droplet was gently dropped on the surface, the computer displayed the WCA measurement. Three readings were taken for each sample at different locations and the average water contact angle were calculated. Reading at a single location gives two angle readings, Left angle and right angle of the water droplet. Figure 34, shows the result displayed by the program for a single reading.

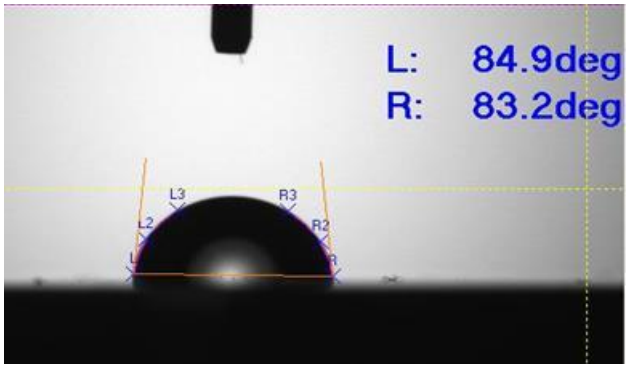

Figure 34: Left and right angle of the water droplet

Water contact angle measurements were recorded, for 3 samples before plasma treatment and after plasma treatment to study the effect of plasma treatment on the titanium substrate the results are tabulated in table 10 and 11.

Table 10: Water contact angles in degrees, before plasma treatment

No. of Readings	Sample 1			Sample 2			Sample 3		
	Left	Right	Avg	Left	Right	Avg	Left	Right	Avg
1	76.6	76.6	76.6	72.8	72.8	72.8	73.2	73	73.1
2	77.8	80.1	79	74.3	76.5	75.4	73.4	74.9	74.2
3	84.9	83.2	84.1	74.6	75.2	74.9	73	66.9	70
			79.9			74.4			72.4

Table 11: Water contact angle in degrees, after plasma treatment

No. of Readings	Sample 1			Samp1le 2			Sample 3		
	Left	Right	Avg	Left	Right	Avg	Left	Right	Avg
1	12.9	14.2	13.55	14.7	19	16.85	15	14.5	14.75
2	13.8	16	14.9	16.7	14.3	15.5	15.2	17.6	16.4
3	14.5	15	14.75	18.1	17.4	17.75	18.3	17.6	17.95
			14.4			16.7			16.4

Figure 35 shows the image of the water droplet for a single reading before and after plasma treatment. From the result displayed by the water contact angle and figures, it is clearly evident that plasma treating the samples successfully decreases the WCA from ~ 75.6 to ~15.8, i.e. a drop of 79.1%. This can be attributed to the increases in surface energy of the surface by carbon cleaning and oxidation effect of the air plasma treatment, resulting in an improved adhesion of the coating material, during the spray coating process as suggested in several studies. [44,47,77]

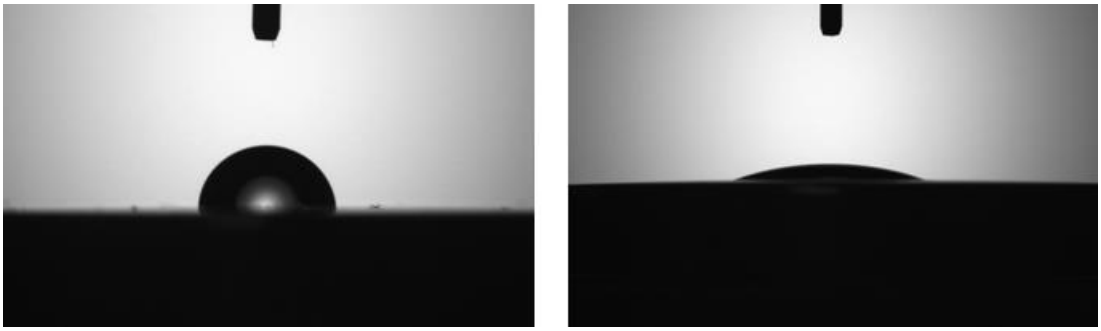

Figure 35: Water droplet before plasma treatment and Water droplet after plasma treatment

The titanium substrate was characterized by ATR-FTIR spectroscopy. Figure 36 (A) shows the ATR-FTIR spectrum of the untreated substrate and (B) shows the ATR-FTIR spectrum of the substrate after 10 minutes of plasma treatment. A large peak at ~ 2000 cm^{-1} arises after treatment due to the C O stretching of ketones, aldehydes and carboxylic acids. [85-87]

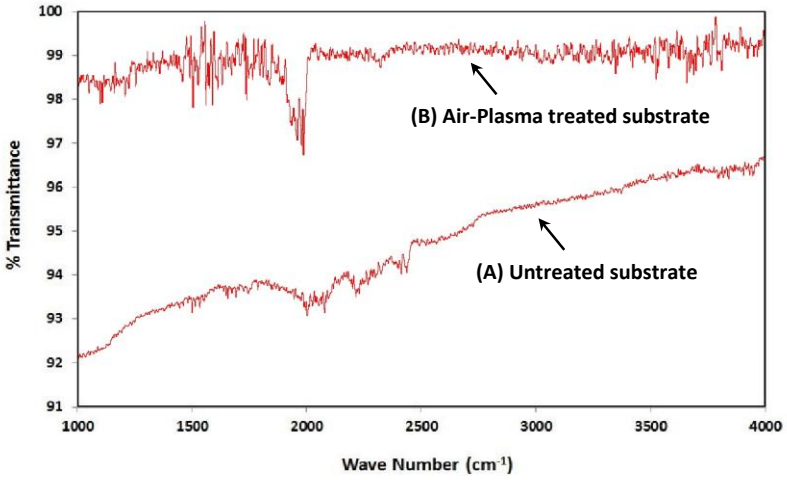

Figure 36: (A) ATR-FTIR spectrum of the untreated titanium substrate (B) and a 10min air-plasma treated titanium substrate

Taking into account the above results, one can conclude that plasma treatment in air leads to the formation of oxygen containing functionalities on the titanium surface, resulting in better adhesion of the coating during the electrostatic spray coating process.

4.1.2 Tribological characterization of bare substrate and pristine UHMWPE coating.

4.1.2.1 COF of bare substrates

Tribology tests were conducted on all the bare substrates prior to any coating to evaluate the COF and understand their individual performance. Figure 37 shows a typical COF vs time graph as displayed on the computer after the test along with the 2-d profiles and ball images. Test was conducted at a normal load of 12N and a sliding velocity of 0.1m/s for ~2400 cycles.

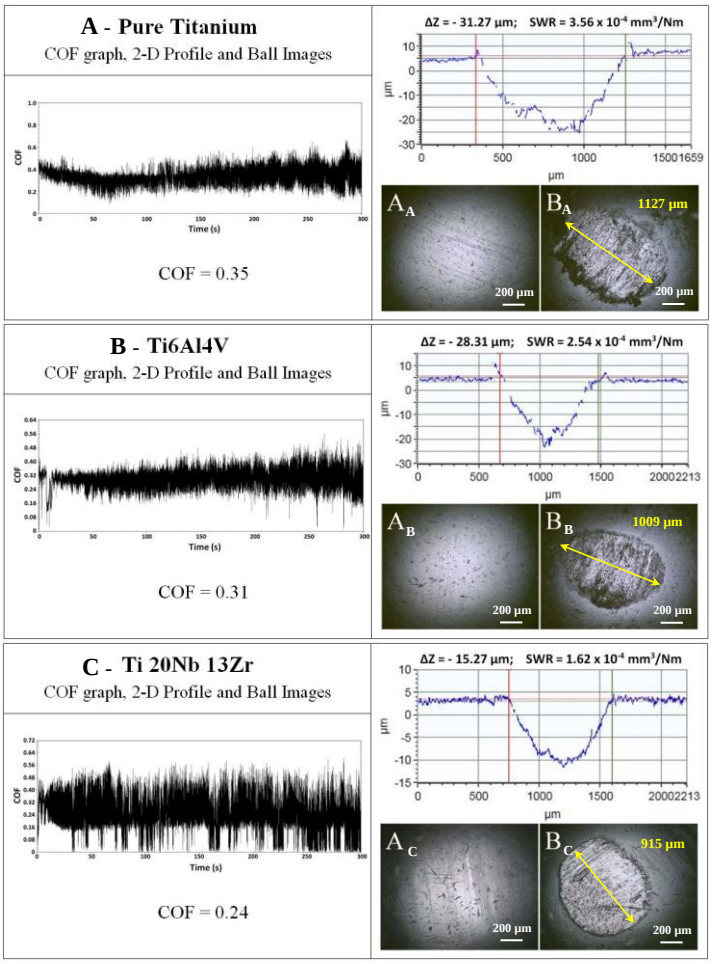

Figure 37: Typical COF graphs, 2-D-wear profiles and counterface ball images (A) before the test (B) after the test for Bare Substrate recorded after a wear test conducted at a normal load of 12N and a sliding velocity of 0.1m/s for ~2400cycles

High friction coefficient of the bare substrates is attributed to the presence of mechanically unstable titanium oxide film leading to adhesive wear [45].

Ball image A was taken before the test and image B after the test, from the figures a substantial loss of material from the counterface ball can be observed , However when comparing the 2-D profiles of different substrates, Ti20Nb13Zr seems to have a less profile depth and low COF compared to Pure titanium and Ti6Al4V.

4.1.2.2 Effect of load on the tribological properties of Pristine UHMWPE

The average wear life of pristine UHMWPE coating on pure titanium substrate was evaluated by applying different normal loads of 7, 9 and 12N respectively, at a constant sliding velocity of 0.1 m/s for 5000 cycles. Table 12 summarizes the test results.

Table 12: Pristine UHMWPE coating – Summary of wear life test

Test #	Applied Load	No. of Cycles	Result
1	7 N	5000	Test did Not Fail
2	9 N	5000	Test did Not Fail
3	12 N	5000	Test Failed

Figure 38 shows, the COF vs Time graph of Pristine UHMWPE with different loads, each tests were repeated three times and the average COF was calculated. The experiment was stopped after 5000 cycles for a 7N and 9 N loads however, as the normal load was increased to 12N the coating failed at an average wear life of 3600 cycles, figure 39 shows the SEM image for a portion of the wear track, peeling off and plowing of the

coating is observed and the EDX analysis shows the elemental peak of titanium which confirms the exposure of the titanium substrate.

Figure 40 shows the average wear life of the coating for applied loads. The tests were repeated three times for each load.

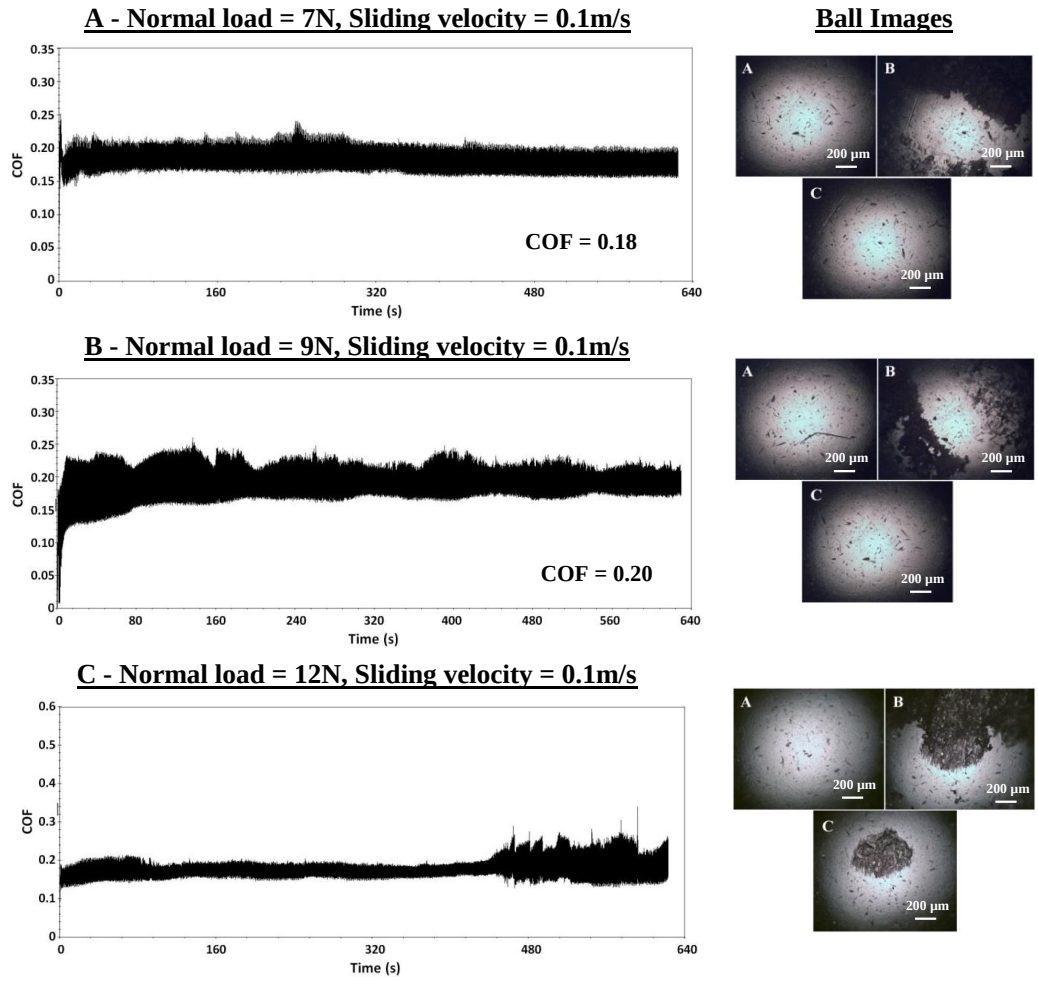

Figure 38: Typical COF graphs and counterface ball images for Pristine UHMWPE coating recorded after a wear test conducted at a normal load of 12N and a sliding velocity of 0.1m/s for 5000 cycles

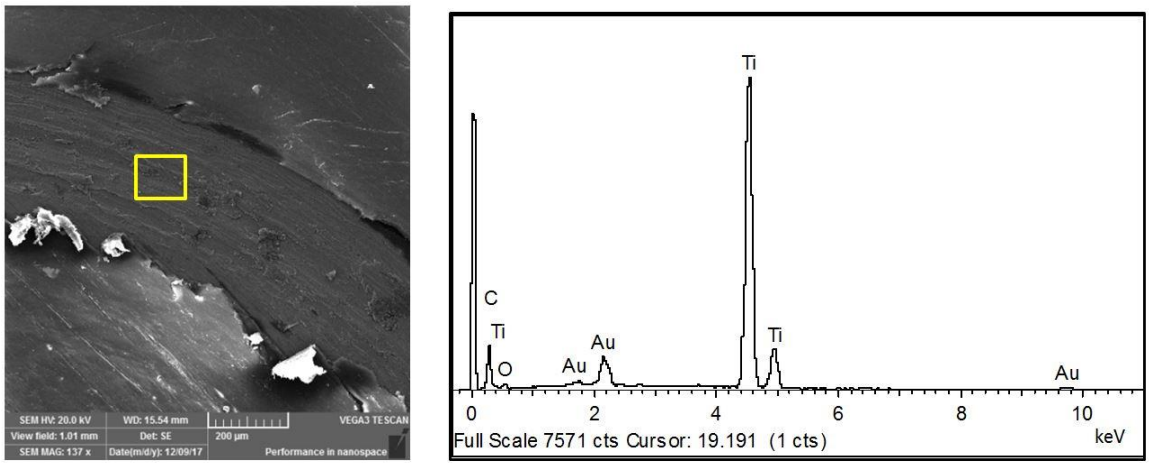

Figure 39: Wear track of Pristine UHMWPE coating & EDX Analysis for F_n= 12N

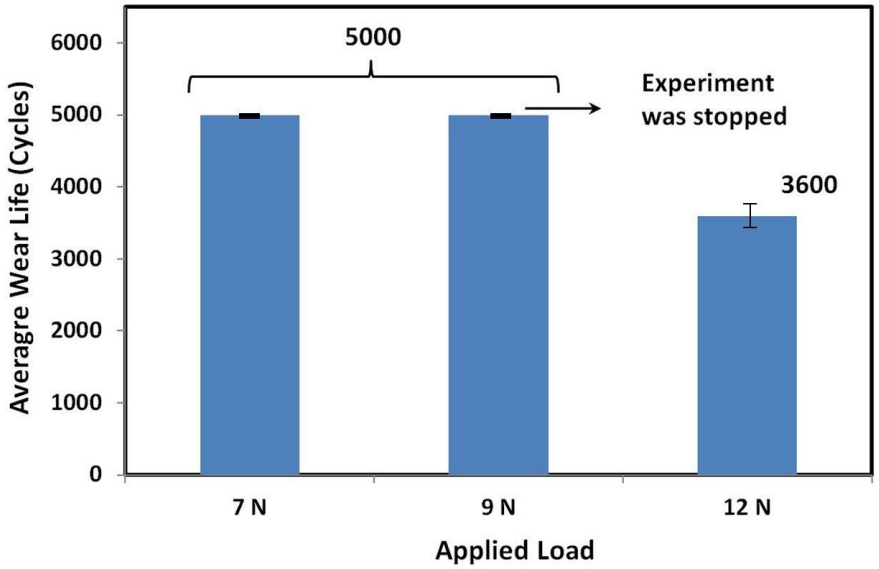

Figure 40: Average wear life of Pristine UHMWPE coating

4.1.3 Evaluation of scratch resistance for pristine UHMWPE coating

Figure 41 shows the acoustic emission with respect to the applied normal load. At an average load of 7.3N the coating fails and the diamond tip comes in contact with the substrate. Complete failure of the coating occurs at a load of 10.2N.

Figure 42(A) shows the length of the complete scratch. Figure 42 (B) shows the point at which the diamond tip has penetrated the coating and initial failure has taken place. At a load of 10.5N considerable peeling off and plowing is observed as shown in the SEM images in figure 42 (C), where complete failure has occurred.

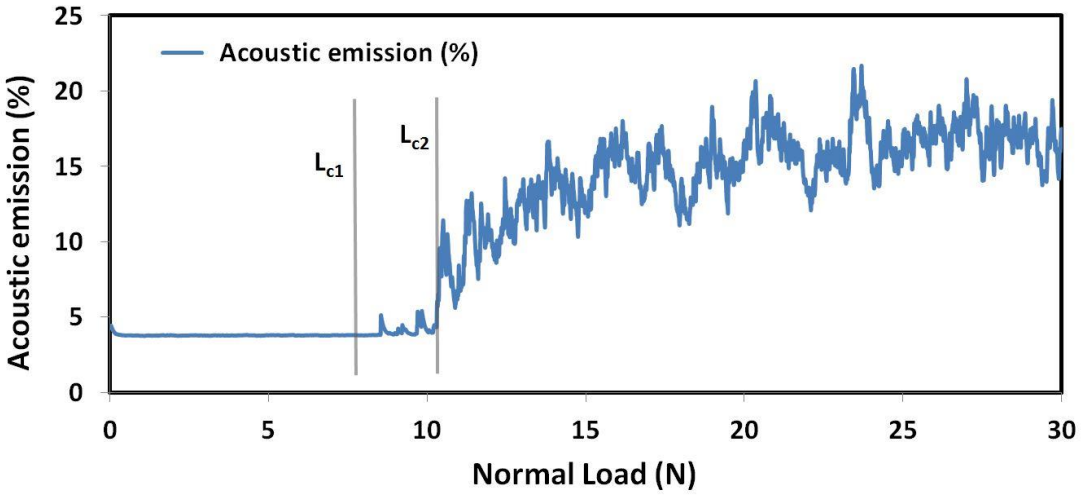

Figure 41: Acoustic emission with respect to applied normal load for Pristine UHMWPE coating

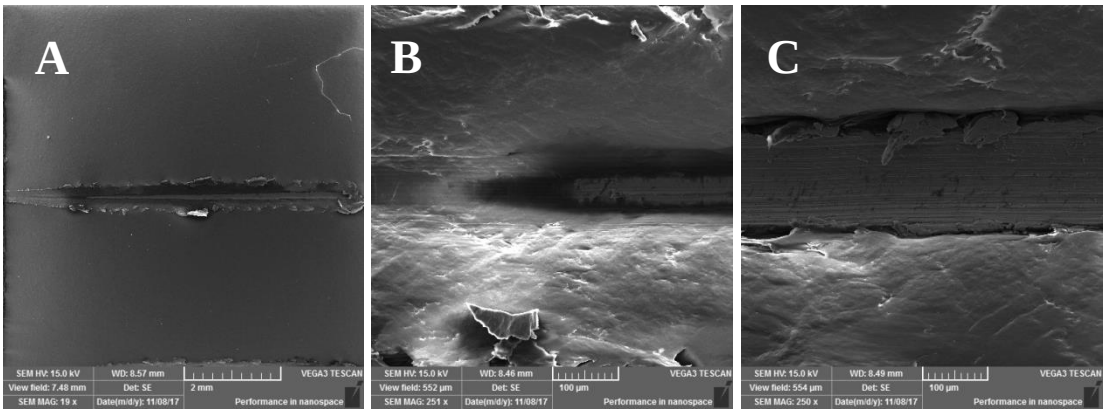

Figure 42: Pristine UHMWPE coating - SEM image of scratch test

Pristine UHMWPE was not able to withstand a load of 12N during tribology characterization and a normal load of 7.3N during scratch analysis due to its low load bearing capacity. To increase the load bearing capacity of pristine UHMWPE we intend to reinforce CNT's into the UHMWPE matrix.

4.2 Phase 2 – Optimization and characterization of nanocomposite UHMWPE reinforced with CNT coating

4.2.1 Evaluation of Interaction of CNT's with UHMWPE Matrix using Raman spectroscopy

Raman spectroscopy was used to study the interfacial interaction between the UHMWPE matrix and CNT's. Figure 43 shows the characteristic Raman peaks of pristine UHMWPE. Points 1-2 are associated with the asymmetric and symmetric stretching modes of the C-C bond whereas points 3-8 are subsequent to the twisting and bending modes of CH_2. All the points marked in the figure are highlighted in table 13 [88].

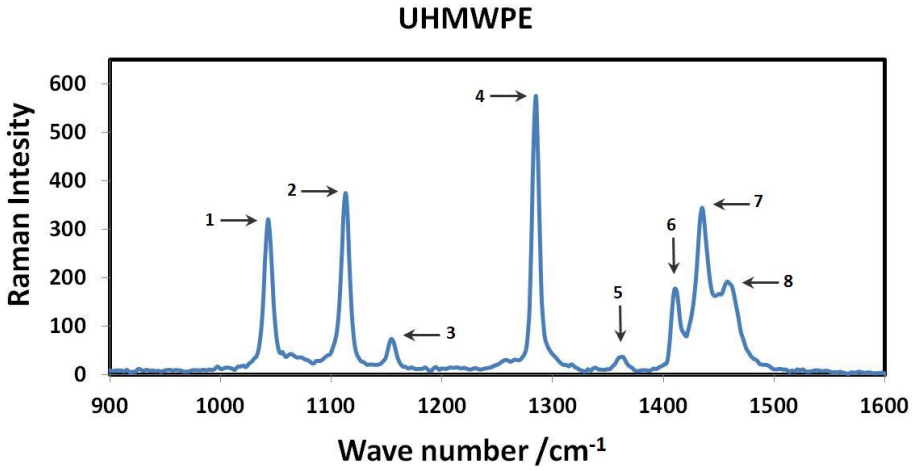

Figure 43: Raman peaks of pristine UHMWPE

Table 13: UHMWPE Raman-peak details

#	Description	Wave number ($^{cm-1}$)
1	Crystalline + Amorphous trans C-C	1043
2	Crystalline + Amorphous trans C-C	1113
3	Crystalline + Amorphous trans CH_2	1156
4	Crystalline CH_2	1285
5	Crystalline + Amorphous CH_2	1361
6	Crystalline CH_2	1412
7	Amorphous trans CH_2	1435
8	Amorphous CH_2	1459

The CNT displayed two characteristic peaks, as shown in figure 44. The first at 1357 cm^{-1} assigned the D band determining disordered graphite structures, the second peak centered at 1574 cm^{-1} assigned the G-band is correlated with the tangential C-C bond stretching motions [89]

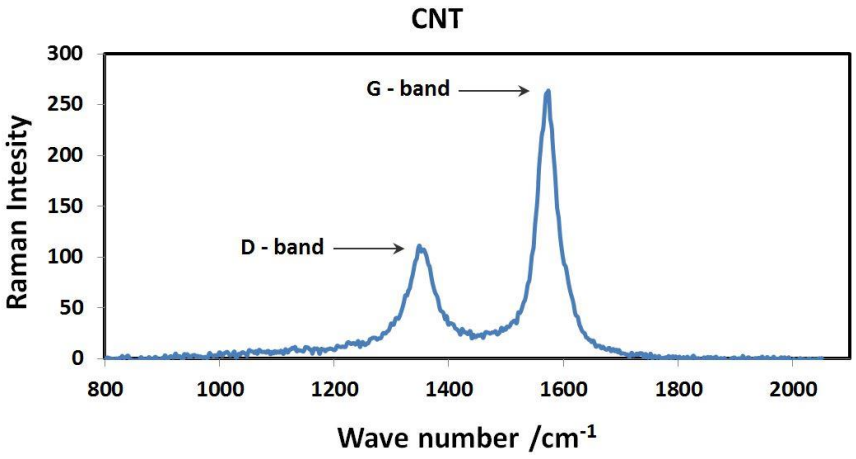

Figure 44: Raman peaks of CNT

Figure 45 shows the high frequency Raman Spectroscopy for UHMWPE, with 0.5, 1.5, and 3wt% addition of CNT. On addition of 1.5wt% CNT the maximum in the G-band peak was up-shifted by 27cm^{-1}. The shifting of the G-Band peak to a higher frequency

can be attributed to the disentanglement and extrication of CNT's as a result of successive dispersion in the UHMWPE matrix. The up-shift of the G-band can also represent stronger compressive forces associated with the UHMWPE chains on CNT's. Similar shifting of the G-band is reported for epoxy and polypropylene reinforced with CNT [83]. However in the case of 3wt% CNT and 0.5wt% CNT the upshift of the G-band was only 19 cm^{-1} and 14^{-1} respectively, which is comparatively a low shift than 1.5wt% CNT.

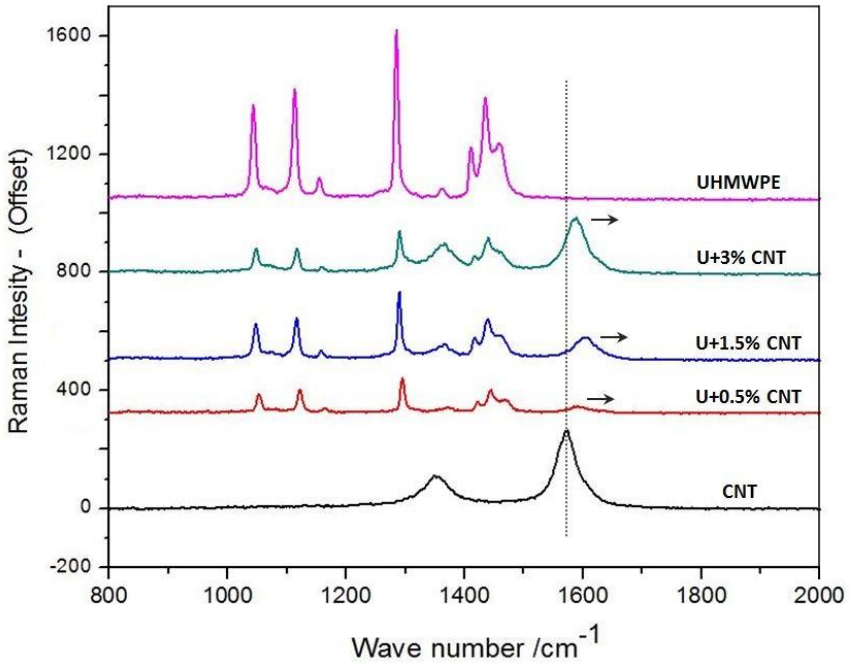

Figure 45: Raman peaks of UHMWPE with 0.5, 1.5 and 3wt% CNT

4.2.2 Dispersion analysis of CNT's in UHMWPE matrix using SEM

The dispersion of 0.5wt% CNT is shown in figure 46, CNT's appear to be evenly distributed however the quantity of CNT seems to be less.

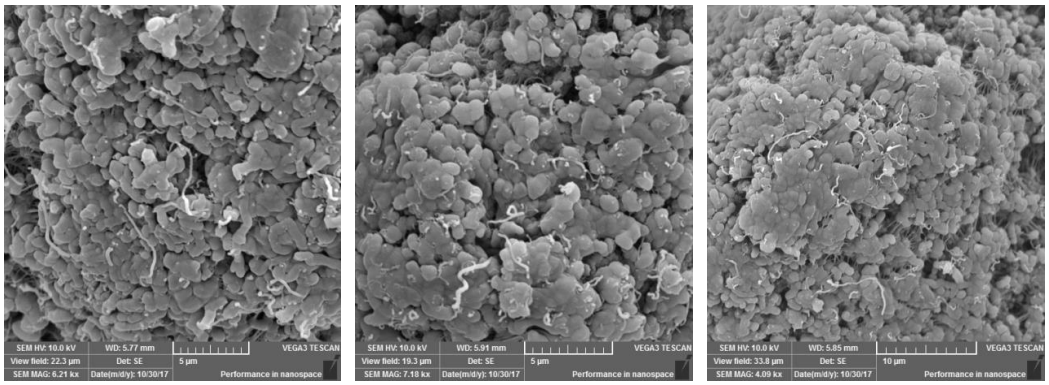

Figure 46: SEM images of 0.5wt% CNT dispersed in UHMWPE matrix

SEM images of UHMWPE reinforced with 1.5wt% CNT is shown in figure 47. The even distribution of the CNT in the UHMWPE matrix can be clearly seen in the figures. The presence of individual CNT's in different locations attributes to good desperation and almost negligible agglomeration. Therefore the sonication process employed is effective in dispersing 1.5wt% CNT's without breaking the CNT's

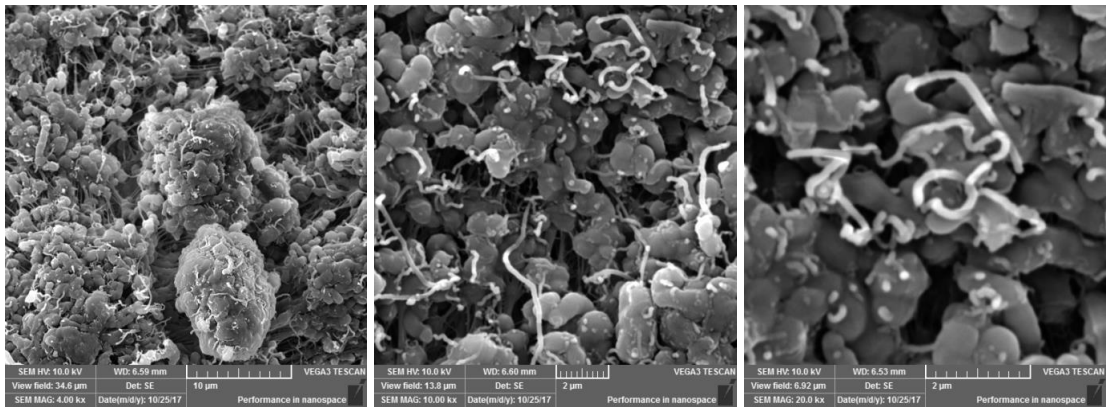

Figure 47: SEM of 1.5wt% CNT dispersed in UHMWPE matrix

When the % of CNT was increased from 1.5wt% to 3wt% traces of agglomeration were observed during the SEM characterization as shown in Figure 48. The presence of agglomeration indicated poor desperation of CNT's for the 3wt% using the sonication

process. The maximum time of sonication was used, increasing the time further will result in breakage of CNT, which will have a negative impact on the properties of CNT's.

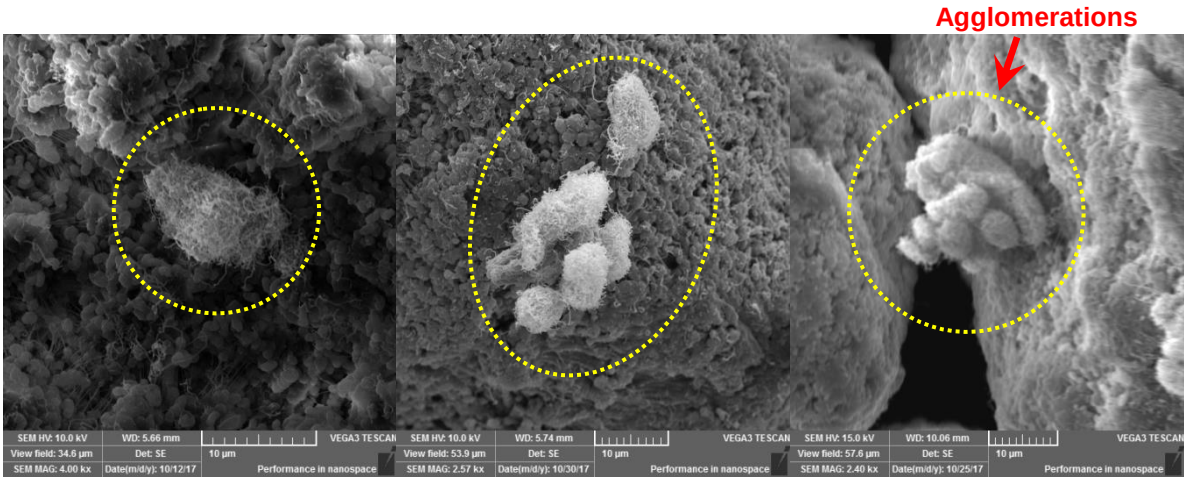

Figure 48: SEM of 3wt% CNT dispersed in UHMWPE matrix

4.2.3 Hardness measurements of nanocomposite coating

Figure 49 shows the change in hardness and penetration depth for different wt% of CNT reinforced in UHMWPE. An increase of approximately 37% in hardness value and a decrease of 24% in penetration depth can be observed as the amount of CNT reinforcement is increased from 0wt% to 3wt%.

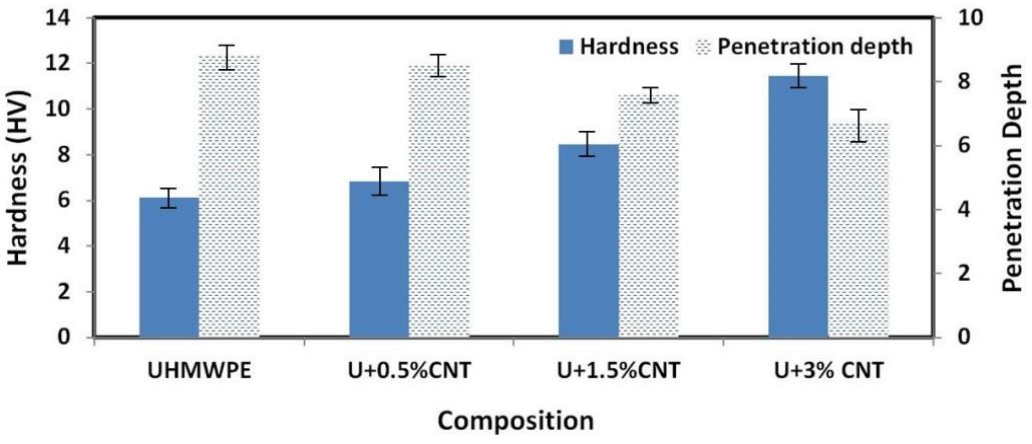

Figure 49: Hardness & Penetration depth Vs composition for U+X% CNT

The reinforcement of CNT in the UHMWPE matrix does not induce any structural or chemical changes in the polymer matrix, therefore the increase in hardness and decrease in penetration depth can be attributed to the excellent load bearing capacity and mechanical properties of CNT [47]

4.2.4 Tribological characterization of UHMWPE reinforced with different wt% of CNT

To improve the load bearing capacity of UHMWPE and enhance its tribological properties, different wt% of CNT were introduced into the UHMWPE matrix, Table 14 shows the initial composition used and tested at a constant number of cycles and with a sliding velocity of 0.1 m/s these parameters were kept constant throughout the tests.

Table 14: Wear life test for UHMWPE reinforced with different wt% of CNT

Test #	Sample Composition	Applied Load	No. of Cycles	Result
1	U + 0.5% CNT	12 N	50,000	Test Failed
2	U + 1.5 % CNT	12 N	50,000	Test did Not Fail
3	U + 3 % CNT	12 N	50,000	Test Failed
4	U + 1.5% CNT	15 N	50,000	Test Failed

The avg COF along with the wear track and EDX analysis shown in figure 50 and the average wear life cycles shown in figure 51, are average results of three repetitions. Figure 52 shows the 3-D and 2-D optical profiles of the track along with the ball images. Ball image denoted as A indicates the image of the ball taken before the test, image B represents the image of the ball taken immediately after the test, therefore wear debris

and the transfer of coating can be observed in the image, finally image C shows the ball image after cleaning the ball using ethanol, to remove the transferred coating.

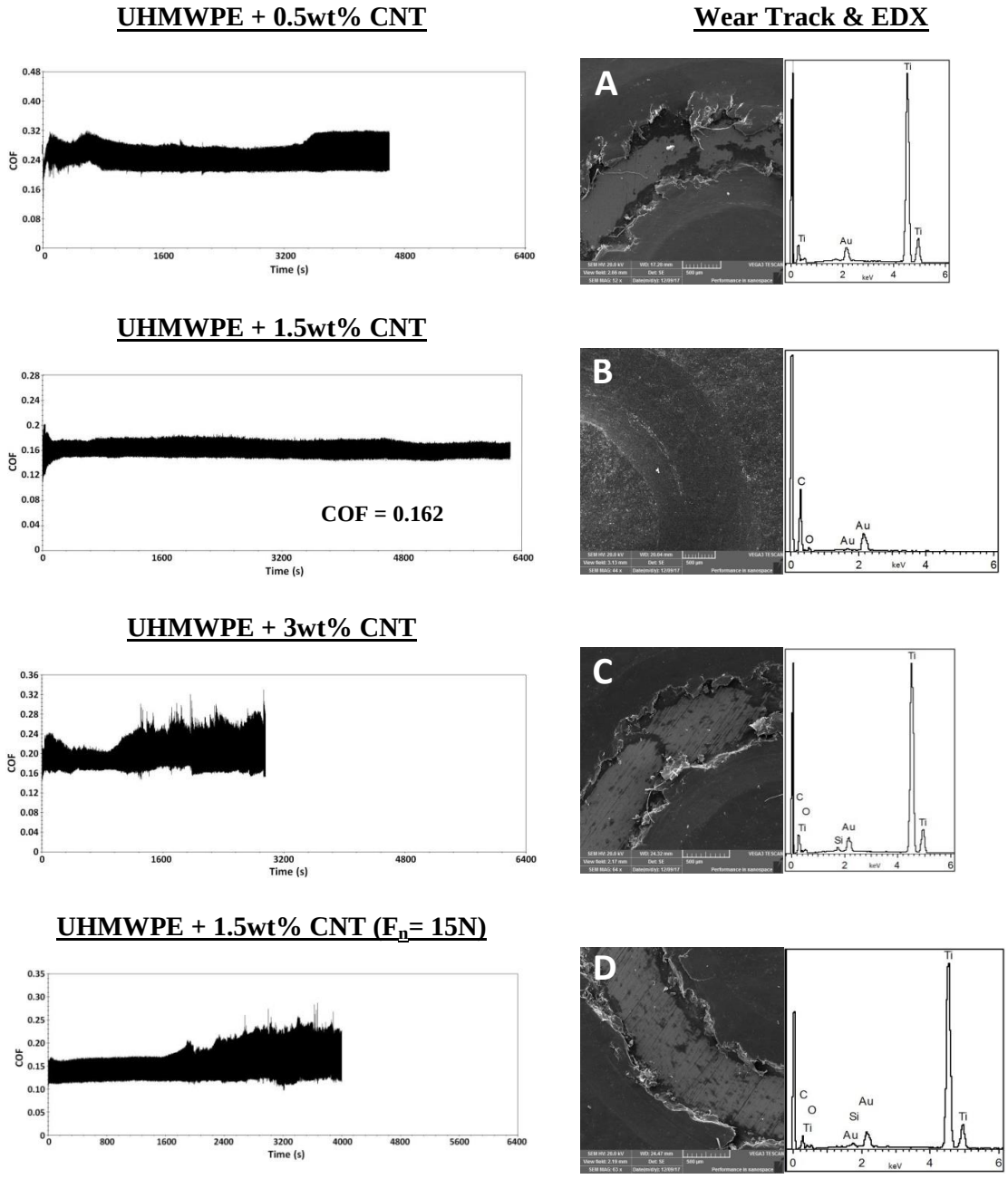

Figure 50: Typical COF graphs, SEM images of wear track and EDX analysis for nanocomposite coatings recorded after a wear test conducted at a normal load of 12N and a sliding velocity of 0.1m/s for 50,000 cycles

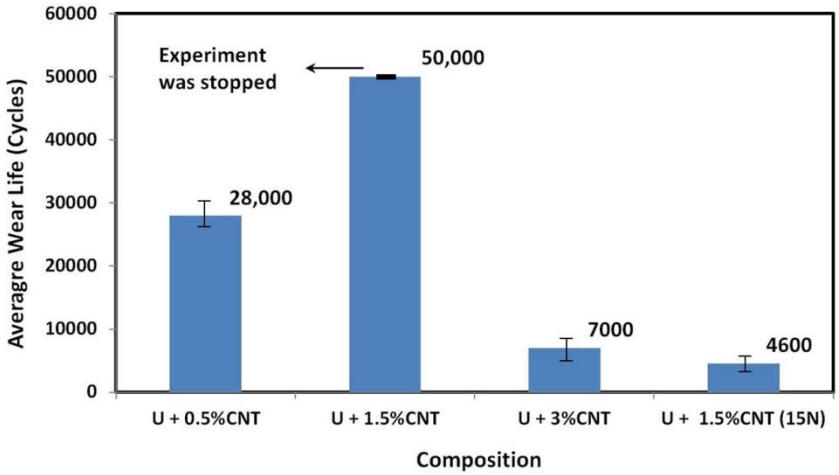

Figure 51: Average wear life of UHMWPE reinforced with different wt% CNT

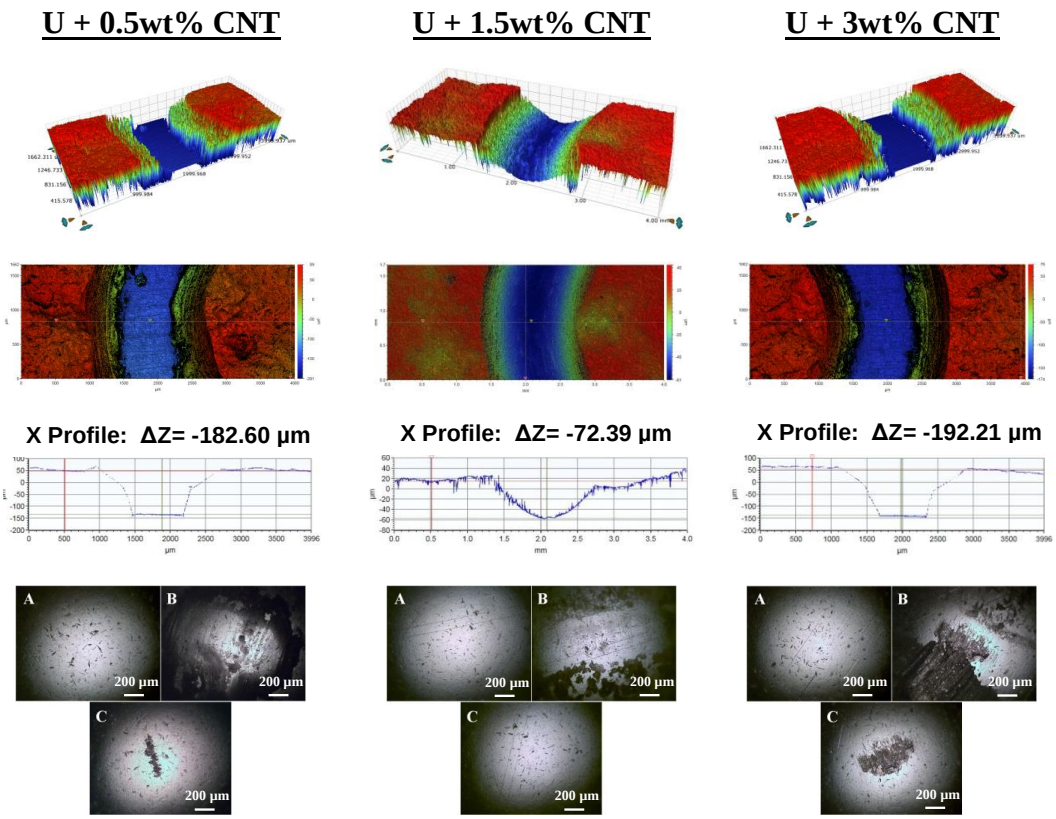

Figure 52: 3-D and 2-D Optical profiles and counterface ball images after the wear test conducted on UHMWPE nanocomposite coating, recorded at F_n=12N and v =0.1m/s for 50,000 cycles

It was observed that an addition of 0.5wt% CNT into the UHMWPE matrix was able to improve the wear life > 5000. However the coatings failed at ~ 28, 000 cycles, Failure of the coating can be seen in the SEM image in table 18, and the EDX analysis confirms the exposure of the substrate and the 2-D profile shows a profile depth of ~182µm which is approximately the coating thickness. However when wt% of CNT was increased to 1.5% CNT the coating did not fail and completed the 50,000 cycle test, whereas when the load was increased to 15N the coating failed < 5000 cycles and increasing the CNT% further to 3wt% also resulted in coating failure at ~ 7000 cycles.

The failure of UHMWPE reinforced with 0.5wt% CNT can be attributed to less quantity of CNT's dispersed in the UHMWPE matrix, therefore not many polymer chains are anchored with CNT's resulting in low load bearing capacity compared to 1.5wt% CNT where the CNT's anchor the polymer chains in a bridged manner. Conversely when UHMWPE is reinforced with 3wt% of CNT the coatings fail at approximately ~ 7000 cycles which can be ascribed to the agglomeration of CNT, clusters of CNT in the UHMWPE matrix as seen in the SEM images in section 4.2.2 resulting in poor tribology, agglomerated CNT's in the polymer matrix create a hard phase on the surface, resulting in an uneven surface morphology which consequently results in coating failure.

4.2.5 Evaluation of scratch resistance for UHMWPE reinforced with 1.5wt% CNT coating

UHMWPE reinforced with 1.5% CNT reaches complete failure at an avg load of 26.4N (see figure 53), which is an increase in 136.2% compared to pristine UHMWPE, thus addition of CNT, tremendously improves the adhesive strength of the coating. Figure 54 shows the SEM image after the coating has failed.

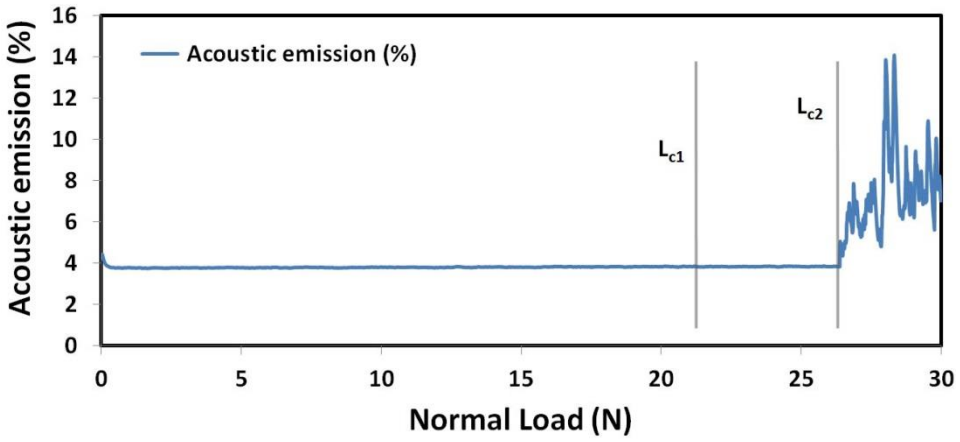

Figure 53: Acoustic emission and COF with respect to the applied normal load for UHMWPE reinforced with 1.5wt% CNT

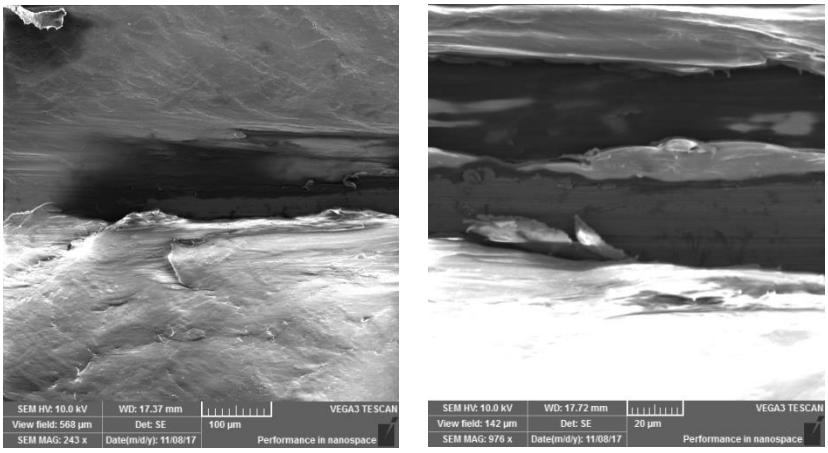

Figure 54: UHMWPE reinforced with 1.5wt% CNT - SEM image of scratch

4.3 Phase 3 – Optimization and characterization of hybrid nanocomposite UHMWPE reinforced with CNT and HA Coating

4.3.1 Dispersion of HA in UHMWPE reinforced with 1.5wt% CNT matrix

Figure 55 shows the SEM images of 3wt% HA reinforced with UHMWPE and 1.5% CNT. It can be observed that the HA plates have been disentangled and evenly distributed in the UHMWPE matrix along with the CNT's.

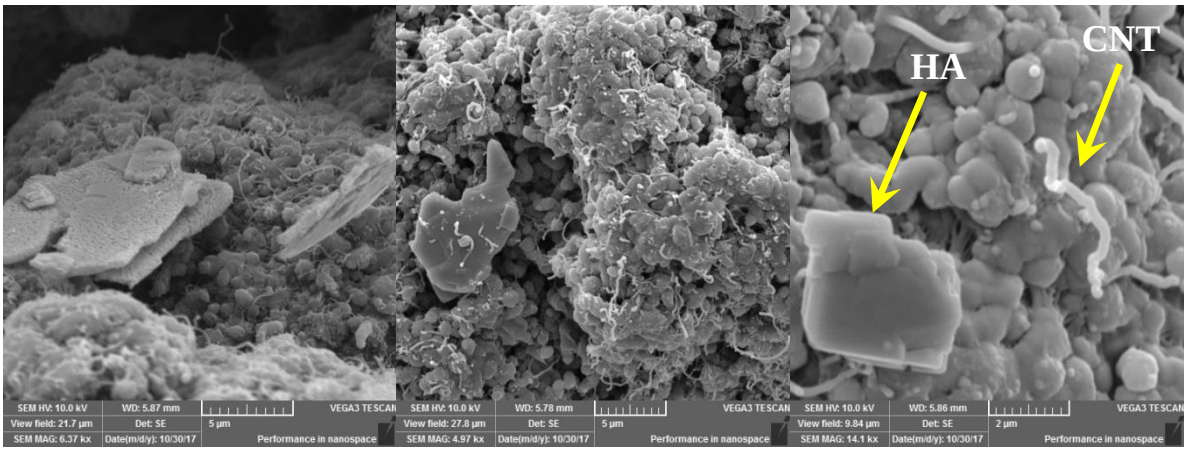

Figure 55: SEM images of UHMWPE reinforced with 1.5 % CNT and 3% HA

However, when the percentage of HA is increased from 3wt% to 5wt%, agglomerated HA plates were spotted as shown in figure 56. The poor dispersal of 5wt% HA in to the UHMWPE and 1.5%CNT matrix could result in diminishing the mechanical properties of the coating.

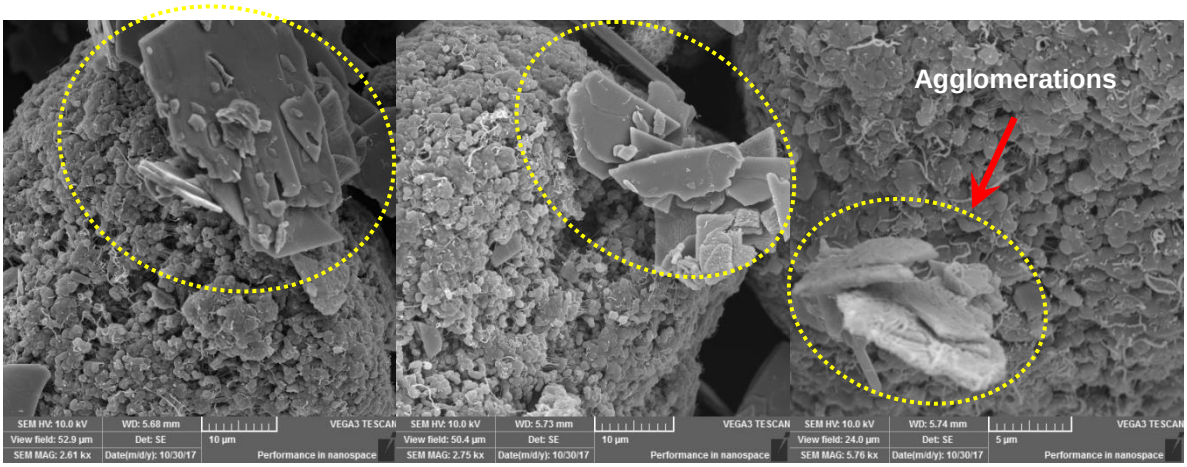

Figure 56: SEM images of UHMWPE reinforced with 1.5 % CNT and 5% HA

4.3.2 Hardness measurements of hybrid nanocomposite coating

Figure 57 shows the change in hardness and penetration depth for different compositions of HA added to UHMWPE reinforced with 1.5wt% CNT. A 22.1% increase in the

hardness value and a 9% decrease in penetration depth is observed for 0wt%HA to 3wt%HA.

The hardness and penetration depth were calculated from the average of 20 different indentations made at different locations on the sample.

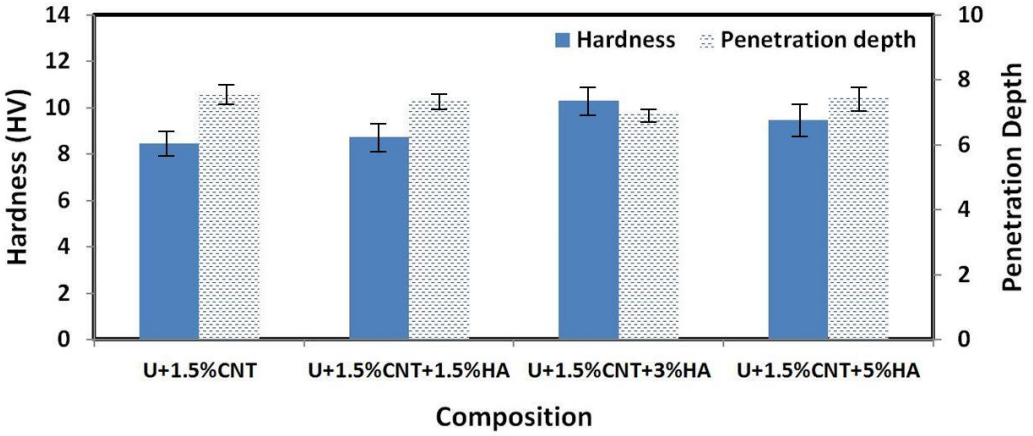

Figure 57: Hardness & Penetration depth Vs composition for U+1.5% CNT+X% HA

4.3.3 Tribological characterization of UHMWPE reinforced with 1.5wt% CNT and different wt% HA

Hydroxyapatite was integrated into the UHMWPE reinforced with 1.5%CNT matrix to improve the bioactivity and osteocoductivity of the coating. Furthermore studies show an improvement in mechanical properties upon addition of HA in UHMWPE matrix [90, 91].

Table 15 shows the different composition used for optimization. The load and number of cycles were kept constant throughout the test at 12N and 100,000 cycles respectively. Figure 58 shows the COF graphs along with the wear track and EDX analysis and figure 59 shows the average wear life for all compositions.

Table 15: Wear life test for UHMWPE reinforced with 1.5wt% CNT and different wt% HA for 100,000 Cycles

Test #	Sample Composition	Applied Load	No.of Cycles	Result
1	U + 1.5% CNT	12 N	100,000	Test did Not Fail
2	U + 1.5 % CNT + 0.5% HA	12N	100,000	Test did Not Fail
3	U + 1.5 % CNT + 1.5% HA	12 N	100,000	Test did Not Fail
4	U + 1.5 % CNT + 3% HA	12 N	100,000	Test did Not Fail
5	U + 1.5 % CNT + 5% HA	12 N	100,000	Test Failed

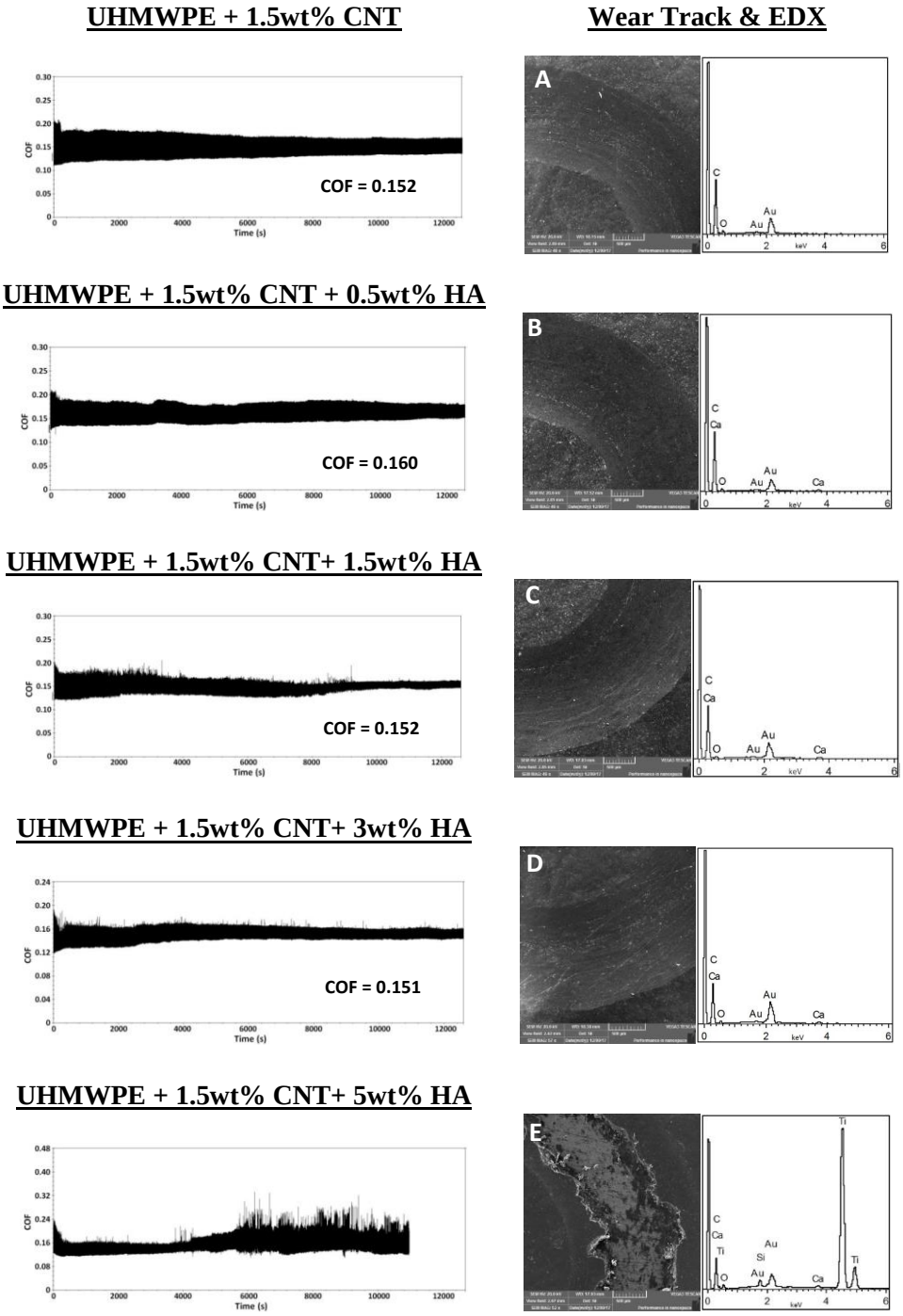

Figure 58: Typical COF graphs, SEM images of wear track and EDX analysis for Hybrid nanocomposite coatings, recorded after a wear test conducted at at FN= 12N, V= 0.1m/s 100,000 cycles

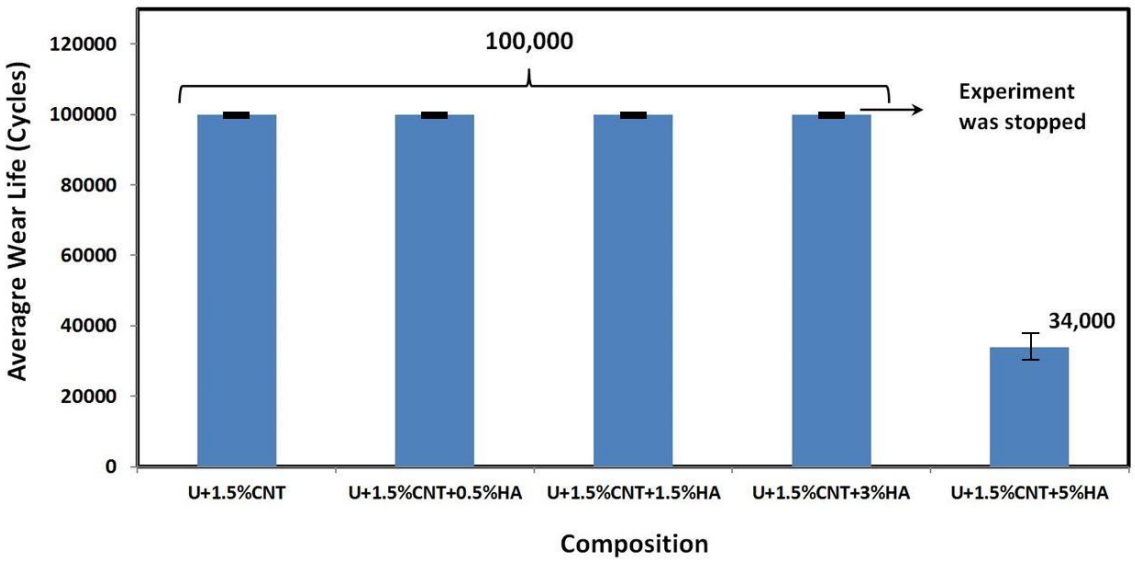

Figure 59: Average wear life of UHMWPE reinforced with 1.5wt% CNT and different wt% of HA for 100,000 cycles

Four compositions, UHMWPE reinforced with 1.5wt% CNT and the addition of 0.5wt% HA, 1.5wt% HA and 3wt% HA, completed the 100,000 cycle test without failure as, however increasing the percentage of HA to 5wt% from 3wt% resulted in failure of coating at ~ 34,000 cycles, due to agglomeration and pile up of HA plates as discussed in section 4.3.1.

Figure 60 shows the 3-D and 2-D optical profiles of the track along with the ball images. From the 2D plot It is observed that the profile depth decreases with the increase of HA content, this is clearly illustrated in figure 61.

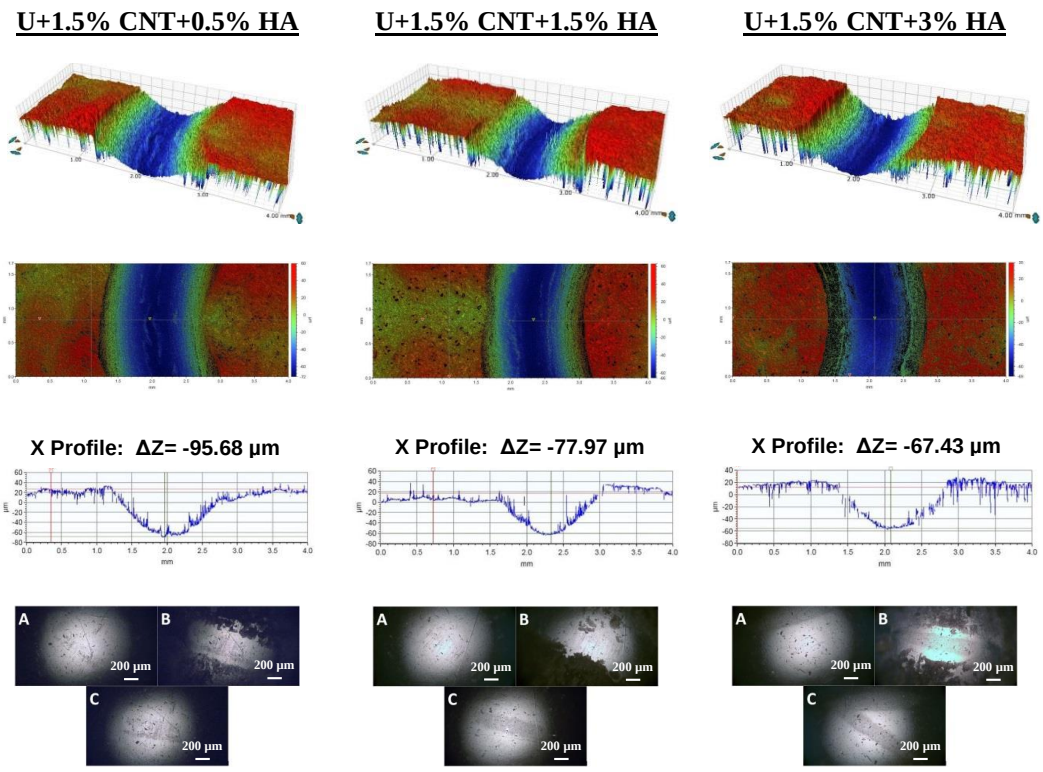

Figure 60: 3-D and 2-D Optical profiles and counterface ball images after the wear test conducted on UHMWPE hybrid nanocomposite coating, recorded at F_n=12N and v =0.1m/s for 100,000 cycles

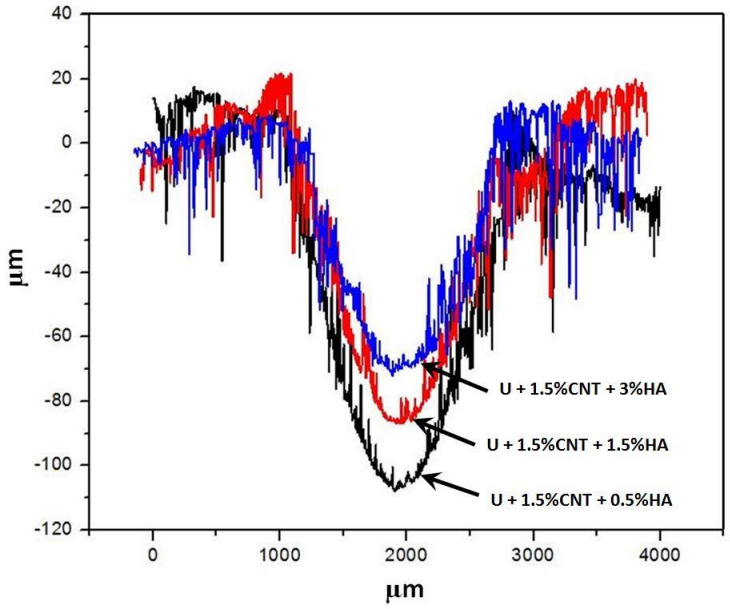

Figure 61: Depth comparison for Hybrid nanocomposite coating (100,000 cycles)

The same compositions were further tested at 250,000 cycles, with all the other parameters unchanged as shown in table 16. SEM image of the wear track along with EDX analysis and the COF graphs are depicted in figure 62 and figure 63 shows the average wear life for 250,000 cycles.

Table 16: Wear life test for UHMWPE reinforced with 1.5wt% CNT and different wt% HA for 250,000 Cycles

Test #	Sample Composition	Applied Load	No. of Cycles	Result
1	U + 1.5 % CNT	12 N	250,000	Test Failed
2	U+ 1.5%CNT+ 0.5%HA	12 N	250,000	Test did Not Fail
3	U+ 1.5%CNT+ 1.5%HA	12 N	250,000	Test did Not Fail
4	U+ 1.5%CNT+ 3%HA	12 N	250,000	Test did Not Fail

UHMWPE + 1.5wt% CNT **Wear Track & EDX**

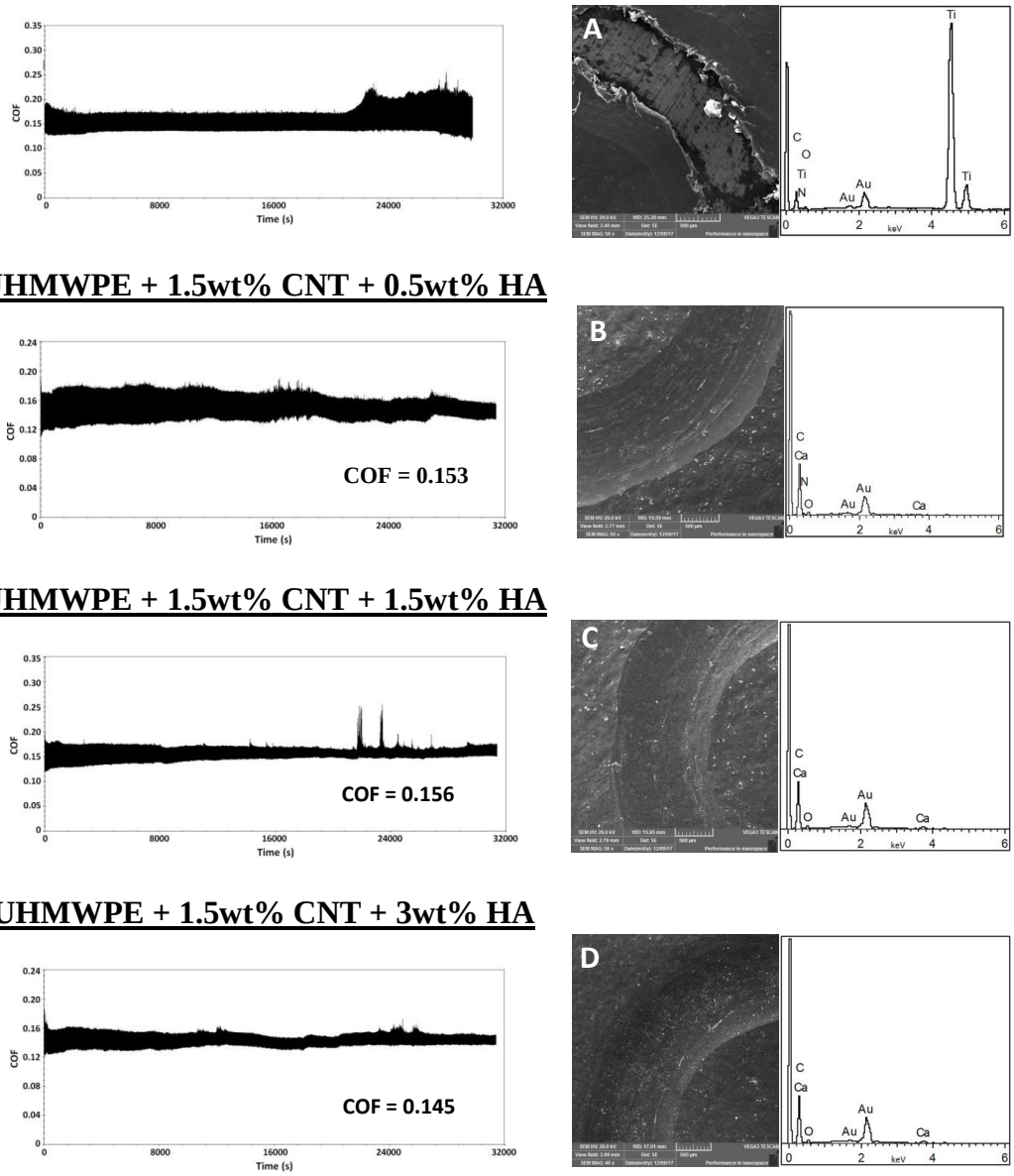

UHMWPE + 1.5wt% CNT + 0.5wt% HA

UHMWPE + 1.5wt% CNT + 1.5wt% HA

UHMWPE + 1.5wt% CNT + 3wt% HA

Figure 62: Typical COF graphs, SEM images of wear track and EDX analysis for Hybrid nanocomposite coatings, recorded after a wear test conducted at at FN= 12N, V= 0.1m/s 250,000 cycles

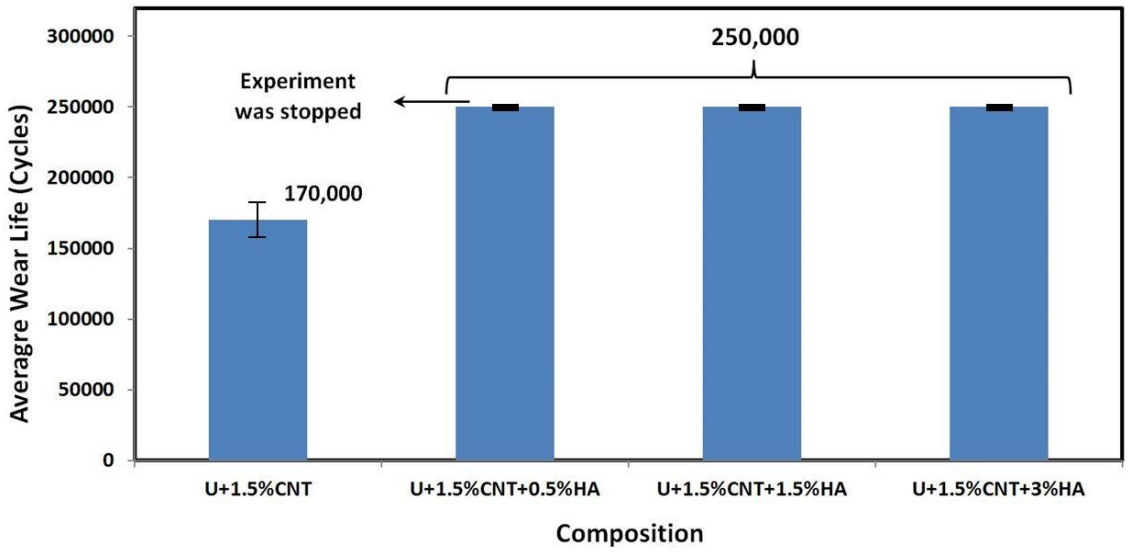

Figure 63: Average wear life of UHMWPE reinforced with 1.5wt% CNT and different wt% of HA for 250,000 cycles

UHMWPE reinforced with 1.5wt% CNT failed at an average wear life of 170,000 cycles. Whereas, the nanocomposite hybrid coating completed the 250,000 cycle test without failure. The 3-D and 2-D profiles of a single test are shown in figure 64. The decrease in profile depth with respect to the addition of HA was also observed for 250,000 cycles, for comparison the track depth for all the three compositions of HA is plotted in figure 65.

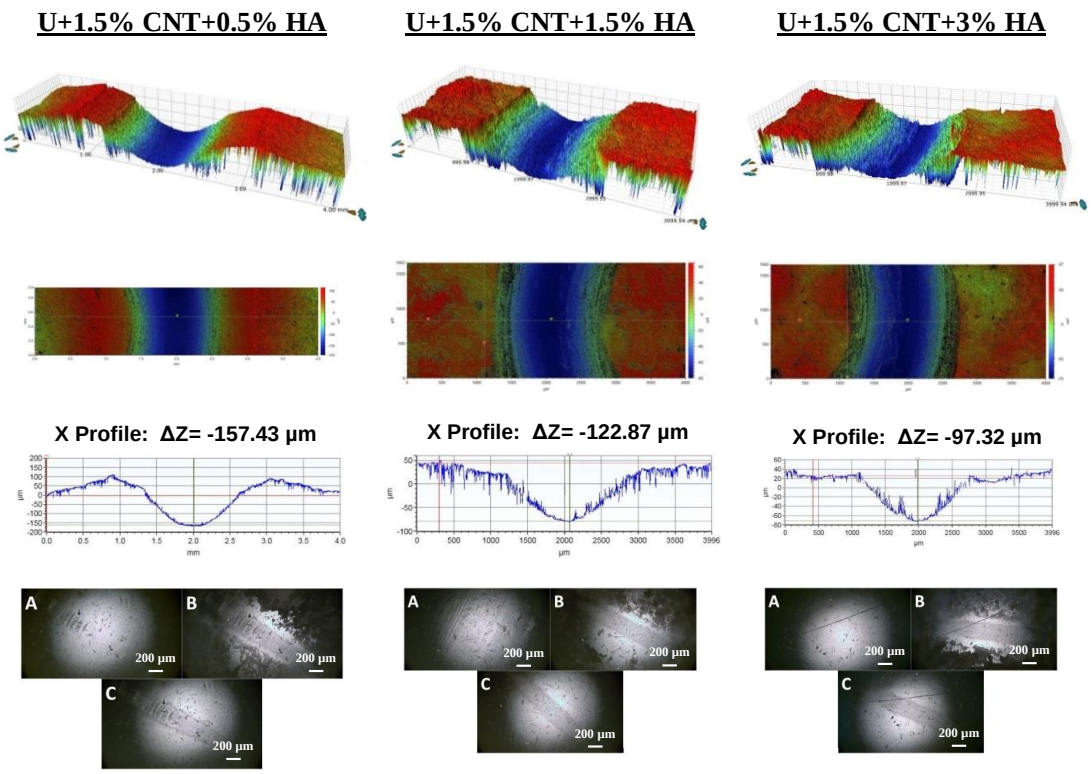

Figure 64: 3-D and 2-D Optical profiles and counterface ball images after the wear test conducted on UHMWPE hybrid nanocomposite coating, recorded at F_n=12N and v =0.1m/s for 250,000 cycles

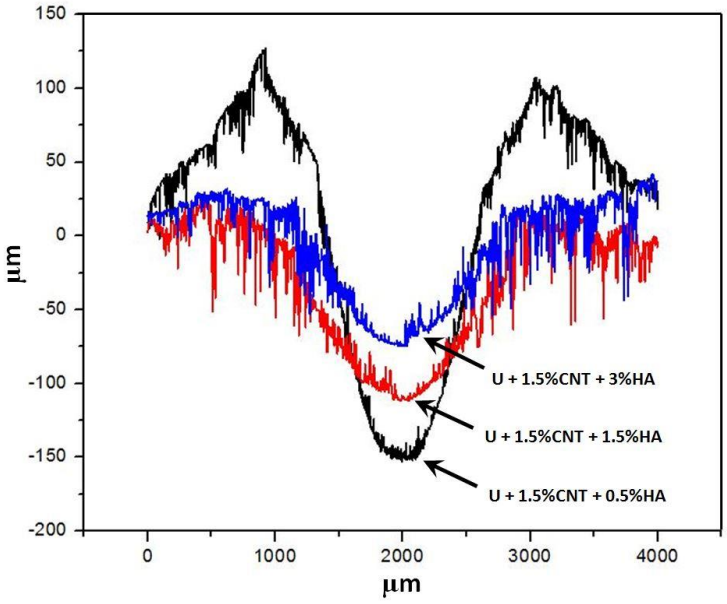

Figure 65: Depth comparison for Hybrid nanocomposite coating for 250,000 cycles

To evaluate and understand the individual performance of these three compositions i.e. 0.5wt%HA, 1.5wt%HA and 3wt% HA with UHMWPE and 1.5% CNT, the wear volume was calculated as shown in table 17.

It is observed that there is a 75.7% and only a 39.2% increase in depth when the number of cycles is increased from 100,000 cycles to 250,000 cycles for 0.5wt%HA and 3wt% HA respectively. Furthermore, a 70.7% and 42% increase in wear volume is seen for 0.5wt%HA and 3%HA upon increasing the number of cycles from 100,000 cycles to 250,000 cycles. Signifying the 3wt%HA as a more wear resistant coating compared to 0.5wt% and 1.5wt%. Figure 66 shows the increase in track depth for 3wt% HA reinforced with UHMWPE and 1.5wt% CNT.

Table 17: Percentage increase of Depth and wear volume for 100,000 cycles and 250,000 cycles

	100,000 Cycles		**250,000 Cycles**		**Depth**	**Wear Volume**
	Avg. Depth (µm)	Wear Volume (mm^3)	Avg. Depth (µm)	Wear Volume (mm^3)	%Increase	%Increase
U+1.5CNT+ 0.5HA	85.70	1.08	150.53	1.84	75.7	70.7
U+1.5CNT+ 1.5HA	79.72	1.06	122.05	1.78	53.1	68.2
U+1.5CNT+ 3HA	71.84	0.85	100.04	1.21	39.2	42

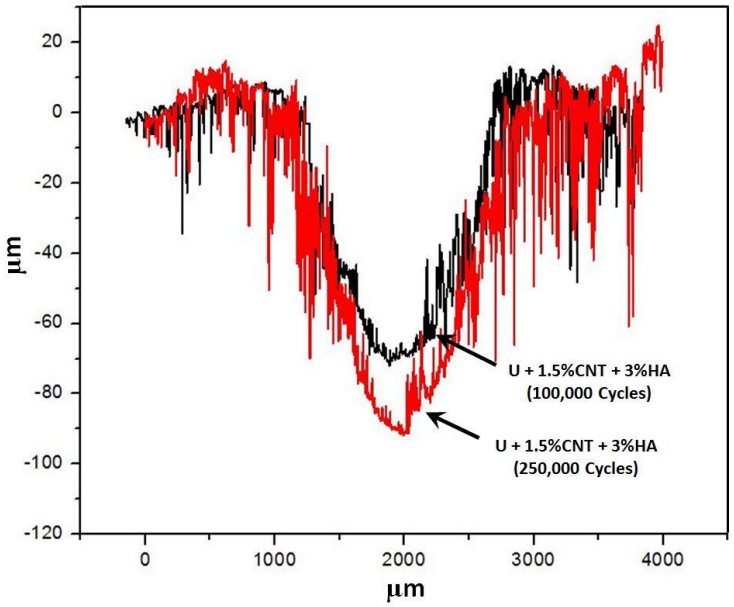

Figure 66: Track depth of UHMWPE reinforced with 1.5wt% CNT and 3wt% HA, for 100,000 cycles and 250,000 Cycles

4.3.4 Evaluation of scratch resistance for UHMWPE reinforced with 1.5wt% of CNT and 3wt% HA

The Hybrid nanocomposite coating, did not fail during scratch test, as shown in figures 67 and 68. Acoustic emission remains constant throughout the test indicating the indenter not being able to penetrate the coating and reach the substrate, implying a very adhesive coating, Fig 68 (A) shows the full length of the scratch and fig 68 (B) shows a location of the scratch at ~ 28N normal load.

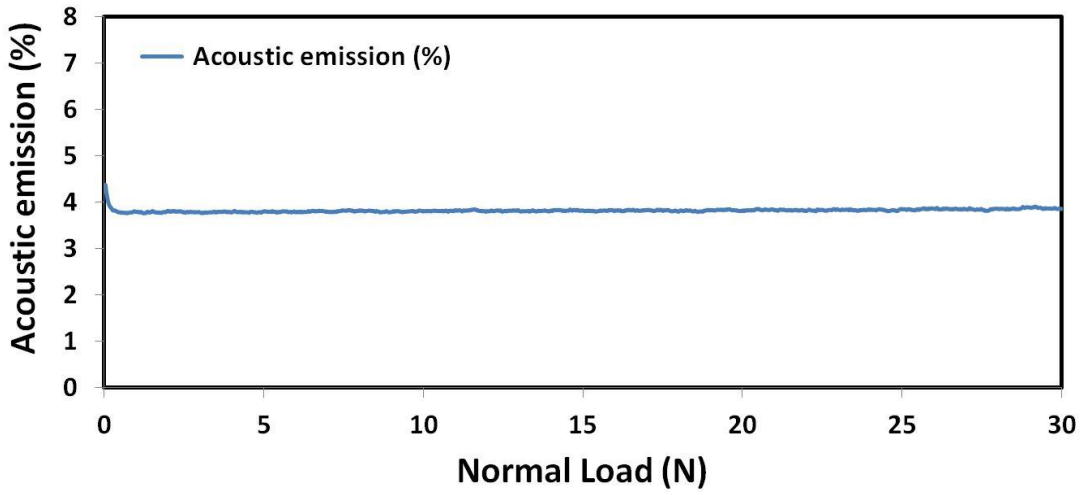

Figure 67: Acoustic emission with respect to the applied normal load for UHMWPE reinforced with 1.5wt% CNT and 3% HA

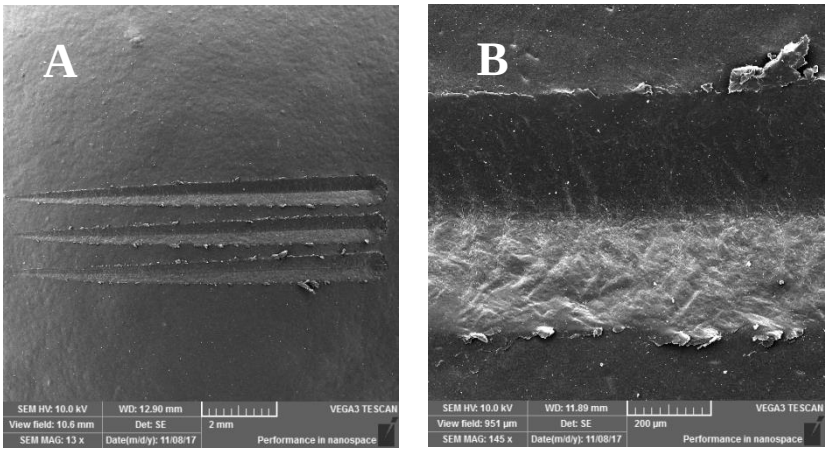

Figure 68: UHMWPE reinforced with 1.5% CNT and 3% HA - SEM image of scratch

4.3.5 Tribological characterization of UHMWPE reinforced with 1.5wt% CNT and 3wt% HA on Ti6Al4V and Ti20Nb13Zr

The optimized hybrid nanocomposite coating was further tested on two different substrates, i.e. Ti6Al4V and TI20Nb13Zr, to study the effect of substrate on the coating.

Figure 69 shows the COF along with the wear track and EDX analysis on titanium alloys and figure 70 and 71 shows the 3-D and 2-D profiles of wear track and Average wear life of the test respectively. The same test parameters were used, and no certain substrate effect was observed. The coating completed the 250,000 test without failure for all three tests for each individual substrate.

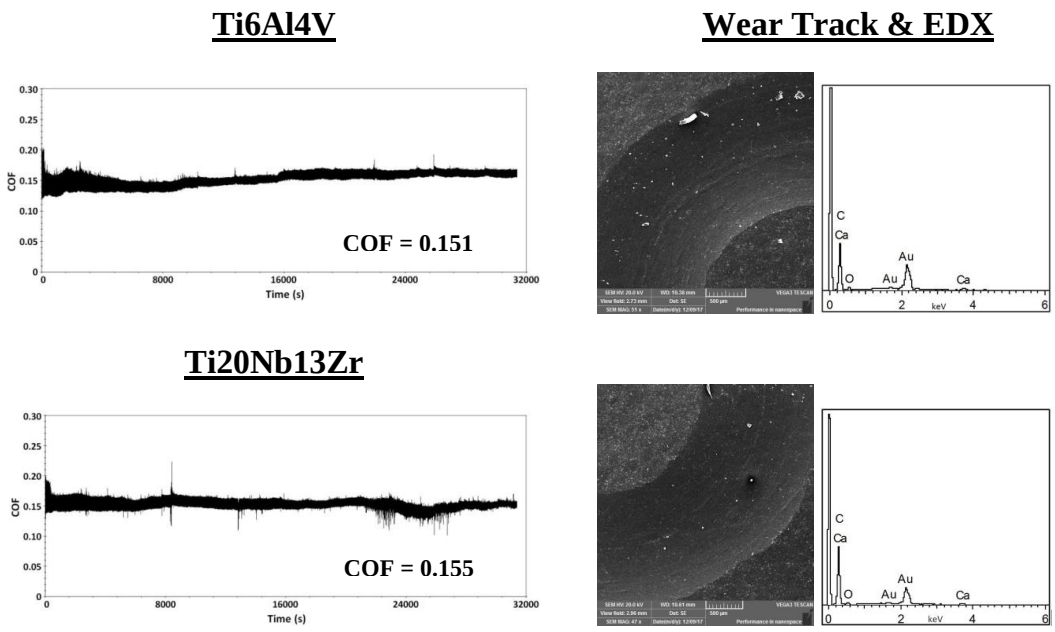

Figure 69: Typical COF graph, SEM images of wear track and EDX analysis of hybrid nanocomposite coating deposited on Titanium alloys, recorded after a wear test conducted at F_N= 12N and V= 0.1m/s for 250,000 cycles

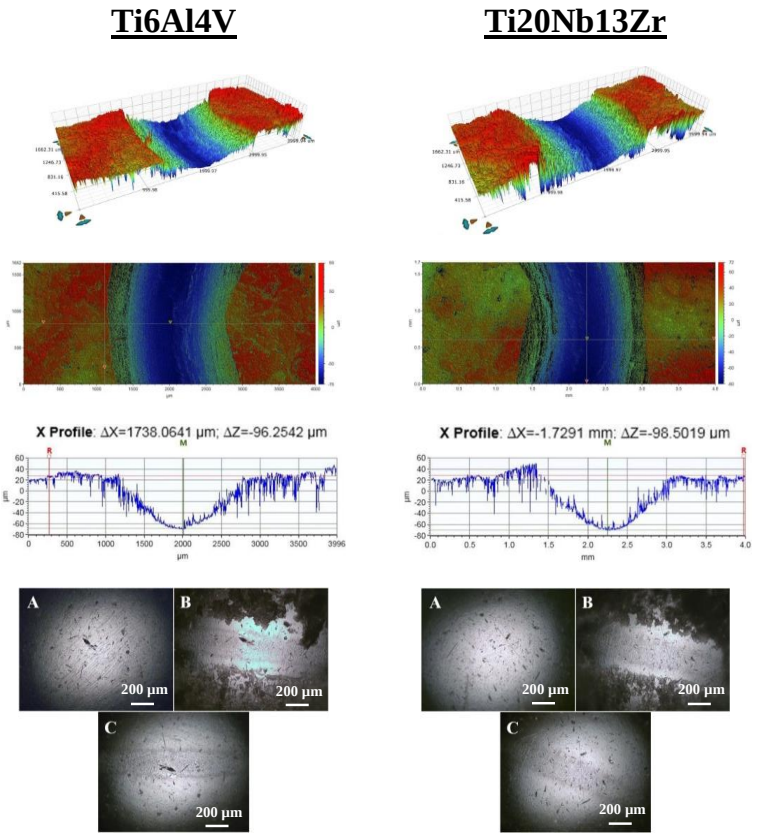

Figure 70: 3-D and 2-D Optical profiles and counterface ball images after the wear test conducted on the optimized Hybrid nanocomposite coating deposited on Ti6Al4V and Ti20Nb13Zr at F_N=12N and V =0.1m/s for 250,000 cycles

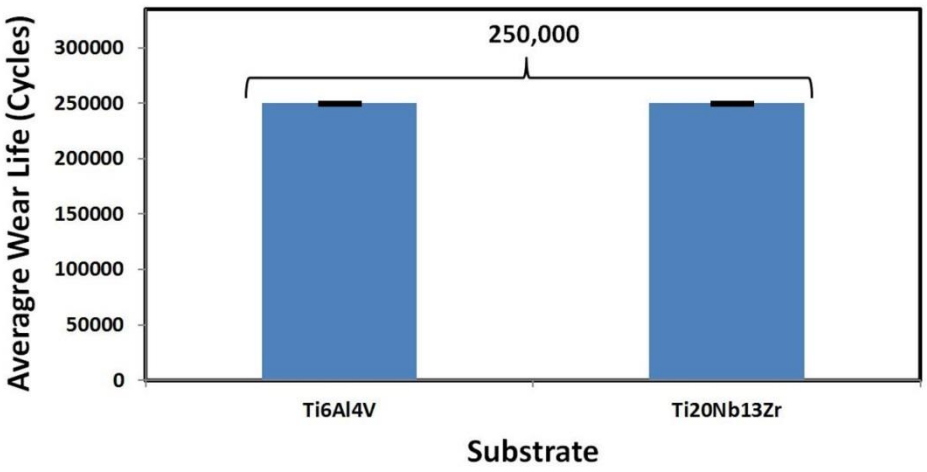

Figure 71: Average wear life of UHMWPE reinforced with 1.5wt% CNT and 3wt% HA on Titanium alloys

4.3.6 Comparison of the tribological performance of all the different bare substrates with the developed optimized hybrid nanocomposite coating

Tribological performance in terms of specific wear rate (SWR) and coefficient of friction (COF) of the developed optimized hybrid nanocomposite coating were compared to that of the different bare substrates to highlight the efficiency of the developed coatings in improving the wear life of the substrates. Specific wear rates (SWR) were calculated for the bare substrates and the optimized UHMWPE hybrid nanocomposite coating reinforced with 1.5wt% CNT and 3wt% HA as shown in Table 18. The coating had a considerable low SWR and low COF compared to all the bare substrates as can be seen from Table 18 and figure 72.

Table 18: Specific Wear Rate

Material	Avg COF	Specific wear rate (mm^3/Nm) x 10^{-4}
Pure Titanium	0.35	3.971
Ti6Al4V	0.31	2.681
Ti20Nb13Zr	0.24	1.498
U+1.5%CNT+3%HA	0.15	0.443

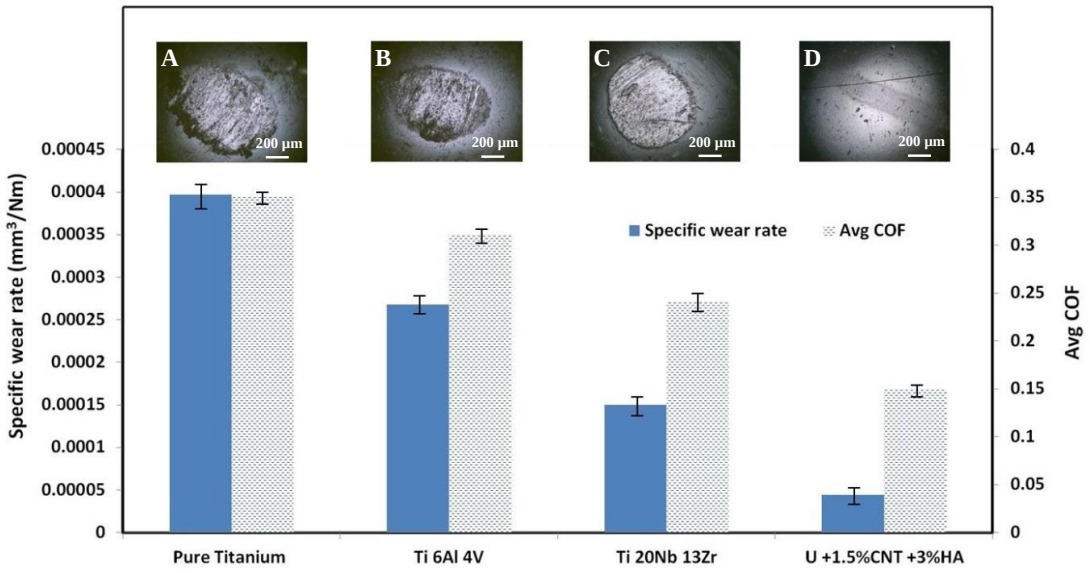

Figure 72: Specific Wear Rates/coefficient of friction for all the bare substrates and the Hybrid nanocomposite coating tested at FN= 12N and V= 0.1 m/s

It is to be noted that in a tribological application, the wear life of both the mating surfaces is of utmost importance. The coating or surface modification done to improve the tribological properties of one of the mating surfaces should be able to protect even the counterface material from wear and tear for a successful tribological performance of the complete system. As can be seen from the figure 64, that the specific wear rate and the COF for the developed hybrid nanocomposite coating is significantly low as compared to that of all the bare substrates. But it is interesting to note that; even the counterface ball which slid against the developed hybrid nanocomposite coating shows no signs of wear and tear as can be clearly seen from the optical image of the ball (figure 64 (d)) recorded after a test of 250,000 cycles signifying the improved tribological performance of the coating to protect the complete system. However, the counterface balls sliding against the bare substrates show big scar marks only after a test run for 2400 cycles as shown in figure 64 (a-c).

Therefore the developed and optimized hybrid nanocomposite coating was not only successful in reducing the COF and SWR of the titanium alloys but also was effective in protecting the wear and tear of the counterface.

4.3.7 Corrosion test of hybrid nanocomposite UHMWPE reinforced with 1.5wt% CNT and 3wt% HA coating

Figure 73 shows the monitoring of Open Circuit Potential (OCP) values for uncoated and coated Ti6al4V alloy substrates in SBF medium. It can be observed that the OCP values of Ti6al4V with UHMWPE coatings shifted to noble direction and in particular UHMWPE reinforced with 1.5wt% CNT and 3wt% HA offered the noblest shift in potential. This behavior indicated that the corrosion protection performance of UHMWPE coatings is enhanced with the incorporation of 1.5tw% CNTs and 3wt% HA. Further to get the clear insight, EIS is performed to validate the obtained OCP results.

Figure 74 represents the EIS data in Bode formats. Initial reflection of the Bode graphs (Fig. 66), all of the coated samples suggests different EIS curves with the uncoated Ti64. For uncoated substrates, large phase angle continued about -80^{o} at mid and low frequency regions while the slope of resistant curves is found to be about -1, representing the distinctive result of a capacitive behavior of native passive layer. In contrast, two maxima in phase angle was obtained at the high and low frequency regions in the case of coated Ti6Al4V samples, which is revealing the association of at least two time constants related with the two-layer structure of the coated Ti6Al4V samples. The impedance in the low frequency region for the coated Ti6Al4V substrates appears to be nearly four order of magnitude higher than that showed by the uncoated Ti6Al4V substrate. The higher impedance is possibly due to a barrier performance where the coating is obstructive

admittance of the hostile electrolytic species toward the metal/coating interface. In particular, the coatings with the incorporation of 1.5wt% CNTs and 3wt% HA exhibited the highest impedance values which confirmed the enhanced behavior of the coatings.

Corrosion potential is shifted to noble direction due to the HA incorporated coatings.

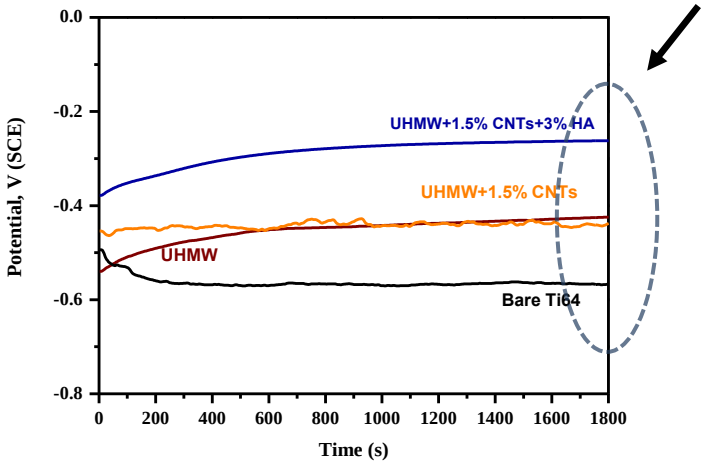

Figure 73: Monitoring of open circuit potential values

Corrosion resistance of Ti64 is increased by the HA incorporated coatings

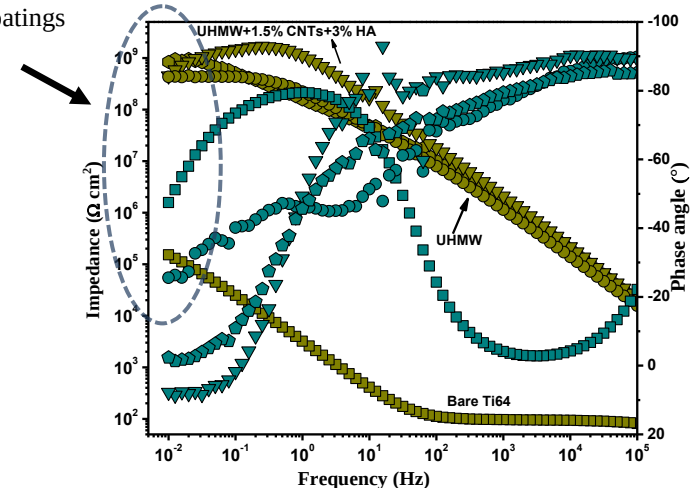

Figure 74: Electrochemical impedance spectroscopy

CHAPTER 5

CONCLUSIONS AND RECOMMENDATIONS

This study was commenced to develop a novel UHMWPE hybrid nanocomposite coating implemented by an electrostatic spray coating technique to modify the surface of titanium and its alloys to enhance its tribological properties.

Carbon nanotubes were used as reinforcement in the UHMWPE matrix to enhance the load bearing capacity of UHMWPE by anchoring the polymer chains in a bridged manner. Different weight percentage (0.5wt%, 1.5wt%, and 3wt %) of CNT's were reinforced in the UHMWPE matrix and optimized based on the tribological results.

Hydroxyapatite was incorporated into the nanocomposite coating to enhance the biocompatibility and improve the mechanical properties of the UHMWPE reinforced with CNT nanocomposite coating. The weight percentages used for optimization hydroxyapatite content were 0.5wt%, 1.5wt%, 3wt% and 5wt%. Similar to the nanocomposite coating the Hybrid nanocomposite coating was also optimized based on the tribological outcome of the coating.

Pure titanium – Grade 2 was used for all the experiments during the optimization process, prior to spray coating the substrates were grinded, ultra-sonic cleaning with acetone, plasma treated and pre-heat treated to improve the adhesion of the coating.

The effect of plasma treatment on the water contact angle was evaluated. There was a significant drop of up to 79.1% in WCA after plasma treatment compared to before

plasma treatment suggesting an increase in surface energy by carbon cleaning and oxidation effect.

Plasma treated substrates were electrostatic spray coated with pristine UHWMPE in phase 1 and in phase 2 CNT's were reinforced in UHMWPE to form a nanocomposite coating (0.5%, 1.5% and 3% CNT), and finally in phase 3, hydroxyapatite was reinforced in the nanocomposite coating to form a hybrid nanocomposite coating (0.5%, 1.5%,3% and 5% HA).

The effect of load on the tribological behavior of pristine UHMWPE was evaluated. The coating failed at approximately 3600 cycles for a load 12N with a sliding velocity of 0.1 m/s. Aadditionally, initial failure was observed at a load of 7.3N and complete failure for a load of 10.2N during a linear progressive scratch test.

Raman spectroscopy of the nanocomposite coating showed a higher shift in the G-band for 1.5wt%CNT compared to 0.5wt% and 3wt% CNT suggesting a much even distribution for 1.5wt% CNT. Also SEM analysis revealed a uniform distribution for 1.5wt% of CNT and less quantity of CNT for 0.5wt% of CNT whereas for 3wt% of CNT, clusters of CNT agglomerates were observed. Hardness measurement revealed increases in ~37% hardness for 0wt% CNT to 3wt% CNT reinforced with UHMWPE. Moreover, 0.5wt% and 3wt% of CNT failed at 28,000 cycles and 7000 cycles during a 50,000 cycle wear test cycles at a load of 12N and a sliding velocity of 0.1m/s, whereas 1.5wt% CNT did not fail as a result of uniform CNT distribution, and the ability to anchor the pristine UHMWPE chains in a bridged manner. The failure of 1.5wt% CNT is due to lack of CNT whereas failure of 3wt% CNT is attributed to agglomeration as observed during SEM

analysis. Scratch analysis indicated an initial failure of 21.8N and a complete failure at 24.8N for 1.5wt% CNT reinforced with UHMWPE nanocomposite coating.

SEM analysis of UHMWPE nanocomposite coating was assessed, A uniform distribution was observed for 3wt%HA, conversely agglomerated and pile up of HA plate were spotted for 5wt%HA. Hardness measurement revealed increases in ~22.1% hardness for 0wt% CNT to 3wt% HA reinforced with UHMWPE and 1.5wt%CNT.

UHMWPE Nanocomposite hybrid coating with 1.5wt% CNT reinforced in UHMWPE and the addition of 0.5wt%HA/ 1.5wt%HA and 3wt%HA did not fail during the 100,000cycle and 250,000cycle wear test. However difference in track depth was observed. U+1.5%CNT + 0.5%HA had the highest increase in track depth ~75.7%, while U+1.5%CNT + 3%HA had the lowest increase in track depth ~37.2%, in addition the coating did not fail during a linear progressive scratch analysis for 3wt% HA.

Wear life test was conducted on Ti6Al4V and Ti20Nb13Zr coated with the optimized UHMWPE nanocomposite coating (UHMWPE reinforced with 1.5wt% CNT and 3wt%HA), the coating did not fail the 250,000 cycle test.

Corrosion test for the optimized hybrid nanocomposite coating revealed a noble shift in potential for the OCP value and the highest impedance value which confirms the enhanced behavior of the coating.

Future research should be focused on evaluating the tribological performance of the nanocomposite coating in SBF solution and performing tribological characterization with different counterface material. Further in vivo and in vitro studies should be conducted to evaluate the biocompatibility of the coating.

REFERENCES

1. Basalah, A.; Shanjani, Y.; Esmaeili, S.; Toyserkani, E. Characterizations of additive manufactured porous titanium implants. *J. Biomed. Mater. Res. - Part B Appl. Biomater.* **2012**, *100 B*, 1970–1979, doi:10.1002/jbm.b.32764.
2. Ramakrishna, S.; Mayer, J.; Wintermantel, E.; Leong, K. W. Biomedical applications of polymer-composite materials: A review. *Compos. Sci. Technol.* **2001**, *61*, 1189–1224, doi:10.1016/S0266-3538(00)00241-4.
3. Patel, N.; Gohil, P. A review on biomaterials: scope, applications & human anatomy significance. *Int. J. Emerg. Technol. Adv. Eng.* **2012**, *2*, 91–101.
4. Saleh, K. J.; Thongtrangan, I.; Schwarz, E. M. Osteolysis: medical and surgical approaches. *Clin. Orthop. Relat. Res.* **2004**, 138–147, doi:10.1097/01.blo.0000142288.66246.4d.
5. Ching, H. A.; Choudhury, D.; Nine, M. J.; Azuan, N.; Osman, A. Effects of surface coating on reducing friction and wear of orthopaedic implants. *Sci. Technol. Adv. Mater. Sci. Technol. Adv. Mater* **2014**, *15*, 14402–21, doi:10.1088/1468-6996/15/1/014402.
6. Teoh, S. H. Fatigue of biomaterials: A review. *Int. J. Fatigue* **2000**, *22*, 825–837, doi:10.1016/S0142-1123(00)00052-9.
7. Manhabosco, T. M.; Muller, I. L. Electrodeposition of diamond-like carbon (DLC) films on Ti. *Appl. Surf. Sci.* **2009**, *255*, 4082–4086, doi:10.1016/j.apsusc.2008.10.087.
8. Niinomi, M. Fatigue characteristics of metallic biomaterials. *Int. J. Fatigue* **2007**, *29*, 992–1000, doi:10.1016/j.ijfatigue.2006.09.021.

9. Minn, M.; Sinha, S. K. DLC and UHMWPE as hard / soft composite film on Si for improved tribological performance. **2008**, *202*, 3698–3708, doi:10.1016/j.surfcoat.2008.01.012.

10. Bakshi, S. R.; Balani, K.; Laha, T.; Tercero, J.; Agarwal, A. The Nanomechanical and Nanoscratch Properties of MWNT- Reinforced Ultrahigh-Molecular- Weight Polyethylene Coatings *. **2007**, 50–53.

11. Bao, Y.; Zhang, T.; Systems, E.; South, L. Influence of composition and process parameters on the thermal spray deposition of UHMWPE coatings. **2015**, *0*, 77–85.

12. Samad, M. A.; Satyanarayana, N.; Sinha, S. K. Surface & Coatings Technology Tribology of UHMWPE film on air-plasma treated tool steel and the effect of PFPE overcoat. *Surf. Coat. Technol.* **2010**, *204*, 1330–1338, doi:10.1016/j.surfcoat.2009.09.011.

13. Samad, M. A.; Sinha, S. K. Dry sliding and boundary lubrication performance of a UHMWPE/CNTs nanocomposite coating on steel substrates at elevated temperatures. *Wear* **2011**, *270*, 395–402, doi:10.1016/j.wear.2010.11.011.

14. Balani, K.; Chen, Y.; Harimkar, S. P.; Dahotre, N. B.; Agarwal, A. Tribological behavior of plasma-sprayed carbon nanotube-reinforced hydroxyapatite coating in physiological solution. *Acta Biomater.* **2007**, *3*, 944–951, doi:10.1016/j.actbio.2007.06.001.

15. Bakshi, S. R.; Balani, K.; Laha, T.; Tercero, J.; Agarwal, A.; Anderson, R.; Laha, T.; Andara, M.; Tercero, J.; Crumpler, E.; Agarwal, A.; Chen, Y.; Harimkar, S. P.; Dahotre, N. B.; Gupta, A.; Tripathi, G.; Basu, B.; Lahiri, D.; Balani, K. Plasma-

sprayed carbon nanotube reinforced hydroxyapatite coatings and their interaction with human osteoblasts in vitro. *Biomaterials* **2007**, *28*, 618–624, doi:10.1016/j.biomaterials.2006.09.013.

16. Robert M. Pilliar *Biomedical materials*; 2009; ISBN 9780387848716.
17. Niinomi, M. Metallic biomaterials. *Biomed. Mater.* **2008**, 41–81, doi:10.1007/978-0-387-84872-3_2.
18. Loir, A. S.; Garrelie, F.; Donnet, C.; Subtil, J. L.; Belin, M.; Forest, B.; Rogemond, F.; Laporte, P. Mechanical and tribological characterization of tetrahedral diamond-like carbon deposited by femtosecond pulsed laser deposition on pre-treated orthopaedic biomaterials. *Appl. Surf. Sci.* **2005**, *247*, 225–231, doi:10.1016/j.apsusc.2005.01.129.
19. Hoseini, M.; Jedenmalm, A.; Boldizar, A. Tribological investigation of coatings for artificial joints. *Wear* **2008**, *264*, 958–966, doi:10.1016/j.wear.2007.07.003.
20. Navarro, M.; Michiardi, a; Castaño, O.; Planell, J. a Biomaterials in orthopaedics. *J. R. Soc. Interface* **2008**, *5*, 1137–1158, doi:10.1098/rsif.2008.0151.
21. Hussein, M.; Mohammed, A.; Al-Aqeeli, N. Wear Characteristics of Metallic Biomaterials: A Review. *Materials (Basel).* **2015**, *8*, 2749–2768, doi:10.3390/ma8052749.
22. Balagna, C.; Faga, M. G.; Spriano, S. Tribological behavior of a Ta-based coating on a Co-Cr-Mo alloy. *Surf. Coatings Technol.* **2014**, *258*, 1159–1170, doi:10.1016/j.surfcoat.2014.07.016.
23. Cobb, A. G.; Schmalzreid, T. P. The clinical significance of metal ion release from cobalt-chromium metal-on-metal hip joint arthroplasty. *Proc. Inst. Mech. Eng.*

Part H-Journal Eng. Med. **2006**, *220*, 385–398, doi:10.1243/09544119jeim78.

24. Sidambe, A. T. Biocompatibility of advanced manufactured titanium implants-A review. *Materials (Basel).* **2014**, *7*, 8168–8188, doi:10.3390/ma7128168.

25. Luo, Y.; Ge, S.; Jin, Z.; Fisher, J. Effect of surface modification on surface properties and tribological behaviours of titanium alloys. *Proc. Inst. Mech. Eng. Part JJournal Eng. Tribol.* **2009**, *223*, 311–316, doi:10.1243/13506501jet488.

26. Liu, X.; Chu, P. K.; Ding, C. Surface modification of titanium, titanium alloys, and related materials for biomedical applications. *Mater. Sci. Eng. R Reports* **2004**, *47*, 49–121, doi:10.1016/j.mser.2004.11.001.

27. Kulkarni, M.; Mazare, A.; Schmuki, P.; Iglič, A. Biomaterial surface modification of titanium and titanium alloys for medical applications. *Nanomedicine* **2014**, 111–136, doi:10.1016/j.carbon.2011.02.021.

28. Kurella, A. *Review paper: Surface Modification for Bioimplants: The Role of Laser Surface Engineering*; 2005; Vol. 20; ISBN 0885328205.

29. Forch, R.; Chifen, A. N.; Bousquet, A.; Khor, H. L.; Jungblut, M.; Chu, L. Q.; Zhang, Z.; Osey-Mensah, I.; Sinner, E. K.; Knoll, W. Recent and expected roles of plasma-polymerized films for biomedical applications. *Chem. Vap. Depos.* **2007**, *13*, 280–294, doi:10.1002/cvde.200604035.

30. Kane, S. R.; Ashby, P. D.; Pruitt, L. A. Characterization and tribology of PEG-like coatings on UHMWPE for total hip replacements. *J. Biomed. Mater. Res. - Part A* **2010**, *92*, 1500–1509, doi:10.1002/jbm.a.32484.

31. Koseki, H.; Shindo, H.; Baba, K.; Fujikawa, T.; Sakai, N.; Sawae, Y.; Murakami, T. Surface-engineered metal-on-metal bearings improve the friction and wear

properties of local area contact in total joint arthroplasty. *Surf. Coatings Technol.* **2008**, *202*, 4775–4779, doi:10.1016/j.surfcoat.2008.04.060.

32. Dearnaley, G.; Arps, J. H. Biomedical applications of diamond-like carbon (DLC) coatings: A review. *Surf. Coatings Technol.* **2005**, *200*, 2518–2524, doi:10.1016/j.surfcoat.2005.07.077.

33. Vitu, T.; Polcar, T.; Cvrcek, L.; Novak, R.; Macak, J.; Vyskocil, J.; Cavaleiro, A. Structure and tribology of biocompatible Ti-C:H coatings. *Surf. Coatings Technol.* **2008**, *202*, 5790–5793, doi:10.1016/j.surfcoat.2008.06.040.

34. Kao, W. H.; Su, Y. L.; Yao, S. H. Tribological property and drilling application of Ti-C:H and Cr-C:H coatings on high-speed steel substrates. *Vacuum* **2006**, *80*, 604–614, doi:10.1016/j.vacuum.2005.10.005.

35. Kulikovsky, V.; Kuzmichev, A.; Bohac, P.; Hubička, Z.; Jurek, K.; Jastrabik, L. Composition of Ti-C:H films obtained by pulsed and continuous magnetron sputtering. *Surf. Coatings Technol.* **2005**, *200*, 620–624, doi:10.1016/j.surfcoat.2005.02.130.

36. Zhou, Y.; Li, M.; Cheng, Y.; Zheng, Y. F.; Xi, T. F.; Wei, S. C. Tantalum coated NiTi alloy by PIIID for biomedical application. *Surf. Coatings Technol.* **2013**, *228*, 2–6, doi:10.1016/j.surfcoat.2012.11.002.

37. Balagna, C.; Faga, M. G.; Spriano, S. Tantalum-based multilayer coating on cobalt alloys in total hip and knee replacement. *Mater. Sci. Eng. C* **2012**, *32*, 887–895, doi:10.1016/j.msec.2012.02.007.

38. Balla, V. K.; Banerjee, S.; Bose, S.; Bandyopadhyay, A. Direct laser processing of a tantalum coating on titanium for bone replacement structures. *Acta Biomater.*

2010, *6*, 2329–2334, doi:10.1016/j.actbio.2009.11.021.

39. Hahn, B. D.; Lee, J. M.; Park, D. S.; Choi, J. J.; Ryu, J.; Yoon, W. H.; Lee, B. K.; Shin, D. S.; Kim, H. E. Mechanical and in vitro biological performances of hydroxyapatite-carbon nanotube composite coatings deposited on Ti by aerosol deposition. *Acta Biomater.* **2009**, *5*, 3205–3214, doi:10.1016/j.actbio.2009.05.005.

40. Kwok, C. T.; Wong, P. K.; Cheng, F. T.; Man, H. C. Characterization and corrosion behavior of hydroxyapatite coatings on Ti6Al4V fabricated by electrophoretic deposition. *Appl. Surf. Sci.* **2009**, *255*, 6736–6744, doi:10.1016/j.apsusc.2009.02.086.

41. Chen, Y.; Zhang, Y. Q.; Zhang, T. H.; Gan, C. H.; Zheng, C. Y.; Yu, G. Carbon nanotube reinforced hydroxyapatite composite coatings produced through laser surface alloying. *Carbon N. Y.* **2006**, *44*, 37–45, doi:10.1016/j.carbon.2005.07.011.

42. Balani, K.; Anderson, R.; Laha, T.; Andara, M.; Tercero, J.; Crumpler, E.; Agarwal, A. Plasma-sprayed carbon nanotube reinforced hydroxyapatite coatings and their interaction with human osteoblasts in vitro. *Biomaterials* **2007**, *28*, 618–624, doi:10.1016/j.biomaterials.2006.09.013.

43. Chen, Y.; Zhang, T. H.; Gan, C. H.; Yu, G. Wear studies of hydroxyapatite composite coating reinforced by carbon nanotubes. *Carbon N. Y.* **2007**, *45*, 998–1004, doi:10.1016/j.carbon.2006.12.021.

44. Abdul Samad, M.; Sinha, S. K. Nanocomposite UHMWPE-CNT polymer coatings for boundary lubrication on aluminium substrates. *Tribol. Lett.* **2010**, *38*, 301–311, doi:10.1007/s11249-010-9610-8.

45. Panjwani, B.; Satyanarayana, N.; Sinha, S. K. Tribological characterization of a

biocompatible thin film of UHMWPE on Ti6Al4V and the effects of PFPE as top lubricating layer. *J. Mech. Behav. Biomed. Mater.* **2011**, *4*, 953–960, doi:10.1016/j.jmbbm.2011.02.005.

46. Abdul Samad, M.; Sinha, S. K. Effects of counterface material and UV radiation on the tribological performance of a UHMWPE/CNT nanocomposite coating on steel substrates. *Wear* **2011**, *271*, 2759–2765, doi:10.1016/j.wear.2011.05.025.

47. Samad, M. A.; Sinha, S. K. Mechanical, thermal and tribological characterization of a UHMWPE film reinforced with carbon nanotubes coated on steel. *Tribol. Int.* **2011**, *44*, 1932–1941, doi:10.1016/j.triboint.2011.08.001.

48. Kelly, P. J.; vom Braucke, T.; Liu, Z.; Arnell, R. D.; Doyle, E. D. Pulsed DC titanium nitride coatings for improved tribological performance and tool life. *Surf. Coatings Technol.* **2007**, *202*, 774–780, doi:10.1016/j.surfcoat.2007.07.047.

49. Subramanian, B.; Muraleedharan, C. V.; Ananthakumar, R.; Jayachandran, M. A comparative study of titanium nitride (TiN), titanium oxy nitride (TiON) and titanium aluminum nitride (TiAlN), as surface coatings for bio implants. *Surf. Coatings Technol.* **2011**, *205*, 5014–5020, doi:10.1016/j.surfcoat.2011.05.004.

50. Annunziata, M.; Oliva, A.; Basile, M. A.; Giordano, M.; Mazzola, N.; Rizzo, A.; Lanza, A.; Guida, L. The effects of titanium nitride-coating on the topographic and biological features of TPS implant surfaces. *J. Dent.* **2011**, *39*, 720–728, doi:10.1016/j.jdent.2011.08.003.

51. Bock, N.; Dargaville, T. R.; Woodruff, M. A. Progress in Polymer Science Electrospraying of polymers with therapeutic molecules : State of the art. *Prog. Polym. Sci.* **2012**, *37*, 1510–1551, doi:10.1016/j.progpolymsci.2012.03.002.

52. Huang, J.; Jayasinghe, S. N.; Best, S. M.; Edirisinghe, M. J. Novel deposition of nano-sized silicon substituted hydroxyapatite by electrostatic spraying. **2005**, *6*, 1137–1142.

53. Jagielski, J.; Piatkowska, A.; Aubert, P.; Thomé, L.; Turos, A.; Abdul Kader, A. Ion implantation for surface modification of biomaterials. *Surf. Coatings Technol.* **2006**, *200*, 6355–6361, doi:10.1016/j.surfcoat.2005.11.005.

54. Díaz, C.; Lutz, J.; Mändl, S.; García, J. A.; Martínez, R.; Rodríguez, R. J. Improved bio-tribology of biomedical alloys by ion implantation techniques. *Nucl. Instruments Methods Phys. Res. Sect. B Beam Interact. with Mater. Atoms* **2009**, *267*, 1630–1633, doi:10.1016/j.nimb.2009.01.118.

55. Huang, N.; Yang, P.; Leng, Y. .; Wang, J.; Sun, H.; Chen, J. .; Wan, G. . Surface modification of biomaterials by plasma immersion ion implantation. *Surf. Coatings Technol.* **2004**, *186*, 218–226, doi:10.1016/j.surfcoat.2004.04.041.

56. Mandl, S.; Sader, R.; Thorwarth, G.; Krause, D.; Zeilhofer, H. F.; Horch, H. H.; Rauschenbach, B. Investigation on plasma immersion ion implantation treated medical implants. *Biomol. Eng.* **2002**, *19*, 129–132, doi:10.1016/S1389-0344(02)00025-4.

57. Xie, Y.; Liu, X.; Huang, A.; Ding, C.; Chu, P. K. Improvement of surface bioactivity on titanium by water and hydrogen plasma immersion ion implantation. *Biomaterials* **2005**, *26*, 6129–6135, doi:10.1016/j.biomaterials.2005.03.032.

58. Liu, L. D.; Chen, F. S. Super-carburization of low alloy steel in a vacuum furnace. *Surf. Coatings Technol.* **2004**, *183*, 233–238, doi:10.1016/j.surfcoat.2003.08.079.

59. Tarakci, M.; Korkmaz, K.; Gencer, Y.; Usta, M. Plasma electrolytic surface

carburizing and hardening of pure iron. *Surf. Coatings Technol.* **2005**, *199*, 205–212, doi:10.1016/j.surfcoat.2005.02.117.

60. Güleryüz, H.; Çimenoğlu, H. Effect of thermal oxidation on corrosion and corrosion-wear behaviour of a Ti-6Al-4V alloy. *Biomaterials* **2004**, *25*, 3325–3333, doi:10.1016/j.biomaterials.2003.10.009.

61. Dong, H.; Bell, T. Enhanced wear resistance of titanium surfaces by a new thermal oxidation treatment. *Wear* **2000**, *238*, 131–137, doi:10.1016/S0043-1648(99)00359-2.

62. Xiong, D.; Gao, Z.; Jin, Z. Friction and wear properties of UHMWPE against ion implanted titanium alloy. *Surf. Coatings Technol.* **2007**, *201*, 6847–6850, doi:10.1016/j.surfcoat.2006.09.043.

63. Wen, H. I.; Han-, D. Improvement in the Tribological Properties of UHMWPE Sliding against Ti6AI4V by Surface Modification 1 Introduction. **2005**, *9*, 164–171.

64. Tai, Z.; Chen, Y.; An, Y.; Yan, X.; Xue, Q. Tribological behavior of UHMWPE reinforced with graphene oxide nanosheets. *Tribol. Lett.* **2012**, *46*, 55–63, doi:10.1007/s11249-012-9919-6.

65. Spriano, S.; Vernè, E.; Faga, M. G.; Bugliosi, S.; Maina, G. Surface treatment on an implant cobalt alloy for high biocompatibility and wear resistance. *Wear* **2005**, *259*, 919–925, doi:10.1016/j.wear.2005.02.011.

66. Chi, P. R. Improvement in the Tribological Properties of UHMWPE Sliding against Ti6Al4 V by Surface Modification. *Wear* **2005**, *9*, 164–171.

67. Paz, Adrian, Dainelys, Guadarrama, Mónica, López, Jesús, E González, Nayrim,

Brizuela, Javier, A. Quim. Nova,. **2012**, *35*, 1724–1727.

68. Hussein, M. A.; Suryanarayana, C.; Al-Aqeeli, N. Fabrication of nano-grained Ti-Nb-Zr biomaterials using spark plasma sintering. *Mater. Des.* **2015**, *87*, 693–700, doi:10.1016/j.matdes.2015.08.082.

69. M. A. Huusein, N Al-Aqeeli, ' Titanium alloys for biomedical applications and fabrication methods thereof". Issued 28, 11,2017,US, Patent number: 9828655

70. Hussein, M. A.; Kumar, A. M.; Yilbas, B. S.; Al-Aqeeli, N. Laser Nitriding of the Newly Developed Ti-20Nb-13Zr at.% Biomaterial Alloy to Enhance Its Mechanical and Corrosion Properties in Simulated Body Fluid. *J. Mater. Eng. Perform.* **2017**, *26*, 5553–5562, doi:10.1007/s11665-017-2955-5.

71. Hussein, M.; Kumar, M.; Drew, R.; Al-Aqeeli, N. Electrochemical Corrosion and In Vitro Bioactivity of Nano-Grained Biomedical Ti-20Nb-13Zr Alloy in a Simulated Body Fluid. *Materials (Basel).* **2017**, *11*, 26, doi:10.3390/ma11010026.

72. Loh, J. H. Plasma surface modification in biomedical applications. *Med. Device Technol.* **1999**, *10*, 24–30.

73. Jin, F.; Balasubramaniam, R.; Stebe, K. J. surfactant adsorption to spherical particles: the intrinsic length scale governing the shift from diffusion to kinetic-controlled mass transfer. *J. Adhes.* **2004**, *80*, 773–796, doi:10.1080/00218460490480770.

74. Surface characteristics of AISI 304L stainless steel after an atmospheric pressure plasma treatment. *Surf. Coatings Technol.* **2005**, *195*, 298–306, doi:10.1016/J.SURFCOAT.2004.07.071.

75. Grosso, D.; Marie, P. How to exploit the full potential of the dip-coating process to

better control film formation. **2011**, 17033–17038, doi:10.1039/c1jm12837j.

76. Hull, M. L. A Finite Element Model of the Human Knee Joint for the Study of Tibio-Femoral Contact. *J. Biomech. Eng.* **2002**, *124*, 273, doi:10.1115/1.1470171.

77. Bahraminasab, M.; Sahari, B. B.; Roshdi, M.; Arumugam, M. Finite Element Analysis of the Effect of Shape Memory Alloy on the Stress Distribution and Contact Pressure in Total Knee Replacement. *Heal. (San Fr.* **2011**, *25*, 95–100.

78. Henak, C. R.; Kapron, A. L.; Anderson, A. E.; Ellis, B. J.; Maas, S. A.; Weiss, J. A.; Hodge, W. A.; Fijan, R. S.; Carlson, K. L.; Burgess, R. G.; Harris, W. H.; Mann, R. W.; Hull, M. L.; Bahraminasab, M.; Sahari, B. B.; Roshdi, M.; Arumugam, M.; Anderson, A. E.; Ellis, B. J.; Maas, S. A.; Weiss, J. A. Effects of idealized joint geometry on finite element predictions of cartilage contact stresses in the hip. *J. Biomech. Eng.* **2011**, *83*, 2879–83, doi:10.1115/1.1470171.

79. Henak, C. R.; Kapron, A. L.; Anderson, A. E.; Ellis, B. J.; Maas, S. A.; Weiss, J. A. Specimen-specific predictions of contact stress under physiological loading in the human hip: Validation and sensitivity studies. *Biomech. Model. Mechanobiol.* **2014**, *13*, 387–400, doi:10.1007/s10237-013-0504-1.

80. Bhushan, B. *Introduction to tribology*; John Wiley & Sons, 2013; ISBN 9781119944539.

81. Leng, Y. (Yang) *Materials characterization : introduction to microscopic and spectroscopic methods*; J. Wiley & Sons, 2008; ISBN 0470822996.

82. Sreekanth, P. S. R.; Kanagaraj, S. Restricting the ageing degradation of the mechanical properties of gamma irradiated UHMWPE using MWCNTs. *J. Mech. Behav. Biomed. Mater.* **2013**, *21*, 57–66, doi:10.1016/j.jmbbm.2013.01.028.

83. Halley, P.; Murphy, M.; Martin, D.; Mcnally, T.; Po, P.; Bell, S. E. J.; Brennan, G. P.; Bein, D.; Lemoine, P.; Paul, J. Polyethylene multiwalled carbon nanotube composites. **2005**, *46*, 8222–8232, doi:10.1016/j.polymer.2005.06.094.

84. Puppulin, L.; Miura, Y.; Casagrande, E.; Hasegawa, M.; Marunaka, Y.; Tone, S.; Sudo, A.; Pezzotti, G. Acta Biomaterialia Validation of a protocol based on Raman and infrared spectroscopies to nondestructively estimate the oxidative degradation of UHMWPE used in total joint arthroplasty. *Acta Biomater.* **2016**, *38*, 168–178, doi:10.1016/j.actbio.2016.04.040.

85. Geyter, N. De; Morent, R.; Leys, C. Surface characterization of plasma-modified polyethylene by contact angle experiments and ATR-FTIR spectroscopy. **2008**, 608–611, doi:10.1002/sia.2611.

86. Morent, R.; Geyter, N. De; Leys, C.; Gengembre, L.; Payen, E. Comparison between XPS- and FTIR-analysis of plasma-treated polypropylene film surfaces. **2008**, 597–600, doi:10.1002/sia.2619.

87. Karahan, H. A.; Özdo, E. Improvements of Surface Functionality of Cotton Fibers by Atmospheric Plasma Treatment. **2008**, *9*, 21–26.

88. Affatato, S.; Modena, E.; Carmignato, S.; Taddei, P. The use of Raman spectroscopy in the analysis of UHMWPE uni-condylar bearing systems after run on a force and displacement control knee simulators. *Wear* **2013**, *297*, 781–790, doi:10.1016/j.wear.2012.10.002.

89. Wang, Y.; Vasileva, D.; Zustiak, S. P.; Kuljanishvili, I. Raman spectroscopy enabled investigation of carbon nanotubes quality upon dispersion in aqueous environments. *Biointerphases* **2017**, *12*, 11004, doi:10.1116/1.4978922.

90. Fang, L.; Leng, Y.; Gao, P. Processing and mechanical properties of HA/UHMWPE nanocomposites. *Biomaterials* **2006**, *27*, 3701–3707, doi:10.1016/j.biomaterials.2006.02.023.

91. Cunha, A. M. L. RBIS, F. G. FERREIRA and P. L. GRANJA Department ofMetallurgical Engineering (FEUP) - University ofPorto Rua dos Bragas, 4099 Porto Codex - PORTUGAL. *6*, 163–176.

VITAE

Name: :Zahid Ahmed Uwais

Nationality: :Sri Lankan

Date of Birth: :12/11/2017

Email: :zahid.uwais@gmail.com

Address: :7A, Primrose Road, Kandy, Sri Lanka. Zip code: 20000

Academic Background:

B.Sc. Mechanical Engineering
King Fahd University of Petroleum & Mineral (KFUPM)
Graduated with Honors, (3.24/4 GPA)

M.Sc. Mechanical Engineering
King Fahd University of Petroleum & Minerals (KFUPM)
Specialization: Materials & Manufacturing, (3.46/4 GPA)

Publications:

1. Uwais, Zahid A., et al. "Surface Modification of Metallic Biomaterials for Better Tribological Properties: A Review." *Arabian Journal for Science and Engineering* 42.11 (2017): 4493-4512.

2. Uwais, Zahid A., et al. "Tribological Characterization of a Novel UHMWPE Hybrid Nanocomposite Coating for Biomedical Applications." (Submitted to Applied Surface Science)